

Effects of Applied DC Electric Fields on Water-Oil Interfacial Properties

by

Ye Zhang

A thesis submitted in partial fulfillment of the requirements for the degree of

Master of Science

in

Chemical Engineering

Department of Chemical and Materials Engineering
University of Alberta

© Ye Zhang, 2019

Abstract

Among all the competing methods to enhance the phase separation of water-in-oil emulsions in chemical industries, electric field is considered as one of the best treatment options. To better understand the mechanism by which electric field assists water droplets coalescence and the corresponding physics of skin formation, the interfacial properties of the water/oil interface in a water-in-model oil emulsion system, including interfacial tension, shape factor, crumpling ratio and dilatational rheology, are studied with a tensiometer. The pendant water drop deforms immediately at the onset of electric field application, into either a prolate shape or an oblate shape in the direction of electric field, depending on the properties of the continuous phase. The degree of drop deformation is of positive correlation with the experienced electric field strength and is also affected by the electric field direction and the drop position in between the electrodes. An external electric field is found to enhance the formation of interfacial asphaltene layer elucidated by a higher crumpling ratio, lower interfacial tension, higher shape factor and higher elasticity with increasing electric field strength. This could be due to the induced electrohydrodynamic flow, which triggers the interfacial convection and accelerates asphaltene movements and adsorption. The same trend holds true for measurements with various asphaltene concentration, aging time, water phase pH, and water salinity under electric field application. Although the electric-assisted formation of a stronger interfacial barrier is against drop-drop coalescence, a hypothesis is proposed that the electric-induced drop deformation may dominant, enlarging the interfacial area and generating a patchy film with weak spots for easier drop-drop coalescence.

Acknowledgements

First, I would like to thank Prof. Zhenghe Xu and Prof. Qingxia Liu for supervision and guidance at all time for this thesis project. My appreciation also goes to Prof. Jan Vermant for offering me so much help in electric field simulation and interfacial tension calculation, and kindly invited me to conduct part of my thesis project work in ETH Zurich. I also would like to thank Prof. Johan Sjöblom and Prof. Sebastien Simon for sponsoring the JIP project and organizing meetings which provides me with opportunities to enter the field of electro-coalescence. I appreciate the help from Dr. Nick Jaensson and Dr. Bram Schroyen in ETH Zurich, who filled me with fundamental knowledge in stress-fitting and guided me through simulation. I would like to thank Dr. Sameer Mhatre for all his suggestions and guidance during my thesis project.

I also feel thankful to the assistance from Mr. Jim Skwarok, Ms. Jie Ru and Ms. Lisa Carriero. My appreciation also goes to the entire Oil Sands Extraction research group for their timely help and kind suggestion, especially from Zhen Niu, Rui Li, Peiqi Qiao, Zuoli Li, An Li, and Carol Dwaik.

Finally, I thank NSERC Industrial Research Chair in Oil Sands Engineering for financial support.

This document is dedicated to my beloved parents, who raised me up with love and support.

Table of Contents

Abstract	ii
Acknowledgements	iii
Table of Contents	v
List of Figures	viii
List of Tables	xii
Chapter 1 Introduction	1
1.1 Conventional and unconventional resource	1
1.2 Oil sands and bitumen	3
1.3 Objectives and outline	6
Chapter 2 Literature Research	9
2.1 Emulsion.....	9
2.1.1 Stabilization and destabilization	10
2.2 Interfacial behaviors of asphaltene.....	13
2.2.1 Asphaltene molecular structure	14
2.4.2 Asphaltene aggregates	16
2.4.3 Adsorption kinetics.....	18
2.3 Electrocoalescence	20
2.3.1 Electrophoresis and dielectrophoresis	20
2.3.2 Electrohydrodynamic flows.....	21
2.3.3 Drop deformation	22
2.3.4 Fundamentals of electrocoalescence	25
Chapter 3 Experimental Techniques	28

3.1 Pendant drop tensiometry.....	28
3.1.1 DPT: Drop profile tensiometry.....	28
3.1.2 CPT: Capillary pressure tensiometry.....	29
3.2 Interfacial tension measurement.....	30
3.2.1 Shape factor	30
3.2.2 Correlation of shape factor and interfacial tension.....	32
3.3 Dilatational rheology measurement by oscillating drop method	33
3.3.1 Principle of oscillating drop method	34
3.3.2 Applicability limits	35
3.4 Crumpling ratio measurement	36
Chapter 4 Experimental Setup and Procedure	38
4.1 Materials.....	38
4.1.1 Preparation of asphaltenes	38
4.1.2 Model oil.....	40
4.1.3 Water phase	40
4.2 Instrumentation.....	41
4.2.1 High voltage power supply.....	41
4.2.2 Copper electrodes	43
4.2.3 Syringe and needle.....	45
4.2.4 Glass cell.....	46
4.2.5 Schematic of setup.....	47
4.3 Experimental Procedure	48
4.3.1 Interfacial tension measurement by pendant drop tensiometry	48
4.3.2 Crumpling ratio measurement and calculation	49
4.3.3 Dilatational rheology measurement by pendant drop tensiometry.....	50

4.3.4 Calibration	51
4.3.5 Repeatability	51
Chapter 5 Results and Discussion	53
5.1 Shape evolution of pendant water drop	53
5.1.1 Electric-induced deformation type	53
5.1.2 Deformation with step-wise electric field application.....	56
5.1.3 System reversibility	58
5.1.4 Effect of electric field direction and drop position.....	60
5.2 Effect of electric field strength.....	63
5.2.1 Applicability limits of interfacial tension measurement in electric fields.....	63
5.2.2 Effect of electric field on the interfacial tension	66
5.2.3 Effect of electric field on the shape factor.....	71
5.2.4 Crumpling ratio measurements.....	73
5.2.5 Effects of electric field on dilatational rheology	77
5.2.6 Possible explanation	80
5.3 Effect of asphaltene concentration on shape factor and crumpling ratio under different electric fields	81
5.4 Effect of aging time on shape factor and crumpling ratio under various electric fields	83
5.5 Effect of water phase pH on shape factor and crumpling ratio under different electric fields	86
5.6 Effect of salinity on shape factor and crumpling ratio under various electric fields	89
Chapter 6 Conclusions and Future Work.....	94
6.1 Conclusions	94
6.2 Future work	98
Bibliography	102

List of Figures

Figure 1- 1: Structural differences of well bores applied in conventional and unconventional resources exploitation [1].....	2
Figure 1- 2: Raw bitumen production by region [9].	4
Figure 1- 3: Raw bitumen production by extraction methods [10].....	5
Figure 2 - 1: Schematics of (a) water-in-oil emulsion, and (b) oil-in-water emulsions, with the presence of surfactant containing both hydrophilic and lipophilic groups [20].	11
Figure 2 - 2: The proposed (a) archipelago, and (b) island model compound for describing the asphaltene molecular structure in previous research [41].....	15
Figure 2 - 3: Schematics of the molecular and nano-colloidal structures of asphaltenes according to the previously reported Yen-Mullins model, or the modified Yen model [83] based on references [78], [84]–[86]. Again, this model suggests the dominance of the island molecular structure.....	18
Figure 2 - 4: (a, b) Qualitative simulated electrohydrodynamic flow pattern in and around an isolated drop utilizing the leaky dielectric model [98].	22
Figure 2 - 5: A drop pair of glycerol-water (containing 10% glycerol) coalescing in silicone oil under external uniform DC electric field at 250 kV/m [93].	26
Figure 3 - 1: Schematic and variables of a theoretical drop profile for fitting with an experimental pendant drop image.....	31
Figure 4 - 1: (a) Supernatant collection based on siphon principle, and (b) the fully dried precipitated asphaltenes ready to use in model oil preparation.	39
Figure 4 - 2: Example of external software program operation in controlling the applied voltage. The desired voltage is set to 2 kV and the output voltage is also 2 kV as shown in the window of “VOLTAGE MONITOR (kV)”.	42

Figure 4 - 3: Pictures of (a) the copper electrodes with banana pin on top and wire connection at the bottom and (b) its application in electric field involved experiments.....	43
Figure 4 - 4: Schematic pictures of wire connections to reverse the electrode polarity. The top electrode is (a) positively charged, and (b) grounded.....	45
Figure 4 - 5: Images of (a) connection of the hose barb and the glass capillary, and (b) Teflon tape wrapping on the outside.	46
Figure 4 - 6: Schematic of experimental setup for interfacial tension and crumpling ratio measurement (an automatic liquid dispenser is used in dilatational rheology measurement).	47
Figure 5 - 1: Shape comparison of pendant water drops suspending in model oils of the same concentration at (a) 0 kV/m and (b) 100 kV/m (c) 100 kV/m.	55
Figure 5 - 2: Drop deformation under increased electric field until detachment.	57
Figure 5 - 3: Interfacial tension variation after aging the water drop at 0 kV/m for 15 minutes, followed by altering the applied voltage to 50 kV/m ,100 kV/m, 50 kV/m and 0 kV/m for 5 minutes at each stage for (a) water-in-heptane emulsion system, and (b) water-in-toluene emulsion system.....	58
Figure 5 - 4: Interfacial tension variation for water-in-model oil emulsion system. The water drop is aged at 0 kV/m for 30 minutes, followed by applying electric field at 100 kV/m for 3 minutes and then back to 0 kV/m.	59
Figure 5 - 5: Pendant water drop suspending in model oil tends to detach from the glass capillary during 40 minutes of aging time, when the direction of electric field is opposite to gravity.	62
Figure 5 - 6: Examples of drop image and the corresponding shape factor for a water-in-0.05 g/L model oil system after 40 mins aging under various electric field strength.	64
Figure 5 - 7: Variation trend of interfacial tension and shape factor of a water/model oil interface at (a) electric field application process, and (b) electric field removal process.....	67
Figure 5 - 8: The interfacial tension of water/oil interface at 0 kV/m and aged for 60 minutes. .	68
Figure 5 - 9: The interfacial tension of a water/model oil interface aged for 40 minutes under electric field and relaxed for 20 minutes without electric field.	69
Figure 5 - 10: Variation trend of the interfacial tension as a function of time for a water-in-model oil system aged for 40 minutes under various electric field strength.	72

Figure 5 - 11: The apparent interfacial tension and the measured shape factor for a water-in-model oil system aged for 40 minutes as a function of electric field strength.....	73
Figure 5 - 12: Example of crumpling process at (a) the initial status, (b) the status right before crumpling occurs, and (c) the crumpling point. The deionized water drop is immersed in 0.05 g/L model oil at 100 kV/m.	74
Figure 5 - 13: The crumpling ratio results of water-in-0.05 g/L model oil under different electric field strength.	77
Figure 5 - 14: The average elastic modulus variations as a function of time during 40 minutes of aging under electric field of (a) 0 kV/m, (b) 50 kV/m and (c) 100 kV/m.	79
Figure 5 - 15: Schematic of asphaltenes aggregates' movement along the interface under an electric field in the same direction as gravity.	81
Figure 5 - 16: The shape factor for a water-in-model oil system aged for 40 minutes at different concentrations as a function of electric field strength.	82
Figure 5 - 17: The crumpling ratio results of both water-in-0.01 g/L, 0.05 g/L, and 0.1 g/L model oil system under various electric field strength.	83
Figure 5 - 18: The shape factor for a water-in-model oil system aged for 30, 40, and 50 minutes under various electric field strength.....	84
Figure 5 - 19: The crumpling ratio results for water drops aged for 30 minutes, 40 minutes and 50 minutes respectively under various electric field strength.....	85
Figure 5 - 20: The shape factor of a pendant water drop immersed in model oil as an implication for the interfacial tension versus different water pH at various electric field strength.	86
Figure 5 - 21: The crumpling ratio results of water phase at various pH suspending in 0.05 g/L model oil under different electric field strength.	88
Figure 5 - 22: Shape factor results as a function of salt content with addition of: (a) NaCl, and (b) CaCl ₂ at 0, 0.01 and 0.1 mol/L in the aqueous phase for pendant drop immersed in model oil under various electric field.....	90
Figure 5 - 23: Crumpling ratio results as a function of salt content with addition of: (a) NaCl, and (b) CaCl ₂ at 0, 0.01 and 0.1 mol/L in the aqueous phase for pendant drop immersed in model oil under various electric field.....	91

Figure 5 - 24: Crumpling ratio results as a function of electric field strength with addition of NaCl, and CaCl₂ at 0.01 and 0.1 mol/L in the aqueous phase for pendant drop immersed in model oil under various electric field. 93

Figure 6 - 1: Schematics of the proposed mechanism on water drop-drop electrocoalescence in the oil phase. A homogeneous interfacial film of asphaltene is formed (a) without electric field application, but cracks are created (b) with electric field application, due to the enlarged interface..... 97

Figure 6 - 2: Interfacial tension of water/model oil interface as a function of time with interfacial tension hysteresis and electric stress marked. The water drop is aged at 0 kV/m for 30 minutes, followed by applying electric field at 100 kV/m for 3 minutes and then back to 0 kV/m. 100

List of Tables

Table 5 - 1: The effect of electric field direction and drop position on drop deformation and the range of voltage applied.	61
Table 5 - 2: A summary of power off testing on γ_{real} , β_{on} , β_{off} and $\Delta\beta$ under different electric field strength.	70
Table 5 - 3: Images of a pendant water drop in 0.05 g/L model oil at initial status and right before crumpling point under various electric field strength. The shape factor and crumpling ratio are also included.	75

Chapter 1 Introduction

1.1 Conventional and unconventional resource

Conventional resources are considered as the oil and natural gas discretely accumulates in rock formations with relatively high porosity and permeability. They are trapped below a layer of impervious rock formation so that the hydrocarbon migration is restrained. Due to the simplicity in recovery, vertical well bores combined with minimal stimulation are generally applied in the production of conventional resources. By the year of 2006 in western Canada, exploitation of conventional resources were the primary objective [1]. However, conventional resources have been extensively exploited over the last few decades, so unconventional resources have come into notice and been developed more and more.

Unconventional resource usually refers to oil and natural gas resources that locate in special formations and require particular extraction and production methods to recover the resource from the reservoir, such as tight oil, oil shale, oil sands and bitumen [2]. It is estimated that unconventional resources exhibit in a larger amount than conventional resources and is of significant potential to satisfy the growing need for fuels worldwide [3]. The oil and natural gas-bearing units are usually deposited in rock formation with extremely low porosity and permeability, so that advanced stimulation technologies are needed for economic production. Compared with vertical well bores widely used for conventional resources, horizontal drilling combined with hydraulic fracturing are more commonly used for unconventional resources. Horizontal drilling

technology also enables the application of steam assisted gravity drainage (SAGD), which is of great importance in the bitumen recovery from oil sands.

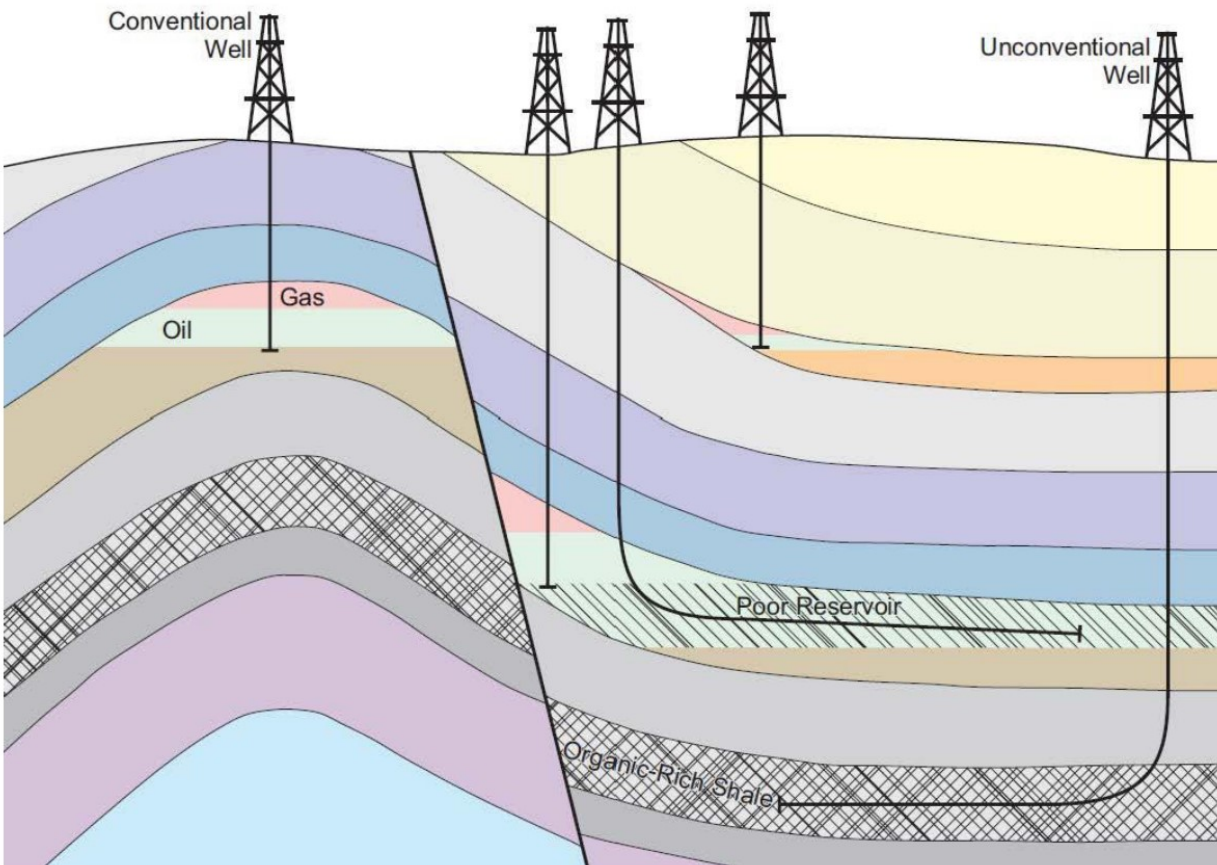


Figure 1- 1: Structural differences of well bores applied in conventional and unconventional resources exploitation [1].

However, the definition of conventional and unconventional resources is not strictly differentiated yet. With the development of more novel methods and evolution of economic and technological conditions, the concept of unconventional resources is subject to change, possibly migrating gradually to the conventional category [4].

1.2 Oil sands and bitumen

Oil sands is a type of unconventional oil that is extremely viscous and heavy, usually exhibits in a mixture of sand, bitumen, minerals or clay, and water. Although it looks very much like and usually referred to as tar sand, oil sand is a petrochemical that naturally exists under the formation compared to tar sand being a synthetic product through destructive distillation from wood, coal, or petroleum [5]. There are a few places around the world that are concerned as the oil sands areas (OSAs), including Russia, Saudi Arabia, the United States, Venezuela and Canada [5]. Around the world, A total area of about 142,000 square kilometers are occupied by the OSAs [6]. The Alberta Energy Regulator has reported that the oil sands deposits in Alberta hold a total reservoir around 165.4 billion Barrels, ranking the third worldwide after the top two being Venezuela and Saudi Arabia. The crude bitumen production, obtained by both open pit mining and recovering in place, amounted up to 2.8 million barrels per day in 2017 [7][8].

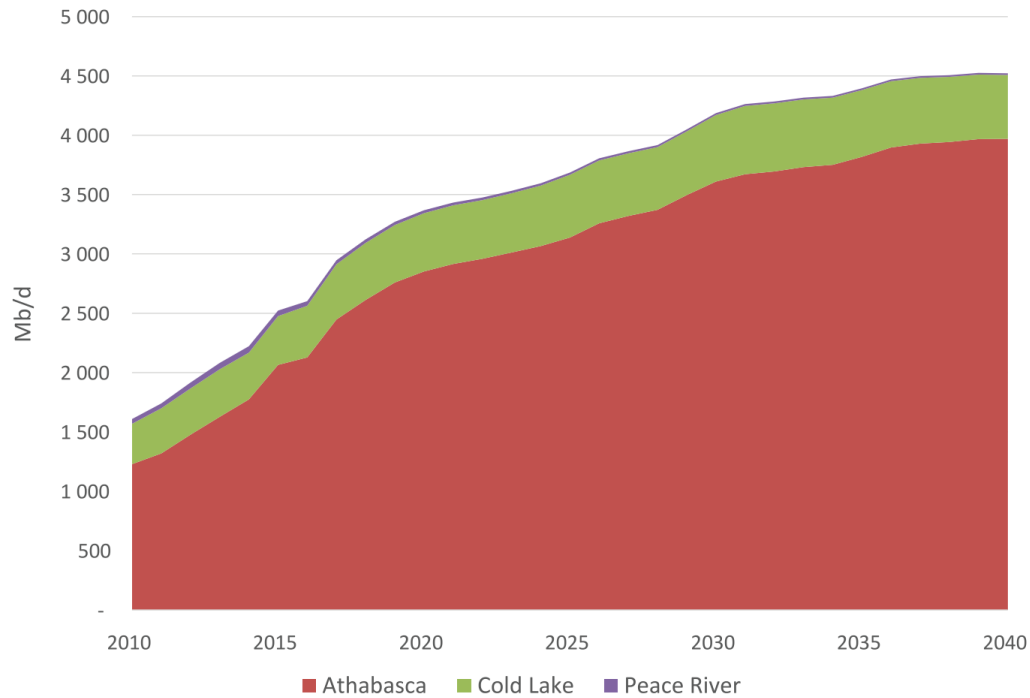


Figure 1- 2: Raw bitumen production by region [9].

It is demonstrated in the figure that the production has been increasing rapidly in the last eight years and will keep growing slightly slower in the next twenty years. The oil sands recovered from the Athabasca region accounts for around 82% of total production, both in the past and in the forecast, with production from Cold Lake region and Peace River region taking up 16% and 2%, respectively [9].

The viscosity of bitumen in its natural state is so high and too thick to flow in a production well, that advanced technologies are required to enhance the production of oil sands [6]. There are mainly four ways to extract the contained bitumen, as shown in the figure below, including steam assisted gravity drainage (SAGD), cyclic steam stimulation (CSS), surface mining (open pit mining) and primary with enhanced oil recovery production [9].

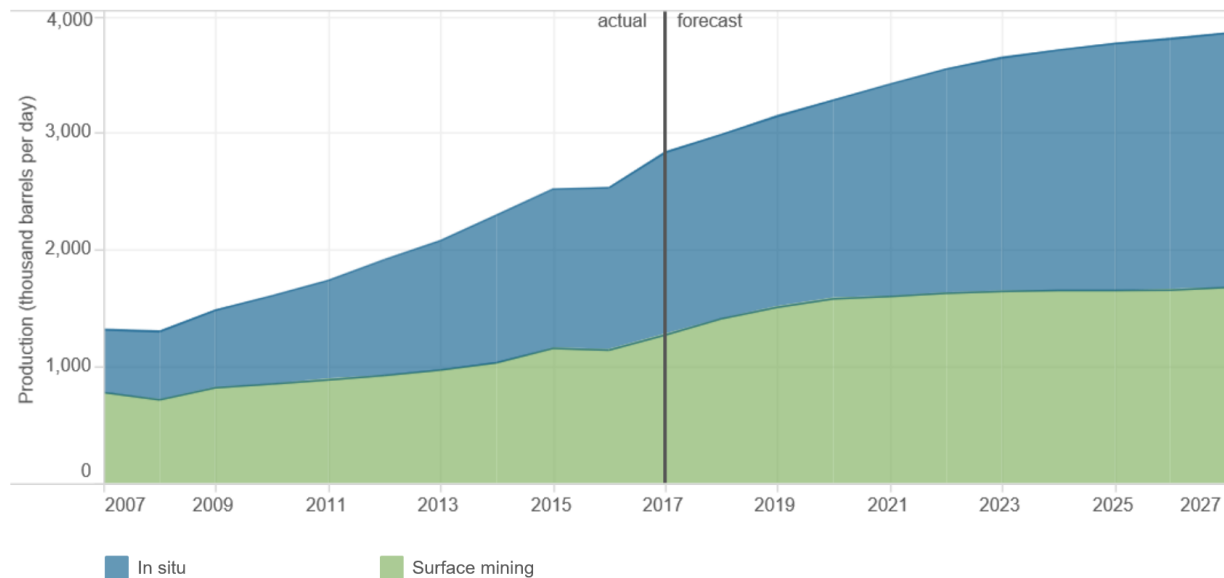


Figure 1- 3: Raw bitumen production by extraction methods in Alberta [10].

Two main methods for oil sands production in Alberta are in situ and surface mining, as shown in the above figure. The surface mining involves using truck and shovel to remove the overburden above the oil sands reservoir, applicable only at a depth smaller than 70 meters. However, 80 percent of the oil sands reservoirs locate deeper and are no longer economical to be mined [6][11], where in situ methods by drilling wells to recover in place is much easier and cause minimum disturbance to the land. This method is primarily combined with SAGD, heating the reservoir with steam to reduce the viscosity at high temperature and produce flow into the horizontal well [9]. A pair of long horizontal wells with 5 meters gap in between are usually drilled in SAGD. Steam, generated with recycled salted water, travels through the upper well to heat the oil sands reservoir in the steam chamber, until the bitumen can flow downwards into the bottom well [11]. It is predicted that the raw production from surface mining and in situ will increase by 32.0% and 39.3%

respectively, compared to the amount in 2017. The in situ production is slightly higher due to the development of advanced technologies in new applications in recent years, lowering the operational costs while enhancing efficiencies [10].

To improve the bitumen quality, Facilities for upgrading are required to produce synthetic crude oil from the raw bitumen. Due to the dense and viscous nature of raw bitumen, large oil molecules need to be broken down into smaller ones through chemical fluids injection or heat additions [8]. It is estimated that in Alberta, approximately 43% of raw bitumen was sent for upgrading in 2017. The percentage would shrink to 36% by the year of 2027 as forecasted by the Alberta Energy regulator, due to the limitation of new upgrading projects planned and the increasing production by open-pit mining and in situ recovery [12]. To further converts oil into commercial petroleum products, the oil need to be distilled so that compositions with different boiling points can be separated [8].

1.3 Objectives and outline

In consideration of the popularity in water and oil phase separation with electric field application, numerous researches have been conducted to reveal the influence of various chemical and physical parameters on electro-coalescence. However, the exact mechanism of how electric field is assisting drops attraction and film rupture is still undiscovered. In this research, the role of electric field is studied by looking into the interfacial properties of the water/oil interface, stabilized by asphaltenes as the only surfactant in the emulsion system. Interfacial tension, crumpling ratio and dilatational rheology are measured by pendant drop tensiometry. This study uncovers whether the

electric field benefits drop-drop coalescing by eliminating the adsorbing capacity of asphaltenes onto the interface.

Chapter 1 provides a brief introduction on the definition of conventional and unconventional resource. Advanced stimulation technologies involved in economic production of unconventional resource are presented. Information of oil sands distribution and regional bitumen production are provided. The production methods and upgrading principles of raw bitumen are also elaborated.

Chapter 2 reviews published literatures on emulsion stability and demulsification, interfacial behaviors of asphaltene and its adsorption kinetics are summarized. The mechanisms involved in electro-coalescence are discussed, including electrophoresis and dielectrophoresis, electrohydrodynamic flows, drop deformation under electric field, and fundamentals of electro-coalescence.

Chapter 3 gives detailed information on the operating principles of pendant drop tensiometry and the theoretical background of interfacial tension, crumpling ratio and dilatational rheology measurements. Since all experiments are conducted with the help of a commercially available Tensiometer. The theories related are presented to prove its applicability limits in interfacial tension measurements under electric field.

Chapter 4 describes the experimental materials and setup utilized in this study. The precipitation of asphaltenes and subsequent model oil preparation are elaborated. The instrumentation on electric field application is presented by the high voltage power supply and the copper electrodes design. Other information on the utilized syringe, needle and glass cell and the experimental procedures in each interfacial property measurement are also elaborated.

Chapter 5 provides experimental results on shape deformation under a few physical variables, leading to an optimum selection of the applied voltage range and direction, drop size, and drop position. The applicability limits of interfacial tension measurements by the Theta Optical Tensiometer under electric field is demonstrated. However, it is not the main purpose of this study to uncover the precise formula deduction and pursue the exact value of interfacial tension, but to form a general knowledge of the variation pattern with this experimental technique. One potential experimental method in the pursuit of a close value to the real interfacial tension is presented. Results of the interfacial tension (implied by the shape factor), the crumpling ratio and the elastic modulus are provided. The effect of electric field strength, asphaltene concentration, aging time, water pH, and salinity are tested in this chapter.

Chapter 6 generally concludes the work and findings in this thesis, with some recommendations for future studies in the field of electro-coalescence.

Chapter 2 Literature Research

2.1 Emulsion

An emulsion system stands for a mixture of liquids, usually two and both of which are immiscible. Emulsion is classified as a part of the more general group, as colloids, which is composed of two-phase systems of matters. Most of the time, an emulsion system refers to a system containing two liquid phases, a dispersed phase and a continuous phase (the dispersions medium, or the external phase). Emulsions are commonly present in numerous applications, including cosmetics, foods, printing, hydraulic fluids, pharmaceutical industry, forest products and metal processing, etc. [13], [14].

Different types of emulsions can be formed with two immiscible liquids. For water and oil, an emulsion is considered as water-in-oil emulsion when the dispersed phase is water and the continuous phase is oil. In reverse, if oil droplets are dispersed in an external continuous phase of water, an oil-in-water emulsion is formed. Note that multiple emulsions are also producible, such as “water-in-oil-in-water” and “oil-in-water-in-oil” emulsions[15], [16]. Moreover, the boundary between the dispersed phase and the continuous phase is known as the interface. The properties of this interface are keystones for emulsion studies.

2.1.1 Stabilization and destabilization

The stability of an emulsions determines the ability in resisting changes in its properties over a certain time period. The lifetime of an emulsion system, ranging from several minutes to a few years, depends on its stability.

To promote and further stabilize an emulsion, one or a combination of emulsifiers are requested [17]. Detergent is a class of emulsifiers that stabilizes the water/oil interface and interacts with both suspending water and oil drops physically. Similar principles also apply to soap, shampoo in grease removal for cleaning purposes. Daily cosmetics, such as lotions, gels and creams, and food products, such as homogenized milk and vinaigrettes are also examples of stable emulsion applications. Surfactant (surface active agents) is another class of emulsifiers containing both hydrophilic and lipophilic (hydrophobic) groups, leading to solubility in both oil and water. The degree of hydrophilic or hydrophobic can be measured by a computable factor, known as the hydrophilic-lipophilic balance (HLB) [18]. An emulsifier with higher solubility in oil tend to form a water-in-oil emulsion, while higher solubility in water lead to an oil-in-water emulsion [19]. Schematic examples of water-in-oil and oil-in-water emulsions with surfactants on the interface is shown in the following figure.

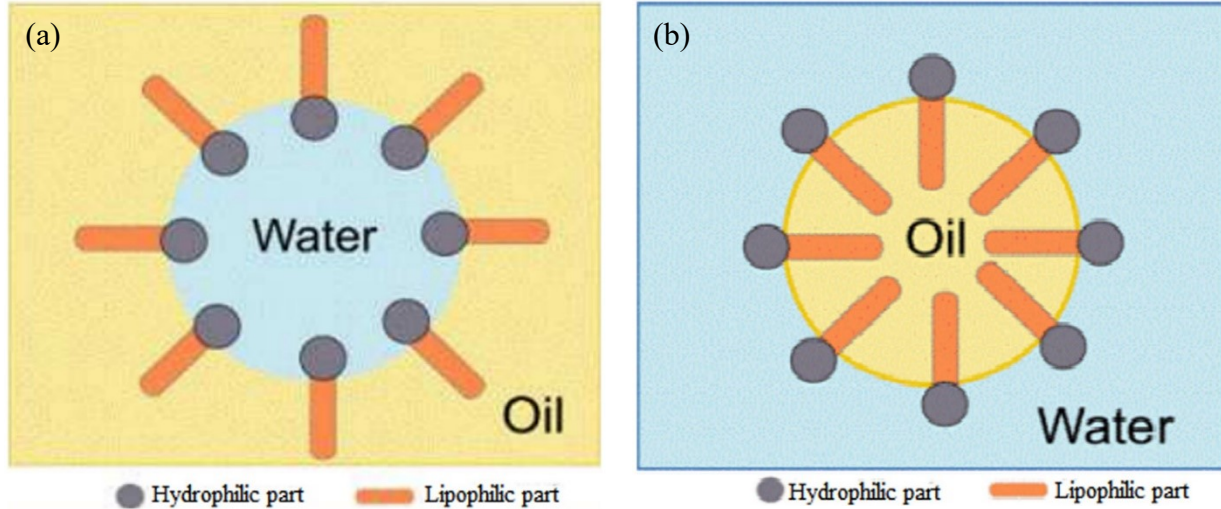


Figure 2 - 1: Schematics of (a) water-in-oil emulsion, and (b) oil-in-water emulsions, with the presence of surfactant containing both hydrophilic and lipophilic groups [20].

The stabilizing mechanism of a water-in-oil emulsion differs from an oil-in-water emulsion. For an oil-in-water emulsion, the stability is subject to both the steric force and the electrostatic repulsion. While in water-in-oil emulsion, the stability is only controlled by the steric force. Because the weak electrostatic force can be neglected due to the low electrical conductivity, permittivity, and ion concentration in the leaky dielectric continuous phase [21], which results in a relatively lower stability than that of an oil-in-water emulsion [22]. Some people advocate that the formation of a steric barrier is the main stabilizing mechanism, preventing small water drops from coalescence and sedimentation. And this steric stability is subject to the hydrodynamic stresses between two neighboring water drops, which also depends on the viscosity [23]. Some disagree and indicate that in oil industries, the thickness of the asphaltene adsorbed layer (a commonly existing surfactant) is only in the order of 2 to 10 nm, too low to work as a traditional steric barrier [24]. It is believed that the asphaltenes cross-link on the interface and form an elastic

or rigid interfacial film, the elasticity or rigidity of which determines the emulsion stability [25]. There are many parameters involved in stabilizing an emulsion system, including drop sizes, volume fractions and their polydispersities, the solubility of the dispersed phase in the external medium, additives of the dispersed phase (such as the pH and salinity of water), and the nature of the surfactants in the continuous phase. These parameters exert coupled effects on emulsion stability and introduce complexities into emulsion processing [26].

Exceeding the lifetime of an emulsion or under demulsification methodologies, destabilization occurs in the form of flocculation, Ostwald ripening, creaming or sedimentation, and coalescence. Flocculation happens when the dispersed drops attract to each other and forms flocs. Ostwald ripening usually occurs in solutions containing solids, where smaller solids dissolve and redeposit onto larger ones. Creaming and sedimentation are similar and follow Stoke's law. Creaming refers to the phenomena that the dispersed drops rise to the surface due to buoyancy or countrification, while sedimentation refers to the dispersed drops accumulating at the bottom of the emulsion by gravitational effect, owing to the higher density in the dispersed phase. Coalescence describes the phenomena that two dispersed drops combine into one and the average drop size in the system increases gradually over time. The two types of emulsion destabilization occurring in water-in-oil emulsion is coalescence and sedimentation.

Just as important as stabilization, destabilization is also widely requested by many industries. In the petroleum industry, a water-in-oil emulsion always exists, wherein a considerable amount of water disperse in crude oil in the form of tiny small droplets with an average size of less than 50 μm [27]. The water consisted can trigger many problems in the industry. Not only will it lower down the oil quality, but also the cost of transportation is largely promoted due to the enhanced volume and viscosity. Also, since salts always coexist with water, catalyst-poisoning and process

equipment corrosion are also serious issue. Therefore, water-oil phase separation (or dewatering, dehydration) from the emulsion is a crucial step in oil treatment in the petroleum industry and has been studied deeply.

Normally, the water can be separated from oil either self-induced or by the influence of external forces. Gravitational settling is a conventional way of self-induced phase separation, where the water droplets coalesce during migration under the effect of gravity and buoyancy. But this method is only limited to relatively large droplets, whereas the drop-size in the petroleum industry is much smaller[27]. Moreover, the difficulties of breaking a water-in-oil emulsion in the industry, i.e. destabilization, or demulsification, mainly lie in the adsorbed surfactants at the water/crude oil interface. These surfactants are naturally existing species, such as the asphaltenes and resins occurring in crude oil, whose capabilities in stabilizing an emulsion have been proved by many publications [28], [29]. The steric interaction together with the mechanical resistance of the adsorbed layer suppress film rupture and inhibits coalescence [30]. In this case, it would be very time-consuming, and less efficient if gravitational settling is applied as a demulsification strategy. Therefore, a majority of demulsification methods applied in the industries take advantage of external forces, including thermal, chemical, mechanical, microwave, electrostatic or a coupling of some of these [31]–[33].

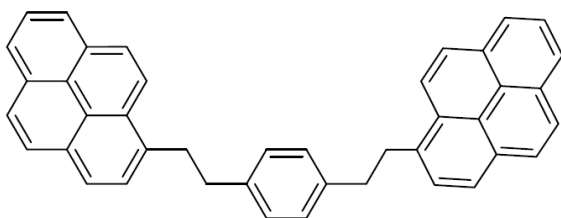
It is crucially important to understand and take advantages of the stabilizing and destabilizing mechanisms, according to the various demands in industrial applications.

2.2 Interfacial behaviors of asphaltene

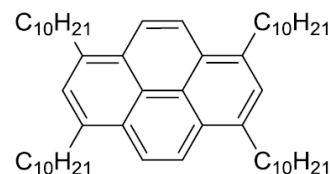
Asphaltenes are defined as the fraction of oil that precipitates in paraffinic solvents but soluble in naphthenic solvents. The asphaltene contents vary to a great extent in different oil fractions, ranking from the lowest in volatile oils, to the highest in crude oils and bitumen. The asphaltene not only controls the viscosity of the oil fraction, but also brings about tremendous disadvantages in oil recovery, storage, treatment and transportation [34]. Especially, as amphiphilic compounds with strong polarity, the asphaltenes tend to adsorb on the oil-water and oil-air interface [35]–[40]. A thick adsorbed layer is spontaneously produced, and thus the drop-drop coalescence is hindered. This strongly stabilized emulsions and foams requires extra effort in further phase separation for petroleum industries. Other constituents of crude oil, such as resins, waxes, and naphthenic acids, are also responsible for the stabilizing mechanism of water-oil emulsion but are not considered for model asphaltene solutions preparation in this study.

2.2.1 Asphaltene molecular structure

The accurate asphaltene molecular structure is still undiscovered owing to its complicity. Among all the competing models proposed, the archipelago and the island model attract the most attention as a description of the molecular structure of asphaltenes. The two model compounds are presented in the figure below.



(a) Archipelago Model Compound
1,4-Bis(2-Pyren-1-yl-thyl)-benzene



(b) Island Model Compound
1,3,6,8-tetradecyl pyrene

Figure 2 - 2: The proposed (a) archipelago, and (b) island model compound for describing the asphaltene molecular structure in previous research [41].

As demonstrated in the figure above, the archipelago model compound consists of a few polycyclic aromatic hydrocarbon (referred to as the PAHs) groups, which are intramolecularly connected by aliphatic chains. As for the island model compound, the aromatic rings are intramolecularly connected to form one polycyclic aromatic hydrocarbon group (a single aromatic core), with peripheral aliphatic side chains. There has been lots of researches on determining the numbers of polycyclic aromatic rings with different experimental techniques, providing a range of 2 to 20 [42]–[48]. And experiments of X-ray scattering [42], [44], fluorescence emission spectroscopy [49], [50], fluorescence depolarization [51] and optical absorption [52] present an average number of less than 10. Ralston and his coworkers also estimated a minimum of four aromatic rings presence in the structure [49]. With the help of scanning tunneling microscopy studies, the average number of aromatic rings is specified to either six or seven [53]. The dominance of the island structure has been proved by laser desorption and mass spectral measurements [54], [55]. Some speculations are made that larger molecular structure are attributed to asphaltenes self-aggregations [34].

The determination of molecular weight also touched off a heated controversy in the history [56] and remains unclear up till today. Concerning that asphaltenes are the heaviest components of crude oils, it is expected that the molecular weight is also high. Experimental techniques have been developed for molecular weight measurements, including neutron scattering (SANS) experiments and small-angle X-ray scattering (SAXS). However, since the concentration of asphaltene solutions utilized is very high, around 10 g/L, asphaltenes self-assemble and the obtained results by these methods are affected [57]–[61]. Advanced techniques are then developed to consider the influence of asphaltene aggregates at high concentration, involving fluorescence correlation spectroscopy [62], [63], mass spectrometry [64], [65], and depolarization [66]–[68]. It has now been widely admitted that asphaltenes exhibits in small molecules with a mean molecular weight of ~ 750 g/mol (Da) [69]–[74].

It is proved by non-aqueous potentiometric titrations of asphaltenes that both acidic and basic functional groups are presented in the asphaltenes molecular structure [75]. This suggests that some asphaltene molecules tend to ionize and then transfer into the water phase at contact. This phenomena is more obvious at high pH, but less at low pH [76].

2.4.2 Asphaltene aggregates

For asphaltenes dissolved into laboratory organic solvents, interactions of asphaltene molecules can lead to a variety of complex structures. Intermolecular attractions mainly occur at the polycyclic aromatic hydrocarbon (PAH) cores located at the center of the molecule. The attraction forces are comprehensive products of various effects, including London dispersion and π - π stacking. Intermolecular repulsion also presence, owing to the steric repulsion forces from the

aliphatic side chains on the molecular exterior. The interfacial behavior of asphaltenes is thus subject to the net force experienced, controlled by the balance of the intermolecular attraction and repulsion [77].

The aggregation process occurs progressively. In the first aggregation process, molecular asphaltene assemble and form nanoaggregates at the critical nanoaggregate concentration of asphaltene (CNAC). And the aggregation number of asphaltenes describes the number of molecules needed in a micelle after reaching the CNAC. The concentration transition from true molecular asphaltene to nanoaggregates is very narrow with small aggregation numbers lower than 10. It is reported by Mullins that asphaltene molecules tend to form nanoaggregates at an aggregation number of six, shaped into a disordered stack of PAHs [78]. The determination of CNAC starts with high-quality (high-Q) ultrasonics experiments, measured by the slope change of sonic velocity versus the concentration. Later, new methodologies for CNAC measurements are developed. The direct current (DC) conductivity technique obtains similar results from high-Q ultrasonics, but sensitive only to a mass fraction at about 10^{-5} of asphaltene molecules [79]. Both NMR measurements and NMR diffusion measurements show the same CNAC value, indicated by a significant variation in hydrogen index [80]. CNAC can also be attained by centrifugation experiments, deducted from a dramatic change in the fraction of the sedimented asphaltene [81]. It should be noted that the CNAC value is subject to both the properties of asphaltenes and the utilized solvent. Additionally, the structure and length of the nanoaggregates can be achieved by SAXS and SANS techniques, by analyzing the absolute cross sections of test results.

In the secondary aggregation progress, at sufficient concentration, nanoaggregates of asphaltenes progressively form into clusters at an aggregation number of eight, with a huge elevation from the CNAC and reaching the critical clustering concentration (CCC) [78]. This flocculation occurring above CCC is controlled by reaction-limited aggregation and loosely bounded into a fractal shape [46], [82]. However, the flocculation induced by heptane addition when the concentration is below CCC is governed by diffusion-limited aggregation [78].

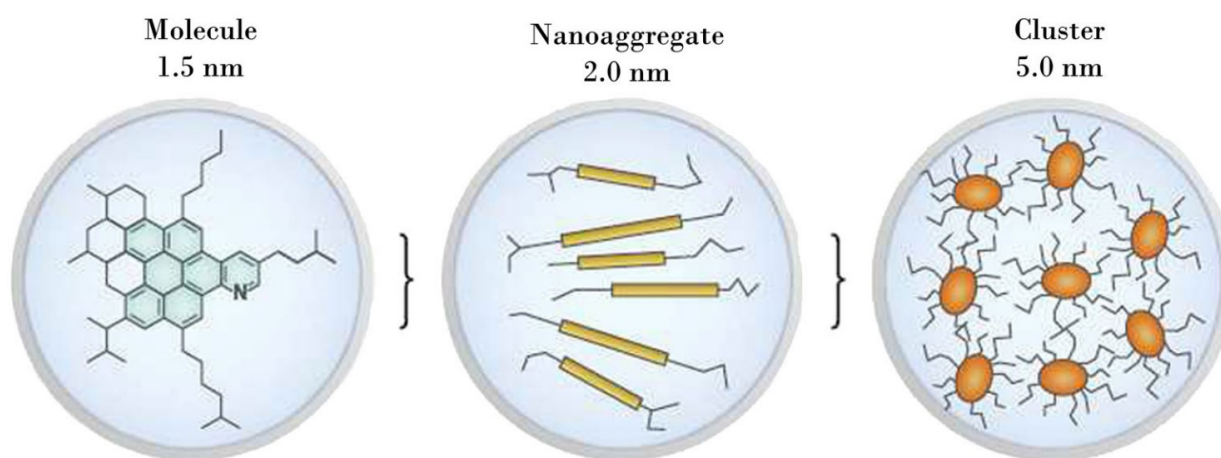


Figure 2 - 3: Schematics of the molecular and nano-colloidal structures of asphaltenes according to the previously reported Yen-Mullins model, or the modified Yen model [83] based on references [78], [84]–[86]. Again, this model suggests the dominance of the island molecular structure.

2.4.3 Adsorption kinetics

The adsorption kinetics of asphaltene is still under debates.

For some surfactants, when the empty sites are fully taken up, the new asphaltene monomers reaching to the crowded interface will return to the bulk, so that back diffusion occurs [87]. But

for asphaltenes, the monomers adsorb onto the interface where there are plenty of unoccupied sites initially. As more and more asphaltene arrive at the interface, the adsorbed layer thickens with longer time [88]. This theory is confirmed by the group of Masliyah that the asphaltene adsorbed at the water/oil interface do not migrate back into the bulk solutions within the experimental time frame of around 1 hour, suggesting that the asphaltene adsorption is irreversible [89].

It is proposed that at short times, the asphaltene adsorption onto the interface starts with a rapid diffusion controlled stage, followed by the progressive buildup of multilayers by redistribution kinetics, proved by the slowly reducing interfacial tension [90]. However, new findings suggest that the later stage is not controlled by either diffusion or redistribution kinetics (relaxation regime), but possibly dominated by adsorption barrier-controlled regime [88].

The adsorption speed is governed by the solubility of asphaltenes, meaning that the quality of solvents utilized for asphaltene solutions preparation matters. Although generally the adsorption process goes slow, even when the bulk concentration of the solution is high. It is observed that with higher concentration, faster adsorption occurs in good asphaltene solvents and slower adsorption happens in poor solvents [88].

The stability of emulsion is also subject to the solubility of asphaltenes. The stability is enhanced as the quality of solvents declines, by the addition of alkane, such as pentane and heptane, into toluene, or temperature reduction [91]. A glassy-rigid and thick interfacial adsorbed layer, due to the formation of clusters, is obtained in the presence of poor solvent. This is supported by the theory that the emulsion stability reaches the maximum when the asphaltene is close to the critical point of precipitation [92]. Only soluble asphaltene molecules tend to adsorb on the interface, while the precipitated asphaltene is not capable of stabilizing emulsions, as proved by Yarranton and his coworker [37].

2.3 Electrocoalescence

In petroleum industry, introducing electric field into the emulsion system to expedite water and oil separation by enhancing drop-drop coalescing, usually referred as electrocoalescence, is of remarkable effect and has been widely adopted at a commercial scale for a long time. The electrocoalescence has gained its popularity not only because the speed of separation is greatly enhanced, but also that electricity serves as a clean energy and no chemical fluids need to be injected into the emulsion [93]. More and more researches are conducted to discover the fundamental aspects of this attractive separation technology and uncover the underlying mechanism of the phenomenon. An emulsion system of water drops suspending in oil under applied electric field is widely studied to mimic the dispersed aqueous phase in crude oil [94].

2.3.1 Electrophoresis and dielectrophoresis

Under DC uniform electric field, a dispersed charged drop or particle exhibits a motion relative to the surrounding liquids, the direction of which depends on the polarity of the charge. This phenomenon is referred as electrophoresis and has showed significant potential in various fields, including biochemistry and molecular biology, and so are widely applied in a lot of advanced technologies.

Additionally, an uncharged particle, no matter deformable or rigid, is also influenced by a net force under non-uniform electric field and tend to move in a certain direction, depending on the electrical properties of both the dispersed particle and the continuous phase [95]. This kind of interaction between particle and electric field is known as dielectrophoresis (DEP). Dielectrophoresis is

widely observed when a conducting drop, such as water, is suspending in a leaky dielectric medium under axisymmetric non-uniform AC electric field[96] and under symmetric non-uniform DC electric field [97]. For two conducting drops placed in a leaky dielectric medium, the dielectrophoretic effect always produce attraction interaction in between [98]. The determination of electrophoresis and dielectrophoresis lies in the uniformity of the electric field or the uniformity caused by irregularities of the electrode surface [99], usually a uniform electric field induces electrophoresis and a non-uniform one induces dielectrophoresis.

2.3.2 Electrohydrodynamic flows

In leaky dielectric system, where exists finite electrical conductivity in the continuous phase, the electrical charges accumulate at the dispersed drop interface and generate an electric stress in both normal and tangential direction to the interface. The tangential component of the electric stress (a shear stress) tends to drag the surrounding fluid in motion and thereby forms circulatory electrohydrodynamic (EHD) flows and hydrodynamic stress in and around the drop interface, as shown in Figure 2-4 below. This circulation driven by electrohydrodynamic stress is a joint action of electric stress and viscous stress (hydrodynamic stress).

However, the EHD flow does not exist in perfect dielectric system, where the continuous phase has zero conductivity and only displacement currents can be produced. Here the electric field induced force acting on the drop interface is always in the normal direction and thus no circulatory

EHD flow can be generated. The EHD flows acting in and around the drop interface can increase the heat and mass transfer [100][101].

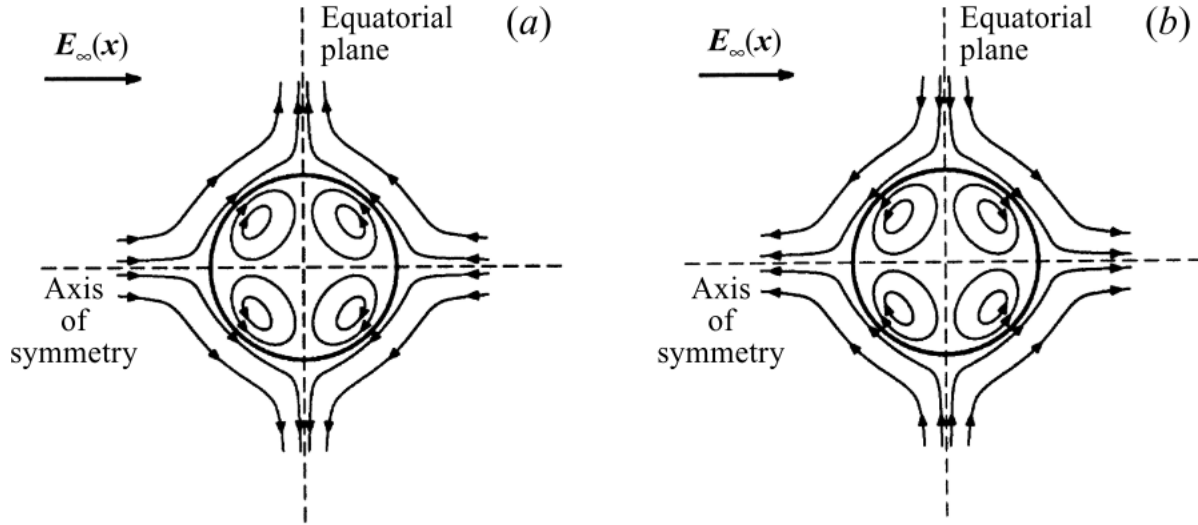


Figure 2 - 4: (a, b) Qualitative simulated electrohydrodynamic flow pattern in and around an isolated drop utilizing the leaky dielectric model [98].

2.3.3 Drop deformation

The dispersed drop deforms in the continuous phase immediately at the onset of electric field application. Understanding the behavior of the dispersed drop in the continuous phase under electric field is of instructional significance in practical applications.

In an ideal situation, where a conducting water drop is immersed in perfect dielectric system, the drop tends to elongate in the direction of the electric field. This is because the geometry of this water drop distorts locally the uniform electric field [102] and the electric stresses induced by the accumulating charges are discontinuous along the interface [103]. Here the electric field induced

force acting on the drop interface is always perpendicular to the interface (in normal direction) and points from a fluid with higher electrical permittivity to the one with lower electrical permittivity [102]. And due to dielectrophoretic effect in the water drop along the electric field line, the water drop should be deforming towards oil and elongating into a prolate shape in the direction of the electric field.

However, the continuous phase is usually a leaky dielectric system and the deformation is much more complicated. The induced electric stress caused by the accumulation of electric charges on the interface can be decoupled into normal and tangential electric stress. The tangential component of the electric stress (a shear stress) has the potential to drive the fluid into circulation both in and outside of the drop and triggers the hydrodynamic stress [104]. And the normal component of the electric stress and the viscous stress account for the drop deformation. Therefore, when gravity is not considered (drop free-floating), the isolated water droplet can deform into not only a prolate shape, as predicted by the electro-hydrostatic theory for perfect dielectric system, but also an oblate shape or even no deformation. The type and degree of deformation is controlled by the coupling effect of normal electric stress, and viscous stress [105]. The leaky dielectric model brought up by Taylor (1966) [104] has been widely used in forecasting the electrohydrodynamic deformation.

An upper limit of applied electric field strength exists, above which, water drops disintegration (drop break-up) occurs and the electric field assists electro-emulsification, instead of electro-coalescence. As the electric field strength raises, the dispersed drop is lengthened in the direction of electric field until the static force experienced can no longer remain equilibrium, above which the drop tend to disintegrate [106]. Smaller drops tend to deform less and can bear stronger electric field before showing instability than bigger drops.

The corresponding mechanism of deformation type and eventual break-up is very complicated, controlled by many related parameters. Apart from the strength of the electric field applied, the uniformity of electric field around the drop and the orientation and position of drops placed in the electric field also matter. Moreover, the local electrohydrodynamic flow circulation pattern along the interface, and the relative physical and electrical properties, involving viscosity, density, flow rate, interfacial tension, conductivity and permittivity, also exert tremendous influence [107]. Generally, higher electrical conductivity and permittivity in the continuous phase produce greater influence on the deformation of the dispersed phase, attributed to the accumulating charges and the induced electric stress on the interface. It is also suggested that drop instability (drop break-up) occurs when the major axis of the drop and the minor one is at a ratio of 1.9, for aqueous drops with a diameter of 1.2 mm [108].

For a multi-drop system under applied electric field, the two neighboring drops display more complicated deformation, which is controlled by the electro-capillary number, also known as the electrical Weber number, given as [109]:

$$C_{aE} = \varepsilon_m a E_0^2 / \gamma \quad \text{Eq. 2-1}$$

When the electro-capillary number is large, the whole drop shows deformation into either a prolate or oblate shape. When the electro-capillary number is small, only the leading poles (the inner-faces) of the two coalescing drops would deform. This phenomenon is attributed to the higher magnitude of electric field in between the two drops (explained later) and the subsequent electrical charges build up at both leading poles of the two drops.

2.3.4 Fundamentals of electrocoalescence

It has been approved that the coalescence of water droplets in oil without electric field goes through a process of drop approaching, film drainage (or film thinning), film rupture and coalescing. When electric field is involved, the mechanisms become more complicated due to the induced dielectrophoretic force. The EHD flow currents is generated by EHD stresses in the emulsion system and the strength of this currents depends on the applied electric field. This circulatory current may interact or counteract with the dielectrophoretic effect, depending on the distance between the two neighboring drops as indicated before [98]. Assume two neighboring drops are placed closely to each other. When the strength of the applied electric field is high, strong flow currents are generated and drop breakup phenomena can be triggered, leading to electro-emulsification. However, when low electric field is introduced into the emulsion system, moderate EHD flow currents benefit drop-drop interaction and result in electro-coalescence [110].

In the expose of electric field, the uncharged water drop becomes polarized and acts as a dipole and moves closer to the other dipoles in the vicinity due to dipole-dipole attraction. In such a multi-drop system with at least two neighboring water drops interacting with each other, the electric field experienced by one droplet is disturbed by the presence of other droplets in the neighborhood, leading to an addition of non-uniform electric field between the drops. Therefore, the magnitude of the electric field in between is always much higher than that of the external electric field applied [111]. As the two drops approaching under attraction, the continuous fluids in between are drained from between and give rise to film thinning. This drainage rate is balanced by many surface forces, including Van der Waals attraction and double-layer repulsion. Additionally, the film drainage is also governed by the deformation of coalescing drops triggered by the electric field. The geometry of the drops makes a tremendous contribution to the resistance of coalescence. The film radius of

a planar film can be the same as drop radius, which is relatively large and requires longer drainage time before coalescing. Nevertheless, drop shape deforms in the direction of electric field, due to the elevation of electric stresses on the approaching side, and exhibits conical-shaped at the inner faces, as presented in the figure below.

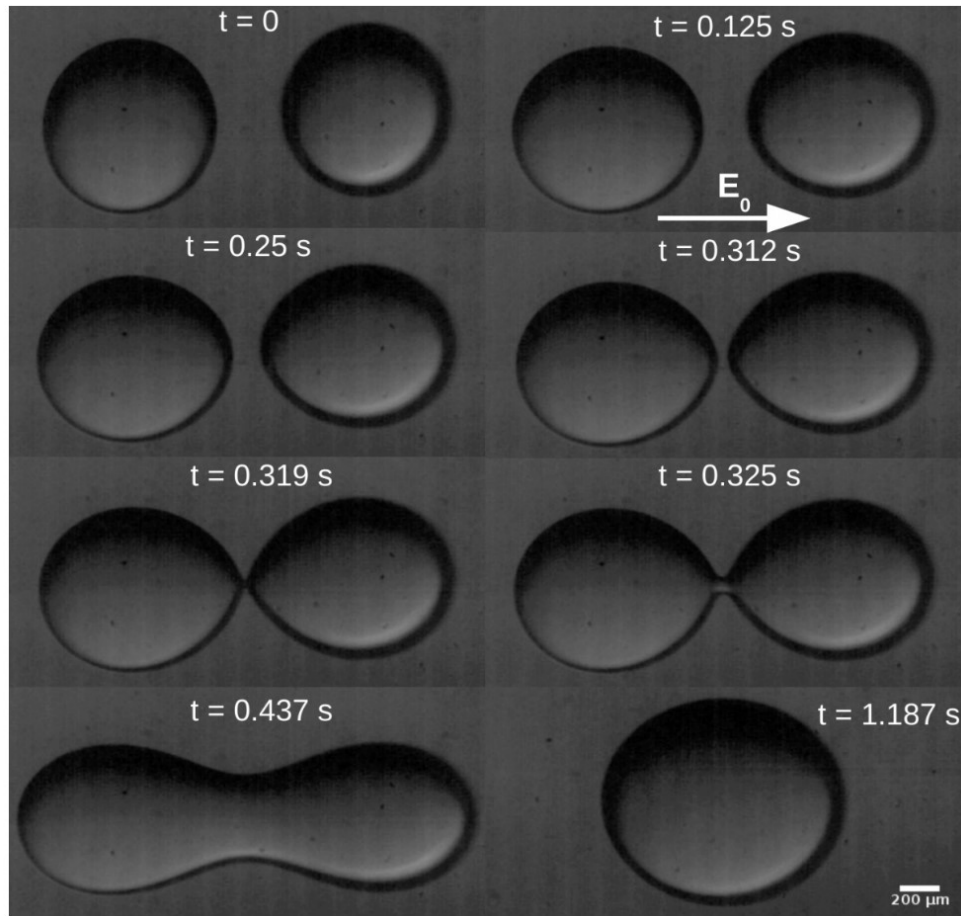


Figure 2 - 5: A drop pair of glycerol-water (containing 10% glycerol) coalescing in silicone oil under external uniform DC electric field at 250 kV/m [93].

This conical shape reduces the radius to a great extent and lowers down the resistance to film drainage [112]. After drop-drop contacting, when the film thickness is subsequently reduced to a

minimum, upon which, the film ruptures and results in coalescing. There are circumstances that the minimum film thickness is not obtained, and the drops retreat instead of coalescing, attributed to the abrupt electrical charge exchange and redistribution at contact [113].

Chapter 3 Experimental Techniques

3.1 Pendant drop tensiometry

To characterize the stability of water-in-oil emulsions under external applied electric field and to understand the underlying mechanism of electro-coalescence, this study focuses on the interfacial properties of the asphaltene films with pendant drop tensiometry.

For pendant drop tensiometry, there are mainly two ways of measuring the interfacial tension, either by analyzing the drop profile, or monitoring the capillary pressure. The first one is usually referred as the drop profile tensiometry (DPT), and the latter one as capillary pressure tensiometry (CPT). Both of these two means comply with the Laplace equation, describing the relationships between the pressure jump across the interface, the interface curvature and the interfacial tension [114].

3.1.1 DPT: Drop profile tensiometry

The drop profile tensiometry, also referred as the axisymmetric drop shape analysis (ADSA), or drop shape analysis (DSA), has numerous advantages. Only a small volume of dispersed phase is needed for generating a pendant drop. Measurements can be conducted on either liquid-air or liquid-liquid interface, including pure solvents and concentrated solutions. Drop profile tensiometry is widely used for interfacial tension measurements and is originally brought up by

Neumann and his coworkers [115], based on fitting the real experimental drop profile with the Young-Laplace equation [116].

In drop profile tensiometry, usually the monitored pendant drops are relatively bigger than the ones in the capillary pressure tensiometry for accurate drop edge detection. Because the applicability of this method relies on a large drop sufficiently deformed by gravity [117], [118]. A curved interface induced by the capillary pressure inside the drop plays a key role. The curvature changes along the interface and thus the local pressure jump can be inferred by the drop profile.

3.1.2 CPT: Capillary pressure tensiometry

In capillary pressure tensiometry, a relatively smaller drop is used compared to the one in drop profile tensiometry. This enables a nearly spherical or hemispherical shaped pendant drop, eliminating the effect of hydrostatic pressure effect and maintaining the curvature at any point on the interface at a constant value along the interface. A thinner capillary is coupled with the capillary pressure tensiometry to enhance the pressure signal for better accuracy, directly extracted by a pressure transducer. By knowing the pressure inside the pendant drop, namely the capillary pressure, the analyzing procedure is greatly simplified as the only parameter left to determine is the curvature [119]. Therefore, the CPT method is especially appropriate when a complicated mechanism is acting on the interface, such as the coupled effect of electric field-induced force and gravity in this research. On such a complex interface, the interfacial tension itself is not reliable enough to describe the dynamically varying interfacial properties, especially when a considerably big deviation may exist in shape fitting from the Laplacian one.

3.2 Interfacial tension measurement

The interfacial tension measurements of water/oil interface are carried out with pendant drop tensiometry on Theta Optical Tensiometer and One Attension software (Biolin Scientific, Finland). The pendant water drop is suspending from a glass capillary immersed in model oil. When mechanical equilibrium is reached, the drop can be considered as a static drop, fully deformed by only gravity and interfacial tension, where the Young-Laplace equation is applicable for inferring the interfacial tension. The drop profile data can be extracted as stated in numerous studies, and advanced technologies allow edge detection to be done automatically by programmed software. The drop shape is fitted to the Young-Laplace equation to determine the interfacial tension.

3.2.1 Shape factor

The tensiometer can analyze the experimental drop profile dynamically, and generate many variables describing the drop profile, including the shape factor, the radius at apex, the volume, the drop height, the tilt, etc. The shape factor, or the gravitational Bond number, is one of the most important variables. The shape deformation induced by gravity, the only form of external force acting on the drop, is correlated with the interfacial tension by the shape factor.

The shape factor is defined as these three first order differential equation, [120] the variables in which are described in figure 3-1:

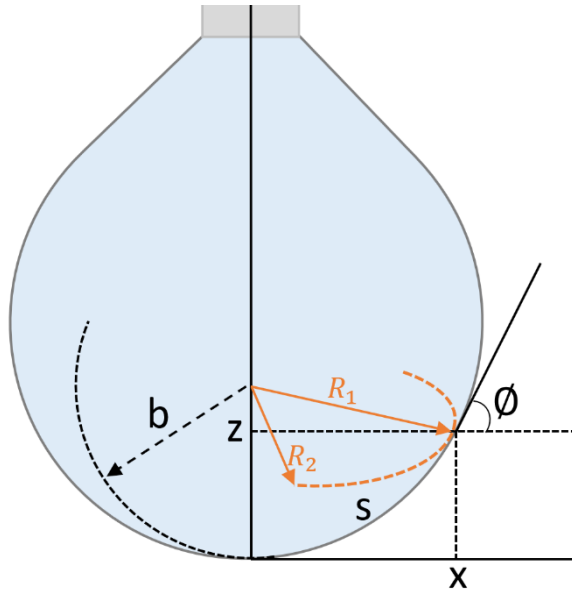


Figure 3 - 1: Schematic and variables of a theoretical drop profile for fitting with an experimental pendant drop image.

$$\frac{dx}{ds} = \cos\emptyset \quad \text{Eq. 3-1}$$

$$\frac{dz}{ds} = \sin\emptyset \quad \text{Eq. 3-2}$$

$$\frac{d\emptyset}{ds} = 2 + \beta z - \frac{\sin\emptyset}{x} \quad \text{Eq. 3-3}$$

In which, if the drop apex is considered as the reference point, s , x and z respectively represents the arc length, the radial and vertical coordinates from any point on the interface to the reference point. ϕ stands for the tangential angle.

3.2.2 Correlation of shape factor and interfacial tension

The Young-Laplace equation is applicable, describing the relationship of drop curvature, pressure difference across the interface and the interfacial tension.

$$\gamma \left(\frac{1}{R_1} + \frac{1}{R_2} \right) = \Delta P_0 - \Delta \rho g z \quad \text{Eq. 3-4}$$

Where γ and $\Delta \rho$ stand for the interfacial tension and density difference of the dispersed phase and continuous phase, R_1 and R_2 are the principle radii of drop curvature, as shown in Figure 3-1. ΔP_0 represents the pressure difference at drop apex, g for the gravitational acceleration and z for the vertical coordinates of a local point on the interface.

Therefore, at the drop apex,

$$R_1 = R_2 = b \quad \text{Eq. 3-5}$$

$$\Delta P_0 = 2\gamma/b \quad \text{Eq. 3-6}$$

Where b denotes the radius of curvature at drop apex.

The principle radii of the interface can also be written as a function of the variables in the theoretical profile:

$$\frac{1}{R_1} = \frac{d\phi}{ds} \quad \text{Eq. 3-7}$$

$$\frac{1}{R_2} = \frac{\sin\phi}{x} \quad \text{Eq. 3-8}$$

Therefore, the interfacial tension is correlated with the shape factor by the equation below.

$$\beta = \Delta\rho g b^2 / \gamma \quad \text{Eq. 3-9}$$

The shape factor estimates the degree of shape deformation caused only by gravity. However, when electric field is applied to the emulsion system, the external force acting on the suspending drop is not only limited to gravity, but also electric-induced force. Therefore, in this circumstance, the Eq.3-9 is no longer applicable for interfacial tension calculation. The apparent interfacial tension generated from the One Attension software is not reliable.

3.3 Dilatational rheology measurement by oscillating drop method

To analyze the viscoelasticity and dynamic properties of the adsorbed layer at water/oil interface, either shear rheology or dilatational rheology measurements can be conducted. Dilatation rheology establishes a relevancy from the kinetic process of surfactants transportation to the formation of an adsorbed layer. And the subsequent intermolecular reaction of adsorbed molecules counteracts against the applied strain to the interface, promoting the elastic behavior of interface and hindering drop-drop coalescence [121], [122]. Although the drop profile tensiometry (DPT) is applicable mainly for a drop with constant interfacial area or at slow variation rate to maintain mechanical equilibrium. The DPT, coupled with an harmonic oscillating drop methodology at low frequency

and low amplitude, has become a popular way of analyzing the dynamic characteristics of the adsorbed film and its dilatational rheology. [123]–[125]

3.3.1 Principle of oscillating drop method

By amplifying the potentialities of drop profile tensiometry, the advancing technologies and instrumentations allow the visco-elasticity of water / oil interface be measured with an oscillating drop method. A controlled periodic perturbation is introduced into the program so that the drop can be expanded and compressed following a certain pattern. This applied external perturbation initiates variation in drop surface area, and sequentially the interfacial tension response to the perturbation at the same frequency with a certain phase shift. Every time an extra dilatational stress operates on shape deformation, relaxation process involving diffusion and surfactants rearrangement occur. If the adsorbed film presence purely elastic behavior, the phase shift will be 0, meaning that there is no delay in interfacial tension responding to the external perturbation. Thus, the dilatational stress acting on the interface is proportional to the area variation. Whereas if the adsorbed film presence viscous characteristics due to relaxation, the complex dilatational viscoelasticity should be expressed as

$$E = \frac{\Delta\gamma}{\Delta A/A_0} = E_0 + iE_1 \quad \text{Eq. 3-10}$$

$$\Delta\gamma = \gamma(t) - \gamma_0 \quad \text{Eq. 3-11}$$

$$\Delta A = A(t) - A_0 \quad \text{Eq. 3-12}$$

Where E is the complex visco-elastic modulus, E_0 and E_1 is the real and imaginary part of the elastic modulus, respectively. $\Delta\gamma$ stands for the variation in interfacial tension, with $\gamma(t)$ stands

for the interfacial tension at time t within a cycle and γ_0 as the initial interfacial tension. $\Delta A/A_0$ represents the relative variation in interfacial area, where ΔA corresponds to the difference of $A(t)$ at time t and A_0 the initial interfacial area. The complex visco-elastic modulus is composed of a real part and an imaginary part, the dilatational viscosity modulus. The dilatational elasticity modulus represents the elasticity of the interface, also referred as the storage modulus. The dilatational viscosity modulus relates to the viscosity of the adsorbed films, referred as the loss modulus. Commercial and laboratory tensiometers can extract digital information on amplitudes of interfacial area, variations of interfacial tension and the phase shift as a function of pre-determined frequency, via Discrete Fourier Transform algorithms [126].

Pendant drop remaining at mechanical equilibrium is crucially important for data accuracy.

3.3.2 Applicability limits

Applicability limits in frequency and amplitude do exist when DPT is used in dilatational rheology measurement with oscillating drop method. Applying a periodic oscillation below frequency and amplitude upper-limits serve as the prerequisite, ensuring the pendant drop to remain at mechanical equilibrium state and presenting a Laplacian drop profile.

In terms of pendant drop tensiometry characteristics and tensiometer capabilities, the large time scale in each experiment can cover a wide range of frequency selections for dilatational rheology measurements. However, the frequency limits are subject to the occurrence of non-radial oscillations or other fluidynamic effects [127]. A faster oscillation, namely a higher frequency, would give rise to shape distortion, caused by viscous forces and drop normal oscillation modes [128][129]. It has been studied in water-air system that DPT with oscillating drop method is

capable for analyzing the dilatational rheology at a maximum of 1 Hz [130]. For an even higher frequency, an alternative solutions including capillary waves damping methods need to be applied[131]. However, this frequency threshold vary qualitatively with drop size, surfactant solutions concentration and viscosity[127]. Compared to a water-air system, viscosity of liquid-liquid interface is generally higher, resulting in an even lower frequency limit, around 0.1 Hz, for DPT applications[114]. The viscous effect from the adsorbed layer can introduce an estimation error in interfacial tension, as the dynamically changing interfacial tension during drop deformation is calculated based on the static Young-Laplace equation.

An amplitude threshold also lies in DPT with oscillation drop method, exceeding which, a significant variation in the interfacial area may affect data accuracy. Usually the amplitude is controlled below 10 % of the pendant drop volume[130].

3.4 Crumpling ratio measurement

As the surfactants adsorbed onto the liquid-liquid interface accumulates, the surface coverage and thickness of the adsorbed layer increases. Crumpling of the adsorbed layer can be observed visually when the water drop area is decreased greatly, achieved in this study by retracting the inside water at a constant speed back into the glass capillary. Upon further compression, the adsorbed film starts to crumple, and some vertical wrinkle-like lines appears on the interface. This critical point right before crumpling occurs, is usually referred as the crumpling point. The ratio of the projected area of water pendant drop at crumpling point to the initial projected area is defined as the crumpling ratio and presented as below.

$$CR = \frac{A_c}{A_0} \quad \text{Eq. 3-13}$$

In which, CR is the abbreviation of crumpling ratio, A_c is the projected area of pendant water drop at crumpling point, and A_0 stands for the initial projected area. In this study, the projected direction is chosen as the top view. Thus, the calculation of crumpling ratio can be simplified as the square of the ratio of the drop diameter at crumpling point to the initial drop diameter, regarding the projected area of the water drop as circle in the direction of top view. The equation is written as:

$$CR = \frac{\pi r'^2}{\pi r_0^2} = \left(\frac{d_c}{d_0}\right)^2 \quad \text{Eq. 3-14}$$

In which, r' and d_c are the radius and diameter at crumpling point, respectively. r_0 and d_0 are the initial radius and diameter. The diameter of the drop is detected with MATLAB coding, defined as the widest part of the drop when it is in exactly vertical position.

The crumpling is observed at the onset of layer collapse when reaching the a maximum of surface coverage [71]. Therefore, the crumpling ratio represents the amount of irreversibly adsorbed asphaltenes layer and its rigidity. A more rigid and consolidated film hinders water bridging and water-water coalescing. It is also found by the group of Yarranton that the crumpling ratio correlates well with the elastic compression modulus[22].

Chapter 4 Experimental Setup and Procedure

4.1 Materials

4.1.1 Preparation of asphaltenes

Asphaltenes are the heaviest components of crude oil with very high molecular weight, which always exist in oil recovery and form stable emulsions leading to difficulties in water-oil separation afterwards. In this research, to mimic the water-oil interface in actual oil industry, asphaltenes are extracted from the Athabasca coker feed bitumen (provided by Syncrude Canada Ltd.). This solids-free asphaltenes serve as the surfactant in the water-in-oil emulsion system. Due to the insoluble nature of asphaltenes in paraffinic solvent, n-pentane is used to precipitate the asphaltenes from bitumen.

20 g of bitumen was mixed with 800 g n-pentane at a bitumen-to-pentane mass ratio of 1:40 in a 1 L glass bottle with Teflon cap. The mixture was well shaken in a shaker for 2 hours and left overnight for asphaltene precipitation and settling. The supernatant was collected as much as possible before another 800 g of fresh n-pentane was added to the settled phase. The new mixture was well shaken for 2 hours and left stand overnight for further asphaltene precipitation before the supernatant was collected again. This process was repeated around 15 times until the collected supernatant is almost colorless. The settled phase is then mixed with n-pentane and equilibrium for 30 mins before separated by vacuum filtration. A Whatman filter paper of grade 50 is placed on top of the Buchner funnel and wetted with n-heptane to ensure best sealing. After several times of filtration, the permeability of the filter paper decreases and new filter paper is placed for better

seepage rate. Thus, the precipitated phase is washed by n-pentane and separated by vacuum filtration a few times until the dripping solvent through the filter paper is colorless. The precipitates is then collected from the filter paper carefully and dissolved into toluene at a precipitates-to-toluene mass ratio of 1:20. To remove the solids, the mixture is shaken for 20 mins and divided equally into Teflon tubes for centrifuge. For machine protection and safety, the weight difference of each pair of tubes was controlled within 0.01 g. The solutions were centrifuged at 20,000 g for 20 mins and transferred from the tubes into rotary evaporation apparatus. The temperature of water-bath is set to 60 degree Celsius to remove the toluene from the solution. The asphaltenes separate out and clings to the glass wall, which then was placed in the film hood for 3 days before chipped out. Liquid nitrogen could also be used in this step for easier collection and a desiccator should be used to remove any condensed water from the collected asphaltene.

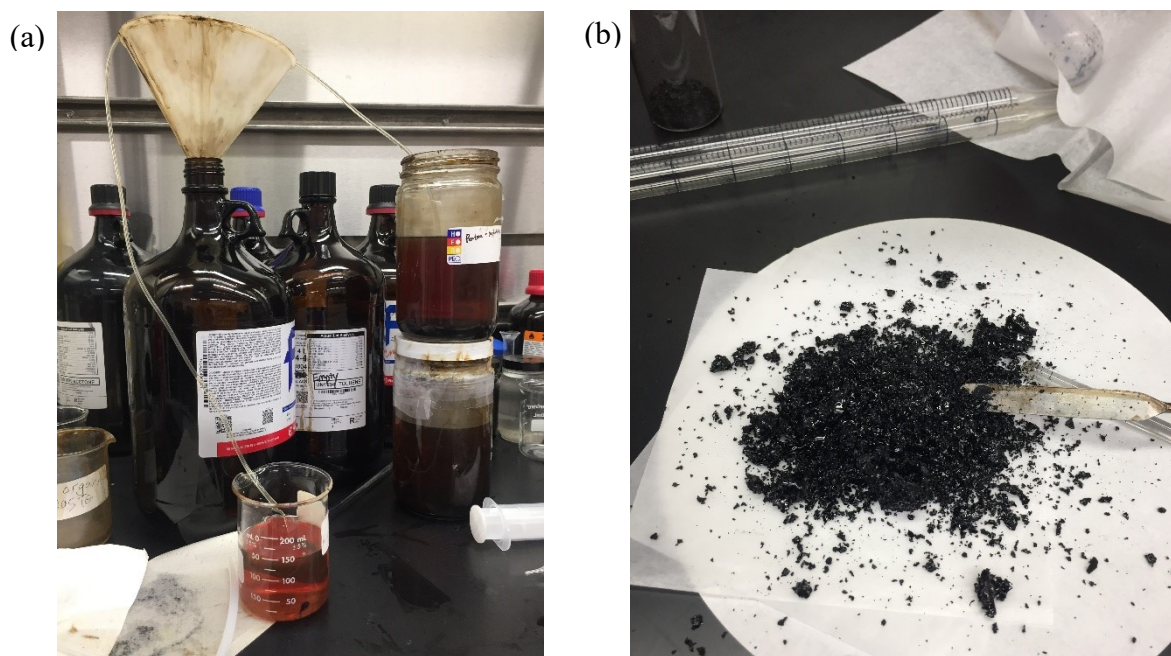


Figure 4 - 1: (a) Supernatant collection based on siphon principle, and (b) the fully dried precipitated asphaltenes ready to use in model oil preparation.

4.1.2 Model oil

To study the effect of electric field on the adsorbed asphaltene layer on water/oil interface, a simplified version of oil containing asphaltenes as the only surfactant was used throughout this study, i.e. the model oil. The n-pentane-extracted asphaltenes were dissolved in 50/50 heptol (a mixture of heptane and toluene at a volume ratio of 1:1) to produce the model oil phase. The asphaltenes were always added to toluene first and well-shaken until totally dissolved before the addition of heptane. The concentration of the model oil was generally 0.05 g/L for most experiments but varied when studying the effect of asphaltene concentration on water-in-oil emulsion.

This model oil was considered as a leaky dielectric medium in this research. The volume of model oil used for each experiment was 28 mL, where the top electrode was submerged, and a capacitor created. To eliminate the change in model oil concentration and properties induced by solvent evaporation, especially toluene, this model oil was made freshly every day for experiments, always well shaken prior to use and disposed after each use to maintain freshness.

4.1.3 Water phase

The water phase involved in most of the experiments was deionized water. When studying the effect of salt type and concentration, NaCl_2 and CaCl_2 was added to the deionized water at various concentrations, respectively. When studying the effect of water phase pH, buffer solution of pH 4, pH 7 and pH 10 was used as water phase compared with deionized water at pH 6.

4.2 Instrumentation

4.2.1 High voltage power supply

The electric field is generated by Spellman high voltage power supply, which operates from 115 - 220V single phase AC line. The DC output voltage and current are continuously adjustable from zero to a maximum of 20kV via two front panel ten-turn locking potentiometers (turn counter-clockwise for unlocking). Voltage and current can also be read from two digital meters, with current meters showing percentage of 500mA and voltage meters presenting in kilovolts unit. A circuit breaker, HV ON switch and HV OFF switch are also on the front panel. An input cable is permanently attached to the power supply and can be connected to AC line. A removable shielded high voltage output cable is provided and can be easily removed from the mating receptacle on the rear of the supply. The polarity of the Spellman high voltage power supply can be reversed internally, which involves changing the multiplier section for one of the opposite polarities. And the high voltage power supply used in this study does come with a negative multiplier.

Although by turning the ten-turn locking potentiometer at the front panel, the voltage applied to the electrodes can be adjusted, whereas the ramp speed and the target voltage cannot be precisely controlled manually. Therefore, an external program is planted into the power supply system, allowing easier adjustment of the applied voltage. For increasing the applied voltage, simply inputting the desired voltage in the column of “Ramp To: (kV)” and ramp speed in the column of “Ramp Rate: V/sec” in the software. However, the ramp speed cannot be controlled by the software while decreasing the applied voltage and it always declines rather slowly.

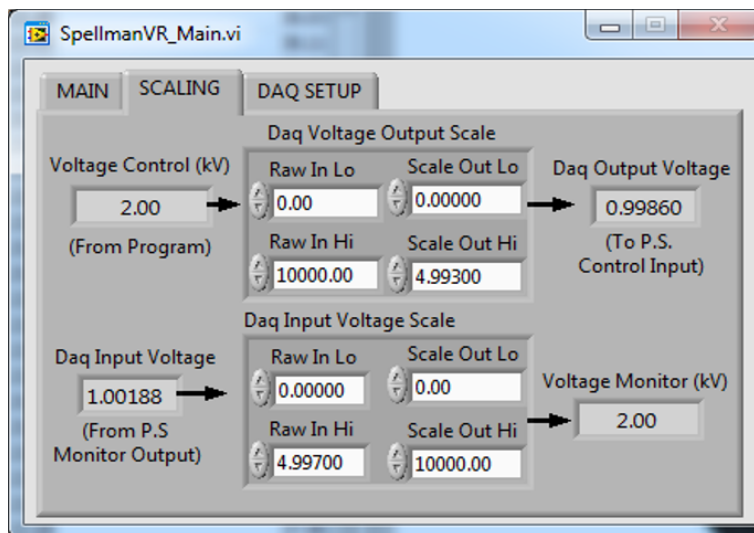
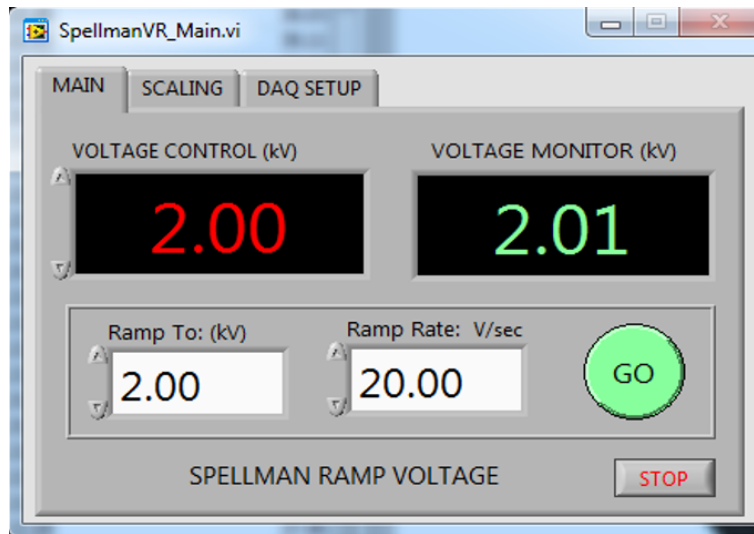


Figure 4 - 2: Example of external software program operation in controlling the applied voltage. The desired voltage is set to 2 kV and the output voltage is also 2 kV as shown in the window of “VOLTAGE MONIOR (kV)”.

4.2.2 Copper electrodes

Two square-shaped flat copper plates, 3.2 cm in side length, are placed in parallel with four 2 cm Teflon columns sandwiched in between at each corner to create a chamber, which is connected by eight Nylon screws. The round hole, sizing 3 mm in diameter, drilled at the center of the top copper plate, allows a glass capillary to go through and suspends a water droplet at the tip. Pictures of this copper electrode and how it is applied during experiments is presented as below.

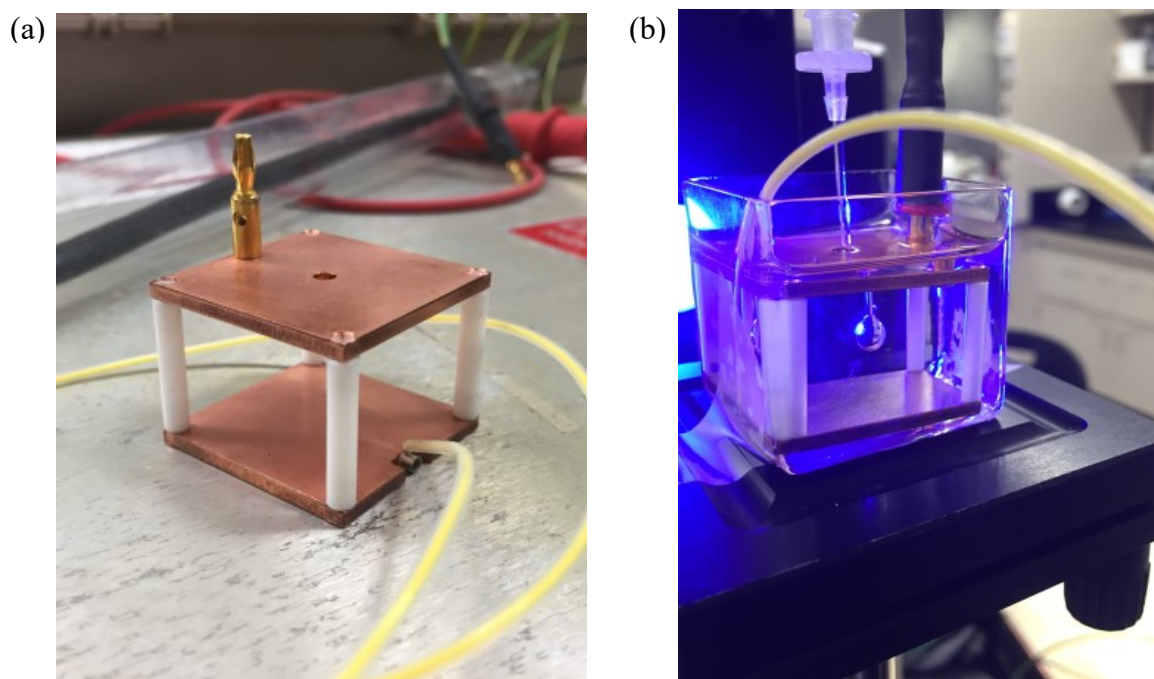
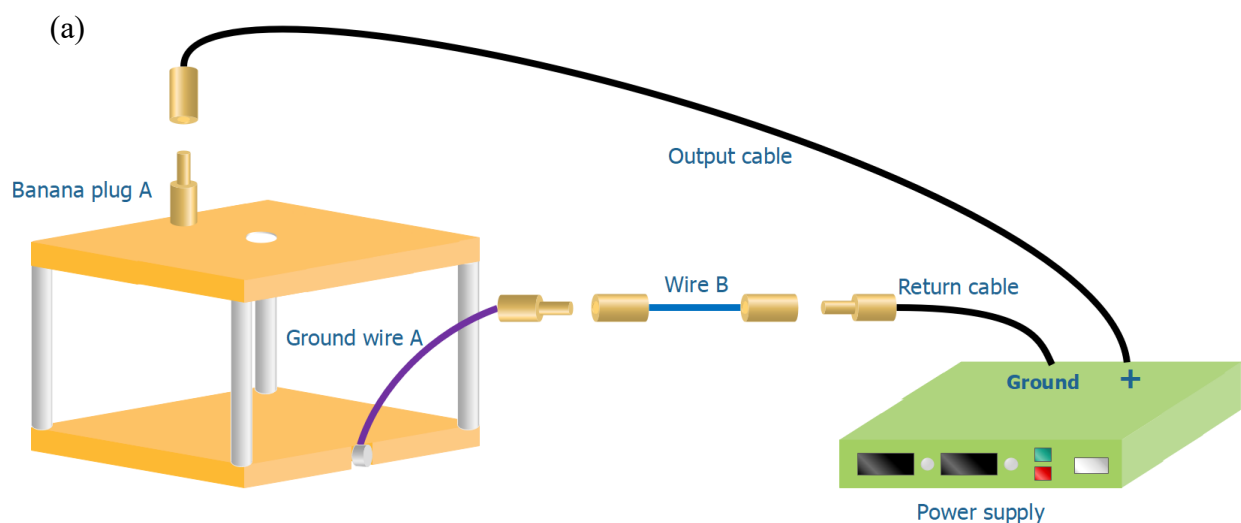


Figure 4 - 3: Pictures of (a) the copper electrodes with banana pin on top and wire connection at the bottom and (b) its application in electric field involved experiments.

Several sets of banana connectors are applied in the electrodes design, each consisting a banana plug (usually referred to the male) and a banana socket (usually referred to the female). The banana

plug A is screwed onto the top plate for connection with the high voltage output cable and the power supply. To ensure a constant distance everywhere between the two plates, the back nuts of the banana plug A is made of Teflon. The notch-out design on one side of the bottom plate allows connection with ground wire A to the bottom plate by screwing it firmly onto the metal bolts. For laboratory safety, ground wire A is typically designed to handle a maximum voltage of 20 kV and is covered with a layer of Teflon outer sheath.

Although the polarity can be reversed internally as mentioned before, exchanging the connection of the leads is much more practical and convenient. To be able to switch the polarity of the two electrodes, another wire B with a banana socket on each side is included in the design. When wire B connects the ground wire A with the return cable, the top electrode is positively charged and the bottom one is grounded, as shown in Figure 4-4(a). When wire B connects the banana plug A with the return cable, the bottom electrode is positively charged and the top one is grounded, as in Figure 4-4(b).



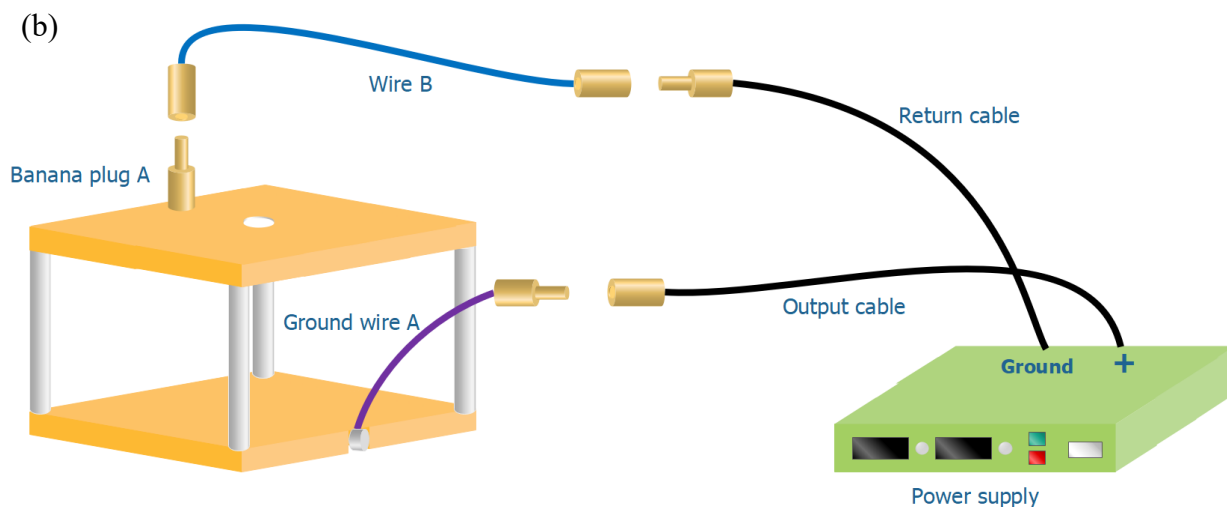


Figure 4 - 4: Schematic pictures of wire connections to reverse the electrode polarity. The top electrode is (a) positively charged, and (b) grounded.

4.2.3 Syringe and needle

Stainless-steel flat needles are widely used in pendant drop tensiometry. However, in the case of electric field involved experiments, stainless-steel flat needles could influence the electric field. Additionally, it is extremely dangerous when the syringe is filled with water or even salted water in some cases. Therefore, in this research, the syringes and needles used are all made of glass and plastic for laboratory safety.

In the pendant drop experiments, the needle is composed of a glass capillary and polypropylene hose barb. The glass capillary and a micrometer syringe are connected by a long and soft plastic tubing. The glass capillary goes through a plastic syringe for stabilization, then clamped by the liquid dispense holder on the Tensiometer. All connection parts are firmly twined with Teflon tapes and parafilm papers to ensure better airtightness control.

In the oscillating drop experiments, the needle is made by joining the tip of the polypropylene hose barb with glass capillary. For stabilization and airtightness concern, they are connected by a small cut of thick plastic tube and layers of Teflon tapes as outer sheath. The needle is then screwed onto the automatic oscillating pump clamped by the liquid dispense holder.

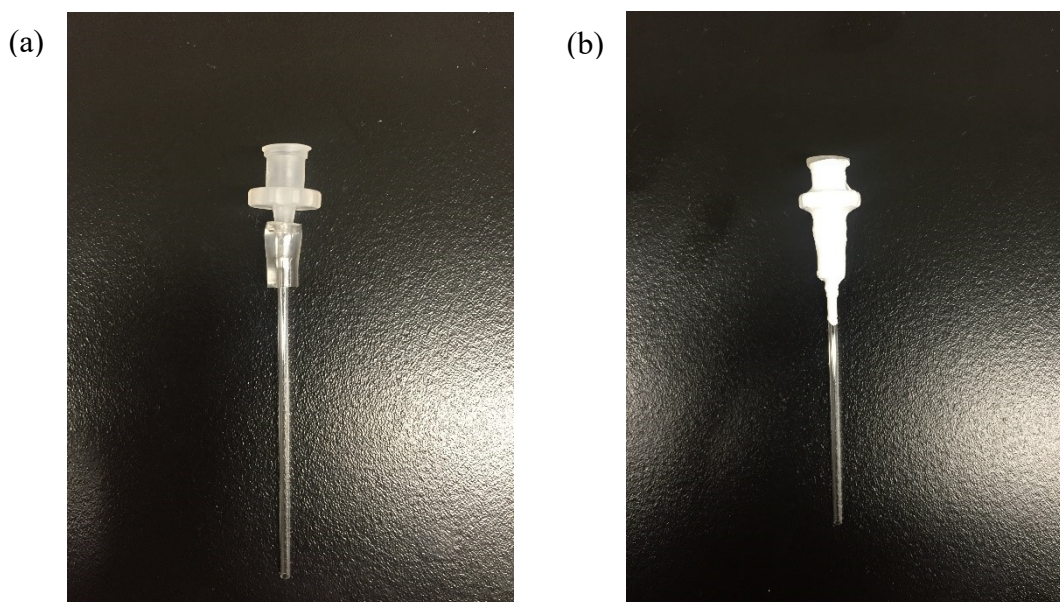


Figure 4 - 5: Images of (a) connection of the hose barb and the glass capillary, and (b) Teflon tape wrapping on the outside.

4.2.4 Glass cell

In pendant drop tensiometry, the cell needs to be transparent and do not react with the continuous phase filled inside it. In this research, the continuous phase to be studied are organic liquids containing toluene, which would react with most plastic materials. Therefore, a cube-shaped glass

cell is used here, with a side length of 3.5 cm. The copper electrodes can fit into this glass cell as well.

4.2.5 Schematic of setup

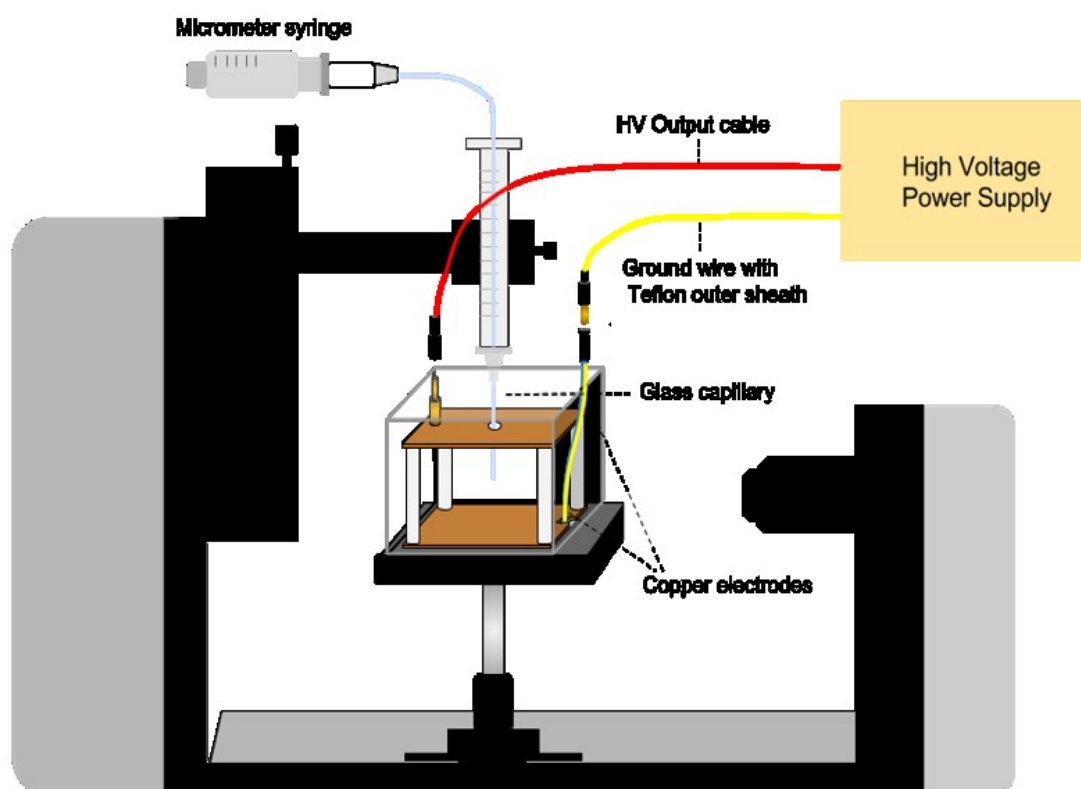


Figure 4 - 6: Schematic of experimental setup for interfacial tension and crumpling ratio measurement (an automatic liquid dispenser is used in dilatational rheology measurement).

The schematic of setup is as shown in the figure. The glass capillary, immobilized by a plastic syringe, is immersed into the model oil phase contained in a transparent glass cell. The water droplet is released from the tip of the inverted capillary and remained vertically. The electric field is applied vertically through the copper electrodes. The water drop shape under electric field is analyzed dynamically by the Theta Optical Tensiometer and the parameters are automatically calculated by the One Attension software.

4.3 Experimental Procedure

4.3.1 Interfacial tension measurement by pendant drop tensiometry

The experiment starts by choosing the “Pendant drop experiment” icon. Experimental parameters were inputted in the recipe sheet, including light phase materials, heavy phase materials, image recording frame rate, analysis mode and total duration. For the light phase material, the density is input as 0.771 kg/m^3 and the heavy phase material is water, selected from the database. Frame rate is 0.6 FPS (frame per second). The total duration is set to 2500 seconds to cover 40 mins of aging time.

The syringe is filled with measured liquid and firmly clamp it onto the liquid dispenser. The glass cell is filled with model oil and placed onto the sample stage. The copper electrodes are immersed into the model oil and connected with the power supply. The sample stage is adjusted to an appropriate level, where the tip of the glass capillary reaches the center of the electrode gap. A water drop is generated in a size of 22 μL . Then, camera parameter and lens focus are adjusted

until the image quality is satisfactory. After recording starts, a target voltage to the electrodes at a ramp speed of 0.4 kV/s is applied and the water drop is aged for 40 minutes. The electric field is removed after the recording stops. The experimental data is collected using automatic baseline. Additional information of shape factor (Y-L β) and drop radius (Y-L r) from the Column selection drop down menu is selected. The image of water drop is saved from the last frame recorded.

4.3.2 Crumpling ratio measurement and calculation

The experiment starts by choosing the “Pendant drop experiment” icon. Experimental parameters are input in the recipe sheet. Light phase material is heptol and the density is set to 0.771 kg/m³. The heavy phase is selected as water from the database.

The syringe is filled with measured liquid and held onto the liquid dispenser. The copper electrodes are placed inside the glass cell and filled with model oil until the top electrode is immersed. The electrodes are connected to the high voltage power supply. The sample stage is raised up to which level that the tip of the glass capillary reaches the gap center. A water drop is released by screwing in the microliter syringe, sizing 22 μ L. Camera parameters and lens focus are adjusted so that a clear image of the drop can be obtained.

The first part of the experiment is water drop aging. The frame rate per second is set to 0.6 FPS and duration time lasts 2400 seconds. A certain voltage is applied to the emulsion system. When recording stops, the recording speed is altered to 30 FPS when the electric field is still on for precisely capturing the initial shape image and the crumpling point. Water is retracted back into the micrometer syringe slowly at a steady speed until vertical wrinkles are observed at the drop interface. The data is collected from the crumpling process with automatic baseline. The images

are observed frame by frame, until the one with wrinkles on the interface is found. The image before wrinkles form and the initial image before water retraction are saved. The above two images are import into MATLAB separately to analyze the diameters of the drop. Assuming that the projected area of the drop from above is round-shaped, the projected area is calculated with drop diameter and an area ratio is obtained as the crumpling ratio.

4.3.3 Dilatational rheology measurement by pendant drop tensiometry

To measure the dilatational rheology, a piezo-pump enclosed in a chamber and an automatic single liquid dispenser should be used.

The experiment starts by choosing the Pulsating drop experiment icon. Experimental details are input in the recipe sheet (materials, densities, frame rate information already given in chapter 4.3.1). Drop out size is set to 22 μL , frequency at 0.1 Hz, amplitude at 0.5 μL and sinusoidal waveform selected. 22 measurement points are set for each experiment, with 10 seconds of waiting time, 10 cycles and 10 seconds of oscillation for each cycle. The total length of experiment is around 2420 seconds, covering 40 minutes of aging time. The glass cell, the solution, electrodes and wire connections are put in place. The camera lens focus are adjusted until a clear drop profile shows on screen. Recording starts and the oscillation begins according to the experimental settings listed above.

After 40 minutes, the 22 measured points are analyzed to get all calculated results. Oscillating drop analysis are carried out for each measured point and the elastic modulus E' is gained. The E' is plot sequentially from the first measured point to the last one as a function of time. The average value

from the last few points represent the elasticity of the studied asphaltene skin on water / model oil interface.

4.3.4 Calibration

Lab experiments always begin with calibration first, to ensure data accuracy. For Theta Optical Tensiometer and One Attension software, the calibration is done with a calibration ball. First, the tensiometer and the software is turned on, and logged in with username and password. An experiment type is chosen from either “sessile drop”, “pendant drop” or “pulsating drop” icon in the instrument home tab. The “Camera Parameters” icon allows adjusting the camera settings automatically or manually if needed. Then, the calibration ball should be placed onto a magnetic holder and put together onto the sample stage, the level of which can be adjusted until an image of the calibration ball shows up on the screen. Lens zoom and lens focus are adjusted appropriately between the camera and the calibration ball. The actual diameter of the calibration ball is 4 mm and is known on the system. By clicking on “Calibration invalid” icon, the diameter of the ball is linked with the image pixels accurately and thus the calibration process is complete.

After calibration with the calibration ball, the interfacial tension of water / air interface is always tested to be at 72.5 mN/m before experiments begin, to ensure data accuracy and DI water purity.

4.3.5 Repeatability

The data presented in this research are based on at least 3 successive parallel measurements under the same conditions, to verify the results. The correlation of each set of results in interfacial tension

and crumpling ratio measurements is high, whereas the repeatability of dilatational rheology results is relatively low.

Chapter 5 Results and Discussion

5.1 Shape evolution of pendant water drop

In pendant drop tensiometry, the equilibrium drop shape of the drop is crucially important as further interfacial properties measurements are based on the shape-fitting. A smooth drop shape is advantageous to the curve fitting accuracy, whereas the fitted shape of an intensely flattened (oblate) or elongated (prolate) drop would lead to a significant amount of deviation. In a normal pendant drop experiment of an aqueous drop immersed in an immiscible liquid, the shape of the drop is balanced by gravity and interfacial tension only. However, when a suspended water drop is exposed to an applied external electric field, extra drop deformation occurs as a result of the non-uniform electric field induced Maxwell stress. To gain a better understanding of drop deformation and an optimum drop shape for curve-fitting, a few physical variables have been tested and are presented in this chapter.

5.1.1 Electric-induced deformation type

In the presence of an external electric field, a conducting drop, immersed in perfect dielectric system (an ideal system), tends to elongate in the direction of the electric field. This is because the geometry of this water drop distorts an originally uniform electric field [102] and the electric stresses induced by the accumulating charges are discontinuous along the interface [103]. Here the electric field induced force acting on the drop interface is always perpendicular to the interface (in normal direction) and points from a fluid with higher electrical permittivity to the one with lower electrical permittivity [102]. This means that for a water-in-oil emulsion system, this electric-induced force is pointing from the dispersed phase of water to the continuous phase of oil. And due to dielectrophoretic effect in the water drop along the electric field line, the water drop should be deforming towards oil and tend to elongate in the direction of the electric field. However, the emulsion is a leaky dielectric system in reality, so the deformation is much more complicated due to the existence of a tangential electric stress and the induced EHD flow. The dispersed drop tends to deform into not only a prolate shape, as predicted by the electro-hydrostatic theory above, but also an oblate shape or even no deformation, depending on the joint action of electric stress, viscous stress, hydrodynamic stress and gravity, etc.



(a) Original drop at 0 kV/m



(b) Elongated drop at 100 kV/m



(c) Flattened drop at 100 kV/m

Figure 5 - 1: Shape comparison of pendant water drops suspending in model oils of the same concentration at (a) 0 kV/m and (b) 100 kV/m (c) 100 kV/m.

In this research, an elongated drop (a prolate shape) is observed in model oil solutions. However, occasionally, the suspended water drops tend to flatten (an oblate shape) at the onset of electric field, in pure solvent system, such as heptane and toluene. Apart from the joint action of mechanical stresses, another reason could be that the water drop is suspending from a glass capillary. The glass capillary could be dielectric polarized as it comes through the central hole of the top charged electrode and attracts the water drop from above. A possible way to eliminate polarization would be Teflon-coating the glass capillary.

Usually, under an applied external electric field, a flattening drop exhibits lower shape factor and higher apparent interfacial tension values (the results directly calculated by the software according to Eq.3-9) than that of the initial status without the electric field. Whereas, an elongated drop exhibits higher shape factor and lower apparent interfacial tension values. However, this apparent interfacial tension values calculated by One Attension software is not the real interfacial tension. Details on this is presented in Chapter 5.2.

5.1.2 Deformation with step-wise electric field application

The moment the electric field is applied, the water drop deforms immediately. For simplification, a pure solvent system is used as the continuous phase in this part, allowing shorter time to reach equilibrium since no surfactant exists in the continuous phase.

In the case of drop flattening, a set of experimental images of a water drop suspending in heptane system is presented as below. A water drop, sizing 35 μL , is released from the glass capillary tip at 0 kV/m (without electric field) and given 10 minutes to reach an equilibrium shape. Then increase the applied voltage to 25 kV/m, 50 kV/m, 75 kV/m, 100 kV/m, 125 kV/m, 150 kV/m, 175 kV/m, 200 kV/m, and 225 kV/m stepwise for 1 minute at each stage. It is observed that as the applied voltage increases, the released water droplet flattens in the direction of electric field. Higher the electric field strength, bigger the deformation. When a critical value is reached, the droplet will deform so drastically that the shape can no longer be fitted to the Young-Laplace equation and a considerable deviation lies in the measured apparent interfacial tension. If applying an even higher voltage then the critical value, the droplet will eventually detach from the capillary and move to the top electrode. An upper limit exists where an extremely high voltage tends to break up the water drop into multiple small droplets. This break-up phenomenon leads to water-oil emulsification and it is not studied in this research.

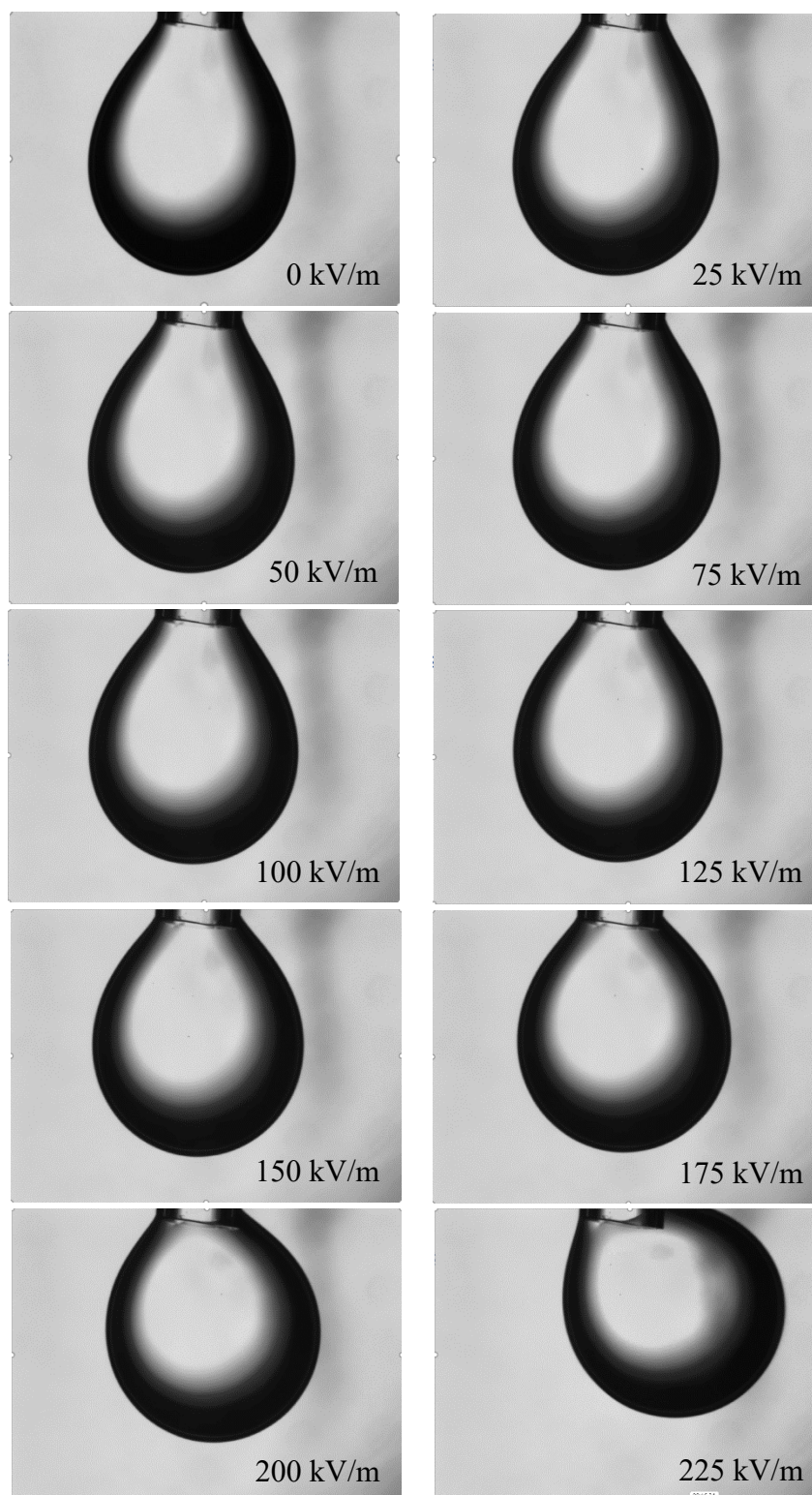


Figure 5 - 2: Drop deformation under increased electric field until detachment.

In the case of drop stretching, the deformation and detach process is very similar. As the applied voltage increases, the degree of deformation raises up. Exceeding a critical voltage, no accurate shape-fitting can be achieved, and the drop tend to detach from the capillary towards the bottom electrode.

For both stretching drops and flattening drops, if the electric field is removed before drop detach, the drop regains the initial shape and the apparent interfacial tension bounce back to the initial value at equilibrium.

5.1.3 System reversibility

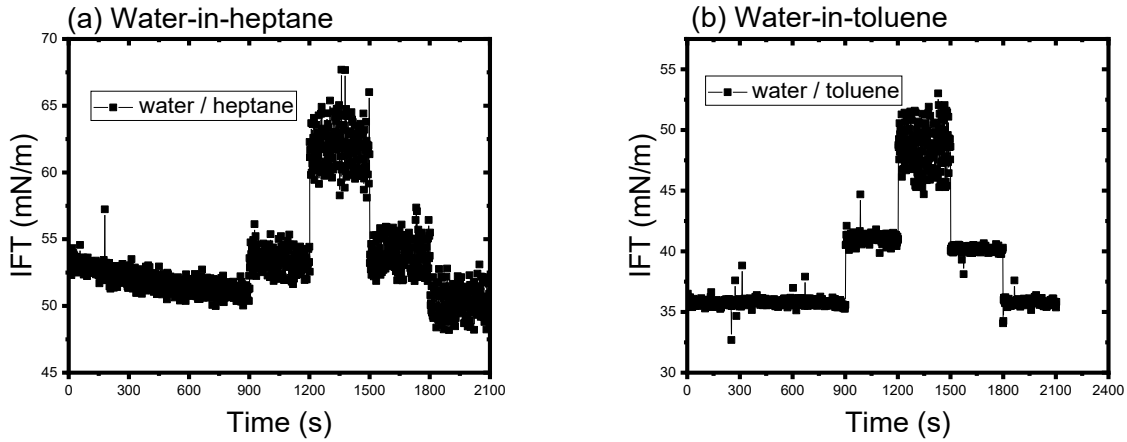


Figure 5 - 3: Interfacial tension variation after aging the water drop at 0 kV/m for 15 minutes, followed by altering the applied voltage to 50 kV/m, 100 kV/m, 50 kV/m and 0 kV/m for 5 minutes at each stage for (a) water-in-heptane emulsion system, and (b) water-in-toluene emulsion system.

For pure solvent system, such as water-in-heptane and water-in-toluene, the shape deformation is reversible. Results in the above figure show that the higher the electric field strength, the bigger the shape deformation. Also, the apparent IFT value (the drop shape) remains the same at the same electric field strength.

However, the real interfacial tension of water and heptane interface should remain constant since no surfactants exist in the continuous phase. And the obtained varied interfacial tension is due to shape deformation affected by the electric-induced force. Therefore, these data indicate that when electric field is involved, extra electric-induced deformation exists. So, the Young-Laplace equation needs to be modified and new methods of calculating the real interfacial tension need to be developed to remove the effect of electric-induced deformation.

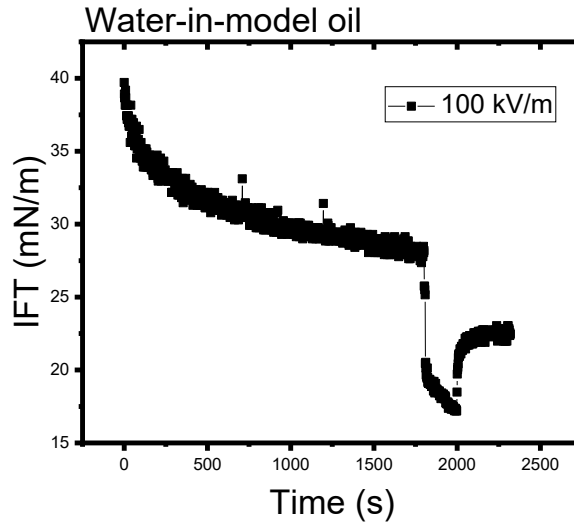


Figure 5 - 4: Interfacial tension variation for water-in-model oil emulsion system. The water drop is aged at 0 kV/m for 30 minutes, followed by applying electric field at 100 kV/m for 3 minutes and then back to 0 kV/m.

Whereas in surfactant system, such as a water-in-model oil system that contains asphaltenes, the IFT after 3 minutes of electric field application is much lower than the original IFT. It is suggested that during electric field application, more surfactants are adsorbed onto the interface, leading to a lower IFT. Therefore, both drop shape and surfactant adsorption are affected by electric field application in surfactant system.

5.1.4 Effect of electric field direction and drop position

The polarity of the electrodes can be reversed as elucidated in Chapter 4.2.2. The direction of electric field can thus be altered in the same orientation as of gravity or the opposite, referred as downwards and upwards, respectively. Various drop positions are also tested under electric field in distinct direction with a deionized water-in-model oil system. A pendant water drop suspending in a position closer to the bottom electrode is referred to as the low position, and a position closer to the top electrode is referred to as the high position accordingly. If the tip of the glass capillary ends up at the center of the electrode gap, the position where the water drop is placed is considered as the middle position. The combined effect of electric field direction and drop position in between the electrode gap is presented in the following.

A table of results is listed as in Table 5-1.

Table 5 - 1: The effect of electric field direction and drop position on drop deformation and the range of voltage applied.

		Field direction - downwards		Field direction - upwards	
		Voltage range, kV/m	Type of deformation	Voltage range, kV/m	Type of deformation
Drop position	Low	0 to 50	Stretch	0 to 50	Stretch
	Medium	0 to 100	Flatten	0 to 100	Stretch
	High	0 to 150	Slightly stretch	0 to 150	Slightly stretch

For a water-in-model oil system, asphaltenes adsorb onto the interface and the polar groups are polarized and stressed by the electric field. In this case, the interface is negatively charged. If the electric field is in the same orientation as of gravity, the type of deformation is determined by the balance of gravity and electric-induced force in distinct direction. If the electric field is applied in the different direction as of gravity, both electric-induced force and the gravity are pointing downwards.

It is indicated that at low positions, the water drop is attracted to the bottom electrode considerably and stretches, whatever direction of electrode is applied. The maximum electric field strength that can be applied is only 50 kV/m, exceeding which, water drop detaches from the glass capillary. For water drops suspending at high positions, the maximum electric field strength is higher, because the glass capillary provides the water drop with support and prevent it from detaching. A flattened drop is observed if the electric field is applied downwards, since the attraction from the top electrode is much stronger than gravity. A stretched drop is observed if applying the e-field

upwards, as both gravity and electric-induced force are pointing downwards. For water drops placed at middle position, an even wider range of applied voltage can be achieved. The electric-induced force and gravity are in a balance and maintain the drop shape to be only slightly stretching, benefiting experiments by forming a stabilized pendant drop.

Experiments have shown that for extensively elongating drops, they tend to detach from the capillary during aging, which is not preferable during experiments.



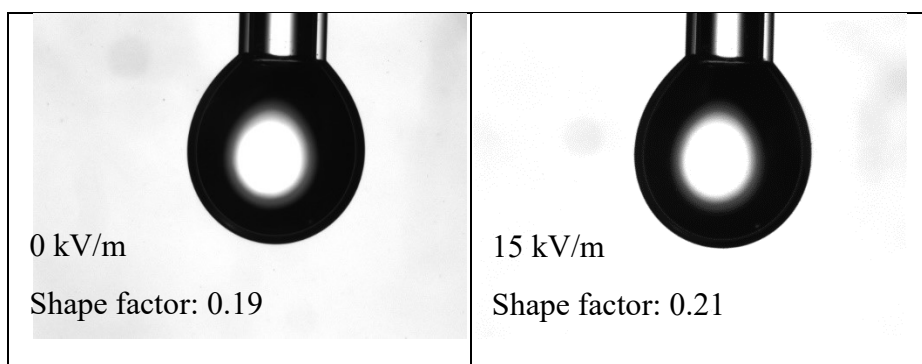
Figure 5 - 5: Pendant water drop suspending in model oil tends to detach from the glass capillary during 40 minutes of aging time, when the direction of electric field is opposite to gravity.

Therefore, in this study, the top electrode is always positively charged and the bottom one grounded, leading to an electric field pointing downwards.

5.2 Effect of electric field strength

5.2.1 Applicability limits of interfacial tension measurement in electric fields

The interfacial tension measurements of water/oil interface are carried out with pendant drop tensiometry on Theta Optical Tensiometer and One Attension software, based on Young-Laplace equation. When a pendant drop is fully deformed by the coupled effect of interfacial tension and gravity, the interfacial measurements can be easily achieved by fitting the drop profile to the Laplacian shape. However, the Young-Laplace equation is applicable for calculating the interfacial tension when a drop is deformed only by gravity and interfacial tension. Under the effect of electric field, the shape of the pendant drop is balanced by the interfacial tension and external forces, such as gravity and electric field induced force. Therefore, in this case, the apparent interfacial tension obtained by the programmed software is not the real interfacial tension.



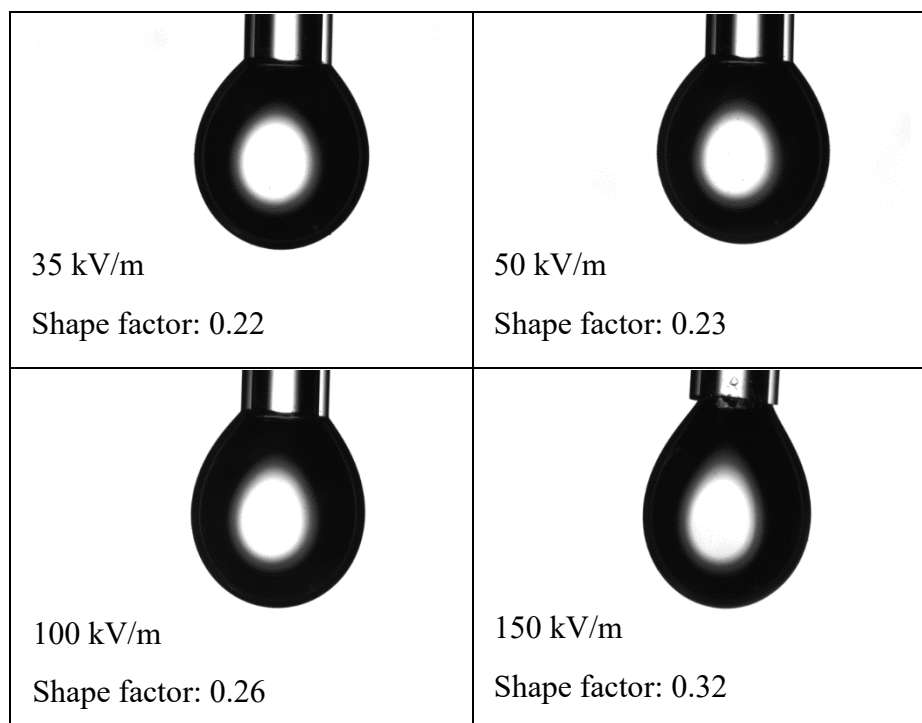


Figure 5 - 6: Examples of drop image and the corresponding shape factor for a water-in-0.05 g/L model oil system after 40 mins aging under various electric field strength.

As shown in Figure 5-6, water drops appear different shapes with and without electric field. A higher shape factor is observed under higher electric field strength, implying lower interfacial tension since the interfacial tension is inversely correlated with the shape factor. No precise conclusion can be reached on whether this reduction in the interfacial tension is caused by surfactants adsorption on the interface or by shape deformation due to electric-induced force, or both. This applicability limit is also implied in Figure 5-3, where the apparent interfacial tension varies with electric field for pure solvent system. But in fact, the real interfacial tension should stay at a constant value, as no surfactant exists in the pure solvent system.

The Young-Laplace equation is used for fitting the captured drop image, based on which an equation for linking the shape factor to the interfacial tension is derived and programmed in the calculating software:

$$\beta = \Delta\rho gb^2/\gamma \quad \text{Eq. 5-1}$$

Detail steps on derivation of this equation is presented in Chapter 3.2. However, the Young-Laplace equation need to be modified considering the electrical pressure jump induced by the Maxwell stress acting on the drop interface [132].

$$\gamma \left(\frac{1}{R_1} + \frac{1}{R_2} \right) = \Delta P_0 + \Delta\rho gz + \Delta P_e \quad \text{Eq. 5-2}$$

Where γ and $\Delta\rho$ stand for the interfacial tension and density difference of the dispersed phase and continuous phase, R_1 and R_2 are the principle radii of drop curvature, as shown in Figure 3-1. ΔP_0 represents the pressure difference at drop apex, g for the gravitational acceleration and z for the vertical coordinates of a local point on the interface. ΔP_e is the electrical pressure jump and is defined as [132]:

$$\Delta P_e = \frac{1}{2} [\epsilon^a E_n^a{}^2 - \epsilon^b E_n^b{}^2 + (\epsilon^b - \epsilon^a) E_t^2] \quad \text{Eq. 5-3}$$

In which, superscripts a and b represents the continuous phase (the model oil) and the dispersed phase (the water), respectively. ϵ is the permittivity of the liquid, E_n and E_t are the normal and tangential component of the electric field, respectively. If the water is considered as a conducting liquid, then the equation above can also be simplified since there is no electric field in the water phase and the electric field is normally distributed on the interface[132]. The equation is given by:

$$\Delta P_e = \frac{1}{2} \epsilon^a E_n^a{}^2 \quad \text{Eq. 5-4}$$

In the pursuit of the real interfacial tension, electric field simulation needs to be conducted as the normal component of the electric field varies along the interface. The simulation and stress-fitting in this field is very complicated and still requires further improvements. Therefore, the numerical method of obtaining the real interfacial tension is not included in this study.

5.2.2 Effect of electric field on the interfacial tension

As mentioned before, when the electric field is involved, there is extra shape deformation induced by the Maxwell stress acting on the drop interface, which causes a significant error in estimating the shape factor from the drop profile and calculating the interfacial tension. The automatically calculated interfacial tension by the One Attension software is no longer reliable. To obtain the real interfacial tension, new methods need to be developed. This part of research comes up with a potential experimental method for acquiring the real interfacial tension, by shutting off the power supply at the end of a 40 minutes aging to remove the effect of electric field on drop shape.

The shape deformation does occur rapidly the moment the electric field is applied. However, when the electric field is removed, the extra deformation induced by the electric field is eliminated rather slowly. This process of regaining the real drop shape at equilibrium is known as the relaxation period, where the adsorbed surfactant rearranges on the interface. It normally takes up to 20 minutes of relaxation time to finally reach a steady state, where the interfacial tension acquired can be considered as the real interfacial tension. Plots of electric field application and removal process is presented as below.

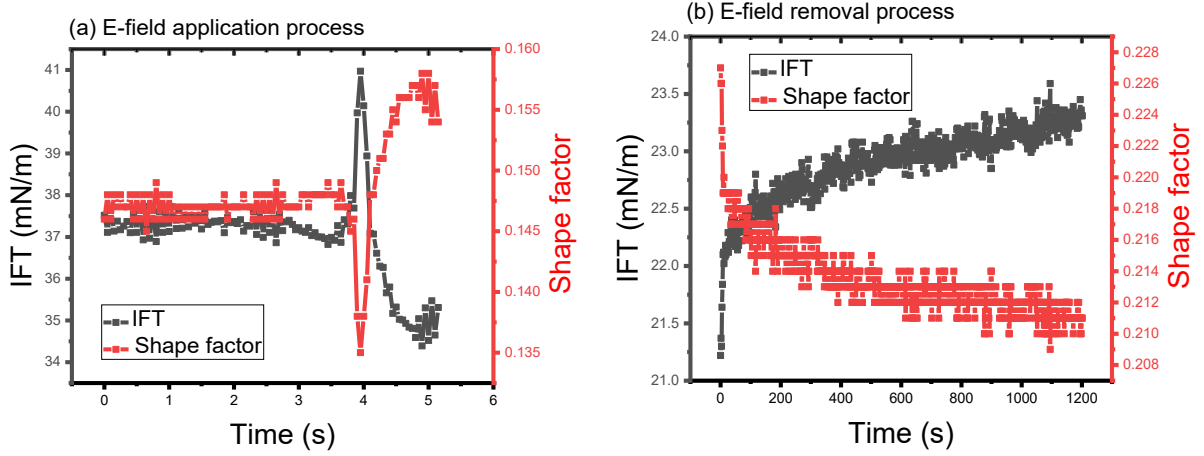


Figure 5 - 7: Variation trend of interfacial tension and shape factor of a water/model oil interface at (a) electric field application process, and (b) electric field removal process.

This experimental method is based on the assumption that the asphaltene films formed on water/oil interface is irreversibly adsorbed, which is supported by papers[133][134][25]. Also, during the relatively long relaxation time, the extra asphaltene adsorption onto the interface is not considered. This assumption is reasonable as the adsorption rate is much lower without electric field, compared to when there is one. And the asphaltene surface coverage of the interface is already very high after 40 minutes of aging under electric field, leaving less sites for new asphaltene adsorption. Figure 5-8 demonstrates that the amount of asphaltene adsorption without electric field in the last 20 minutes is very low, indicated by a slightly and negligibly decreasing interfacial tension.

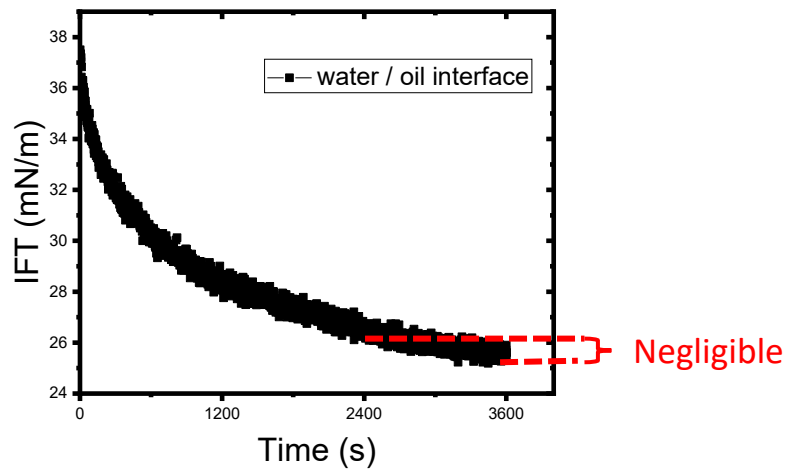


Figure 5 - 8: The interfacial tension of water/oil interface at 0 kV/m and aged for 60 minutes.

Therefore, although the interfacial tension acquired tend to be slightly lower than the real interfacial tension, it still can be considered as the real interfacial tension. A plot of interfacial tension variation during a set of power off testing under distinct electric field strength is presented as below.

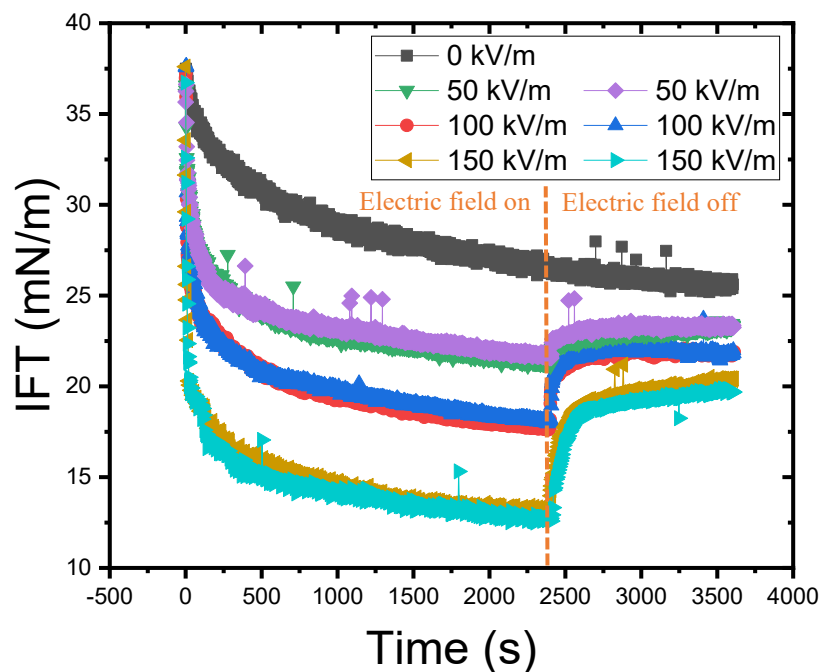


Figure 5 - 9: The interfacial tension of a water/model oil interface aged for 40 minutes under electric field and relaxed for 20 minutes without electric field.

It is indicated in the figure that when the electric field is applied during aging, there is a significant jump in interfacial tension from aging stage to relaxing stage at the onset of electric field removal. And the real interfacial tension obtained after relaxation is still much lower than the one at 0 kV/m. The higher the electric field strength, the lower the interfacial tension. Also, the interfacial tension reduction from 0 kV/m to 50 kV/m is considerably bigger than the ones from 50 kV/m to 100 kV/m and from 100 kV/m to 150 kV/m. These results are consistent with the crumpling ratio results under various electric field strength stated in Chapter 5.3.1. These results imply that

asphaltene adsorption is enhanced under the effect of electric field, giving rise to more asphaltenes adsorbed at the interface. This jump in asphaltene adsorption is significantly bigger at low electric field application (< 50 kV/m) than high electric field (> 50 kV/m).

It is also noteworthy that the bigger the shape deformation, the longer time needed to relax back to the real equilibrium shape. Therefore, this potential experimental method is only suitable when the applied voltage is not very high.

Here we summarize the average value of the real average interfacial tension at each electric field strength, denoted as γ_{real} , the shape factor obtained after 40 minutes of aging under applied voltage, denoted as β_{on} , and the shape factor obtained after relaxation without the electric field for 20 minutes, denoted as β_{off} . The jump of shape factor from β_{on} to β_{off} is denoted as $\Delta\beta$. These variables are listed below as a function of applied electric field strength in the Table 5-2.

Table 5 - 2: A summary of power off testing on γ_{real} , β_{on} , β_{off} and $\Delta\beta$ under different electric field strength.

		γ_{real} , mN/m	β_{on}	β_{off}	$\Delta\beta$
<i>Electric field strength, kV/m</i>	0	25.61	0.192	0.196	0.004
	50	23.28	0.225	0.209	- 0.016
	100	22.04	0.257	0.221	- 0.036
	150	20.06	0.323	0.251	-0.072

The jump of shape factor, $\Delta\beta$, listed in the above table once again implies that the stronger the electric field strength, the bigger shape deformation from the real equilibrium shape when electric field is removed. Even if there is a considerable reduction in shape factor, accordingly a huge jump in interfacial tension, when the electric field is removed, the final shape factor β_{off} with applied electric field is still higher than the one without. These findings infer that the shape factor can be used as a prefigurative tool in the acquisition of interfacial tension variation trend under different electric field. The higher the measured shape factor, indicating the lower the real interfacial tension.

5.2.3 Effect of electric field on the shape factor

The shape factor is measured in this part of the study as an implication of drop shape, not considering the effect of electric field on shape deformation. Obviously, the calculation based on this shape factor does not lead to the exact value of interfacial tension, but still provides enough information on the relative magnitude of the interfacial tension under the same electric field strength. In this part of the study, the β_{on} is called the shape factor for simplicity, referring to the measured shape factor after 40 minutes of aging while the electric field is on.

The effect of electric field strength is tested with deionized water in model oil emulsion system under 5 stages of applied electric field, at 0, 35, 50, 100 and 150 kV/m respectively. The water drop is aged for 40 minutes to ensure sufficient asphaltene adsorption. At least three parallel experiments are conducted at each stage of electric field, and the average value of the dynamically changing interfacial tension is plotted as a function of time in the figure below.

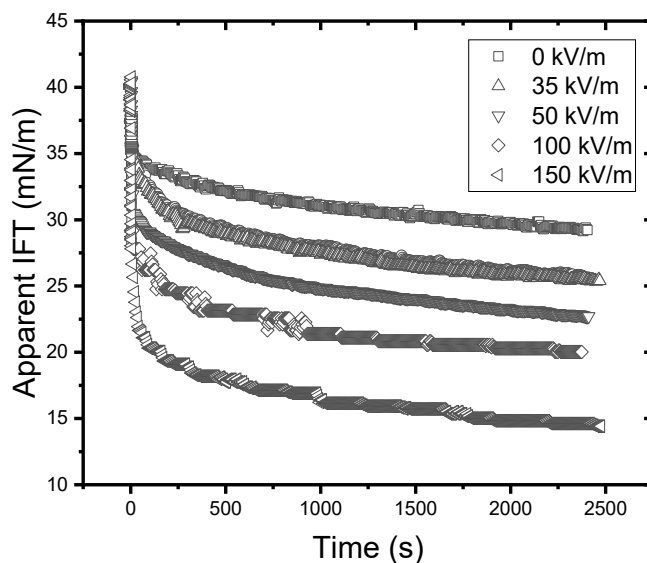


Figure 5 - 10: Variation trend of the interfacial tension as a function of time for a water-in-model oil system aged for 40 minutes under various electric field strength.

It is clearly suggested in the figure that the interfacial tension is changing as a function of time under electric field. The interfacial tension reduces drastically within the first 10 seconds due to a sharp shape deformation induced by the Maxwell stress on the interface. The interfacial tension keeps decreasing later and gradually reaches a plateau as time goes by. The interfacial tension values and the corresponding shape factors obtained at the end of 40 minutes of aging are plotted as a function of electric field strength in the following figure. Studies on other variables in the following chapters, including asphaltene concentration, aging time, water pH and salinity, are carried out in the same manner.

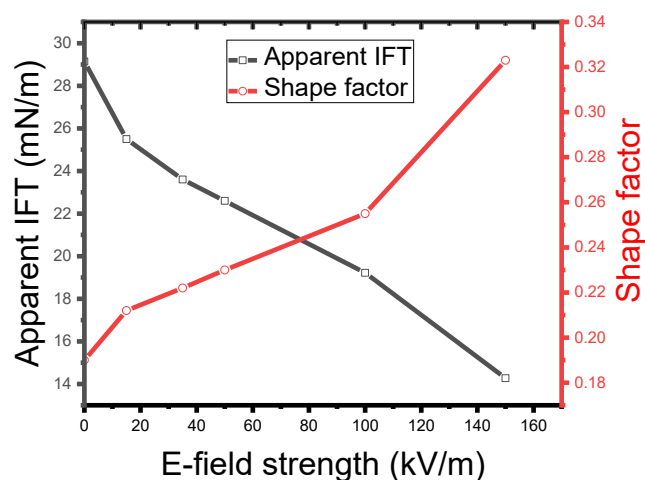


Figure 5 - 11: The apparent interfacial tension and the measured shape factor for a water-in-model oil system aged for 40 minutes as a function of electric field strength.

In the figure above, the apparent interfacial tension is inversely correlated with the shape factor, as the apparent interfacial tension is calculated based on Eq.3-9 and deviates from the real interfacial tension, as mentioned before. Analysing the shape factor results, it is manifested that the stronger the electric field, the bigger the shape deformation.

5.2.4 Crumpling ratio measurements

To determine if the asphaltene adsorption is truly enhanced by the application of external electric field. The crumpling ratio is also measured as another interfacial property for further investigation.

The viscoelastic asphaltene film existing at the water/oil interface is an obstacle that prevents small water droplets from coalescing. A crumpling phenomenon can be observed visually when the water drop area is decreased greatly, achieved in this study by retracting the inside water at a

constant speed back into the glass capillary. At a certain point, named as the crumpling point (as shown in the following figure), the film will crumple, and some vertical wrinkle-like lines appears on the interface.

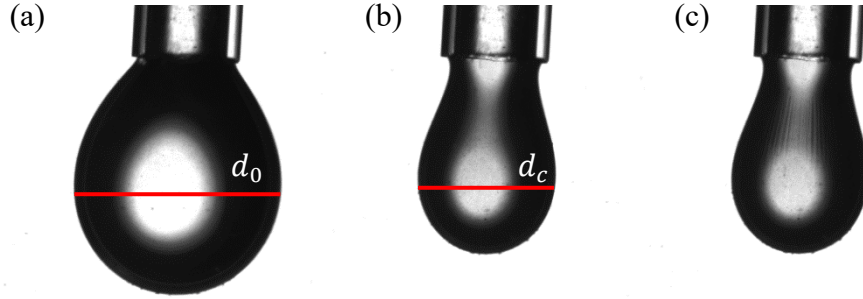








Figure 5 - 12: Example of crumpling process at (a) the initial status, (b) the status right before crumpling occurs, and (c) the crumpling point. The deionized water drop is immersed in 0.05 g/L model oil at 100 kV/m.







The ratio of the projected area of water pendant drop right before crumpling point, as in Figure 5-12(b) to the initial projected area, as in Figure 5-12(a), is defined as the crumpling ratio. In this study, the crumpling ratio is simplified as the square of the ratio of the drop diameter right before crumpling point, d_c , to the initial drop diameter, d_0 , regarding the projected area of the water drop as in circular shape in vertical view. The crumpling ratio here represents the compressibility of the interfacial film. A less compressible (more compact) film hinders water bridging and water-water coalescing without electric field application.

A 0.05 g/L model oil is used for measuring the crumpling ratios under various electric field of 0 kV/m, 15 kV/m, 35 kV/m, 50 kV/m, 100 kV/m and 150 kV/m. Images of pendant water drop at

initial status and right before crumpling occurs are as presented below, each one serves as an example and is selected from many parallel experiments.

Table 5 - 3: Images of a pendant water drop in 0.05 g/L model oil at initial status and right before crumpling point under various electric field strength. The shape factor and crumpling ratio are also included.

Initial status	Right before crumpling point
 <p>0 kV/m Shape factor: 0.19</p>	 <p>0 kV/m Crumpling ratio: 0.338</p>
 <p>15 kV/m Shape factor: 0.21</p>	 <p>15 kV/m Crumpling ratio: 0.586</p>
 <p>35 kV/m Shape factor: 0.22</p>	 <p>35 kV/m Crumpling ratio: 0.708</p>

 <p>50 kV/m Shape factor: 0.23</p>	 <p>50 kV/m Crumpling ratio: 0.717</p>
 <p>100 kV/m Shape factor: 0.26</p>	 <p>100 kV/m Crumpling ratio: 0.732</p>
 <p>150 kV/m Shape factor: 0.32</p>	 <p>150 kV/m Crumpling ratio: 0.789</p>

It is suggested in the table above that the stronger the electric field, the higher the crumpling ratio, the more asphaltene adsorbed, the less compressible (or more compact) the interfacial film. The same trend is also indicated in the figure below, where the average crumpling ratio of parallel experiments is plotted as a function of electric field strength. The crumpling ratio enhances drastically at low electric field strength range, from 0 kV/m to 35 kV/m. Marginal increase is noticed at higher electric field strength. Therefore, the crumpling ratio results consist with the

interfacial tension ones, which imply that the asphaltene adsorption is enhanced by the application of electric field up to 150 kV/m.

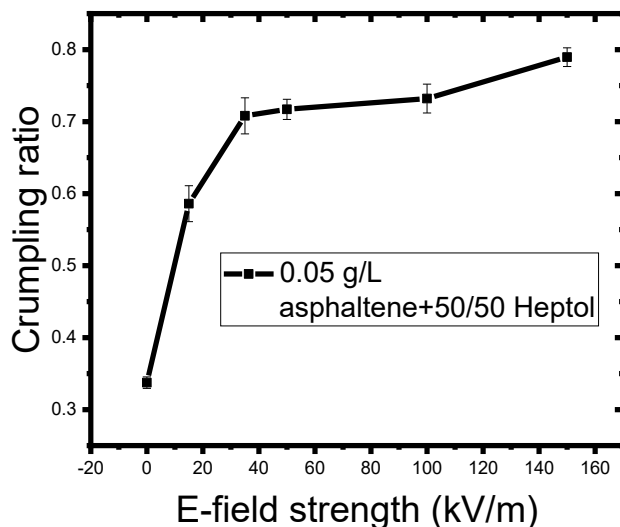


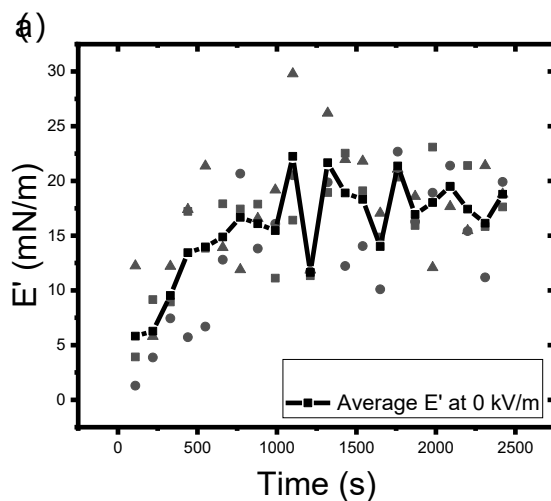
Figure 5 - 13: The crumpling ratio results of water-in-0.05 g/L model oil under different electric field strength.

5.2.5 Effects of electric field on dilatational rheology

This part of study is conducted with a perturbation-controlled oscillating drop method. By applying a sinusoidal oscillation at a low amplitude, a sinusoidal variation in both interfacial tension and surface area is observed, with a phase shift. The dilatational modulus is defined as the ratio of relative change in interfacial tension to that of the surface area. The dilatational modulus consists an elastic modulus, a real component, and a viscous modulus, an imaginary component. This study focuses on the elastic modulus results, representing the elasticity of the asphaltene adsorption layer.

The interfacial elasticity is an even better way of analyzing the asphaltene rearrangements and consolidations than interfacial tension. However, the accuracy of the elastic modulus depends considerably on the real interfacial tension, the calculation of which remains unknown and needs assistance in simulation. The results below serve as an implication instead of the real value of elastic modulus.

The elastic modulus is measured under electric field strength at 0 kV/m, 50 kV/m and 100 kV/m. Under the same electric field, the elastic modulus on each measured point is based on oscillation analysis of 10 cycles at 0.1 Hz in 110 seconds. The elastic modulus at the same time period are then averaged and plotted as a function of aging time. This time dependent elastic modulus increases within the first 1000 seconds and gradually reaches a plateau, where the value obtained can be used to scale the elasticity.



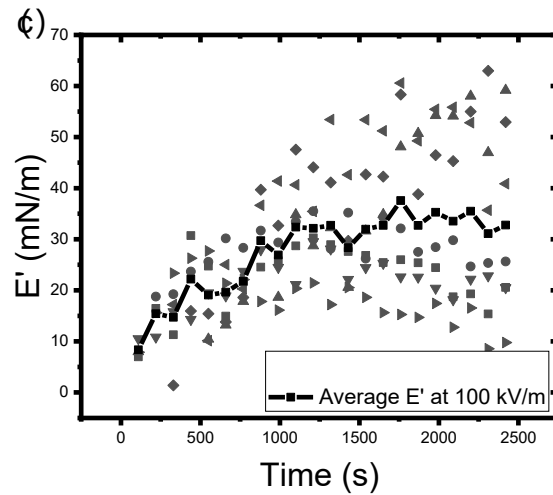
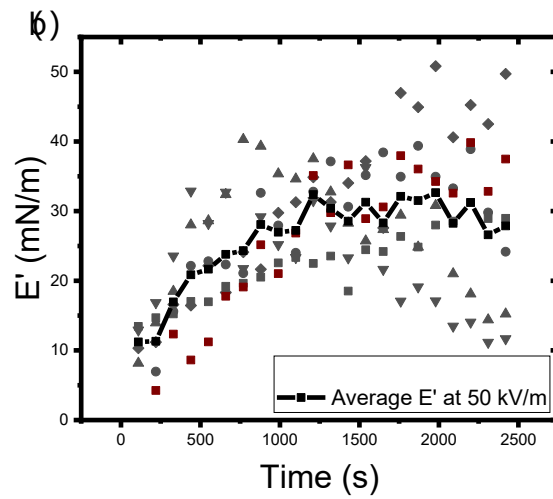


Figure 5 - 14: The average elastic modulus variations as a function of time during 40 minutes of aging under electric field of (a) 0 kV/m, (b) 50 kV/m and (c) 100 kV/m.

It is obviously shown in the figure that the elasticity of the water/oil interface without external electric field is significantly lower than the ones at 50 kV/m and 100 kV/m, roughly maintaining at a value of 18 mN/m. The difference of elasticity for the water/oil interface under 50 kV/m and 100 kV/m is not significant, with the latter one slightly higher than the former one. This trend is

consistent with the crumpling ratio results and interfacial tension results. The assumption is confirmed that in the presence of electric field, the macroscopic EHD flow induces tangential stresses in the leaky dielectric oil phase [110], and thus enhances asphaltenes rearrangements and consolidations on the interface, leaving new sites for more asphaltene adsorption.

5.2.6 Possible explanation

Results of interfacial tension, crumpling ratio and elastic modulus are consistent, indicating that asphaltene adsorption is enhanced with stronger electric field application. This could be due to an enlarged interfacial area by drop stretching, allowing more space for asphaltene molecules occupation than without electric field.

Another possible reason holding a clue for the phenomenon is the electrohydrodynamic (EHD) flow, which increases with higher electric field strength. Due to the EHD flow, the asphaltene molecules adsorbed on the interface keeps rearranging and consolidating, making new sites for more adsorption. This is proved by using a model oil containing asphaltene flocculation, which are bigger and can be visually spotted under high-speed camera. It is shown that the aggregates move randomly and slowly without external electric field but start moving along the interface

following a certain path under electric field. The stronger the electric field, the faster the movement. The path is schematised as presented below.

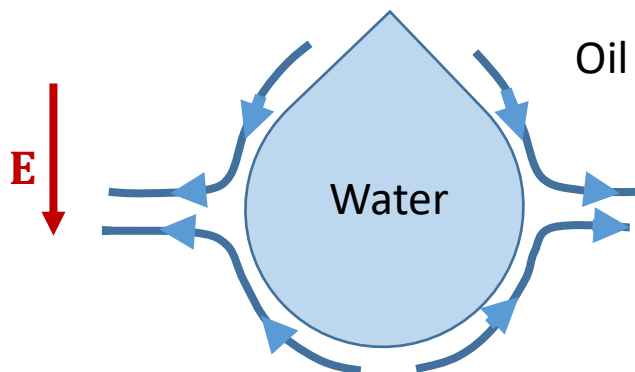


Figure 5 - 15: Schematic of asphaltenes aggregates' movement along the interface under an electric field in the same direction as gravity.

5.3 Effect of asphaltene concentration on shape factor and crumpling ratio under different electric fields

The effect of asphaltene concentration is tested with model oil of three concentrations at 0.01 g/L, 0.05 g/L and 0.1 g/L. Results are showing that the shape factor increases with stronger electric field as indicated and explained in the last section. It is also suggested in the figure that at the same electric field strength, the shape factor goes up, i.e. the real interfacial tension reduces, with higher asphaltenes concentration. This enhancement in asphaltene adsorption has been widely accepted in normal conditions (without electric field application) [122], [135], [136]. As long as the concentration is lower than a critical value, the surface coverage of asphaltenes on the interface will increase with higher asphaltene concentration as the total amount of asphaltenes is larger in

the oil phase. Above this critical value, usually referred to as the saturation point, the stability of the emulsion remains almost at a constant with higher asphaltene content. It is stated that the saturation point is around 2 g/L when asphaltenes are dissolved into a 40/60 heptol (heptane and toluene at a volume ratio of 40:60) [137].

Therefore, when electric field is applied, due to the asphaltene redistribution by electrohydrodynamic flow along the interface, a higher concentration introduces a bigger reservoir for rearranged asphaltenes to form a denser layer, thus decreasing the interfacial tension.

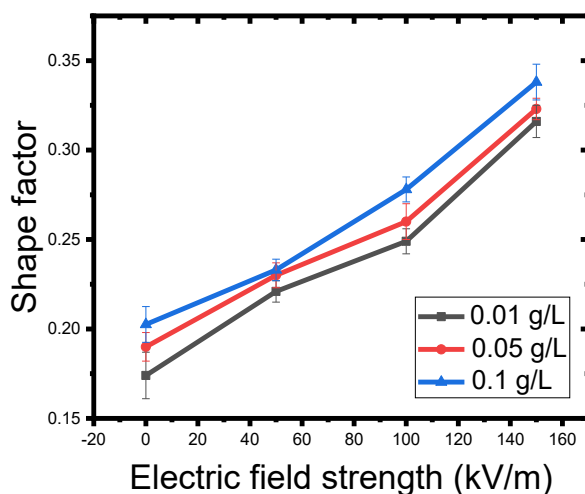


Figure 5 - 16: The shape factor for a water-in-model oil system aged for 40 minutes at different concentrations as a function of electric field strength.

Crumpling ratio are also measured as a function of various asphaltene concentration. It is noticed from the chart that the crumpling ratio increases with higher asphaltene concentration. The higher the asphaltene concentration, the more asphaltene molecules exist in the continuous phase, the more asphaltene can be adsorbed onto the interface in the same amount of time. Since the

asphaltene molecules on the interface are rearranged by electrohydrodynamic flow, the asphaltene distribution at lower concentration is less compact and the surface coverage is lower. At a higher concentration (> 0.1 g/L), the effect of electrohydrodynamic flow may be limited by a saturation point [137], as the maximum surface coverage and compactness can hinder asphaltene adsorption. However, the highest concentration can be applied in this study is 0.1 g/L. Otherwise, the solution is too dark to see through by a high-speed camera.

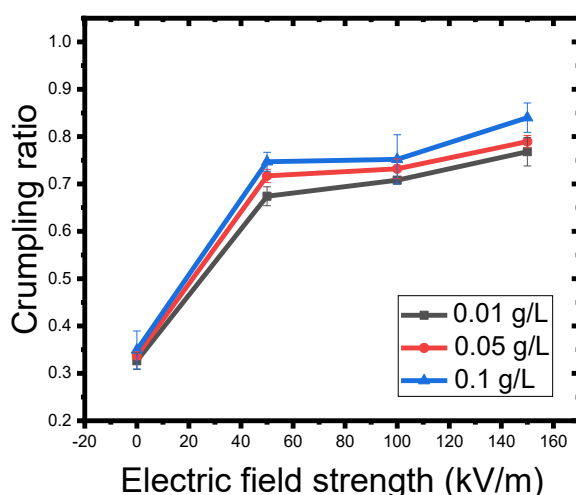


Figure 5 - 17: The crumpling ratio results of both water-in-0.01 g/L, 0.05 g/L, and 0.1 g/L model oil system under various electric field strength.

5.4 Effect of aging time on shape factor and crumpling ratio under various electric fields

The effect of aging time is measured with deionized water drops suspending in model oil, aged for 30 minutes, 40 minutes, and 50 minutes respectively. A plot of the measured shape factor as a

function of aging time under different electric field strength is presented below. As indicated in the figure, the shape factor increases with aging time at each electric field strength, suggesting the real interfacial tension is decreasing. This reduction in interfacial tension is caused by more asphaltene adsorption onto the interface with longer aging time.

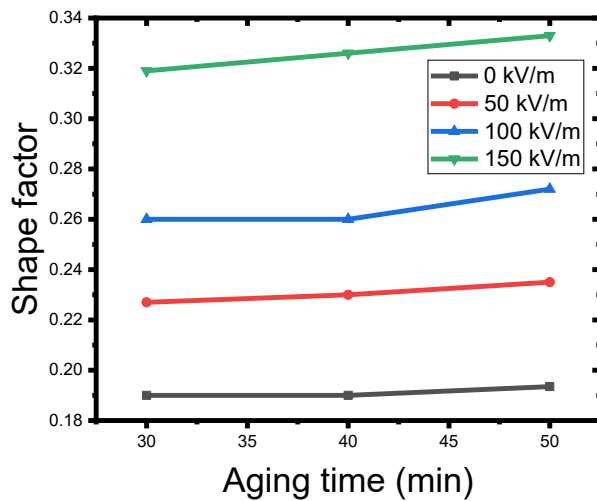


Figure 5 - 18: The shape factor for a water-in-model oil system aged for 30, 40, and 50 minutes under various electric field strength.

The shape factor results alone are not convincing enough to analyze the effect of aging time on water/oil interfacial layers, more inference can be made based on the crumpling ratio results. The effect of aging time is also measured with water-in-0.05 g/L model oil. Results show that the crumpling ratio increases with aging time. But a turning point is reached as time goes, under weak electric field application (0 to 50 kV/m), which is not apparently observed under strong electric field application (100 kV/m to 150 kV/m).

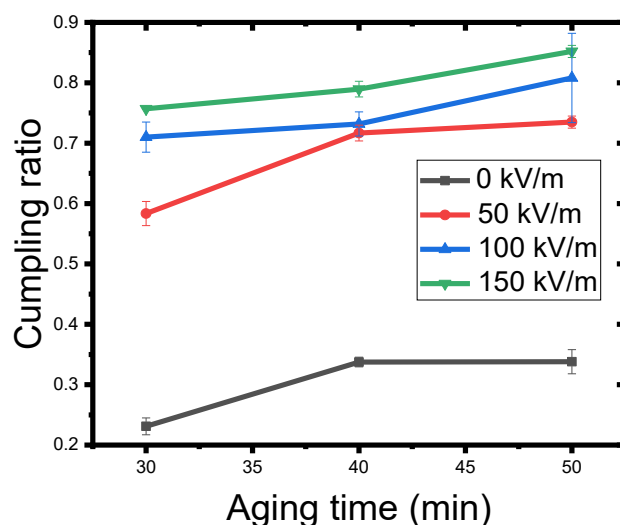


Figure 5 - 19: The crumpling ratio results for water drops aged for 30 minutes, 40 minutes and 50 minutes respectively under various electric field strength.

In the absence of electric field, longer aging time enables more asphaltenes to be adsorbed on the interface. Sites on the interface is filled up with asphaltene molecules gradually, leaving less space for more asphaltene adsorption. A marginal increase in crumpling ratio, or a nearly constant value, is obtained at a longer aging time, where the surface coverage approaches the upper limit. When electric field is applied, the adsorption and redistribution is speeded up due to electrohydrodynamic flow. The turning point appears later in higher applied voltage, due to stronger electrohydrodynamic flow and faster asphaltene redistribution. To find out the turning point of stronger electric field, a higher voltage than 150 kV/m and longer aging time than 50 minutes need to be applied. However, in pendant drop tensiometry, an equilibrium drop shape can no longer be maintained under such strong electric field. And extending the aging time would trigger more air-loss and enlarge experimental error.

5.5 Effect of water phase pH on shape factor and crumpling ratio under different electric fields

Four sets of water pH are tested to study the effect of water pH on the interfacial tension with buffer solutions at pH 4, pH 7 and pH 10, and deionized water at pH6. The influence of different types and concentrations of ions involved are not considered. The results of shape factor are plotted as a function of water phase pH in the following figure.

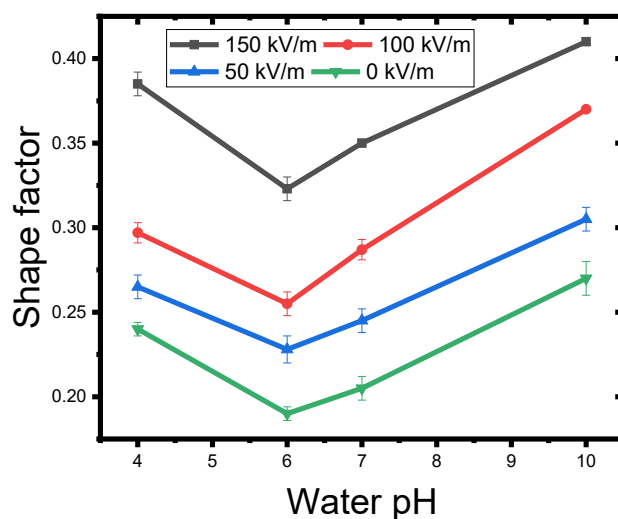


Figure 5 - 20: The shape factor of a pendant water drop immersed in model oil as an implication for the interfacial tension versus different water pH at various electric field strength.

It is clearly demonstrated that in the acidic water phase ($\text{pH} \leq 6$), the shape factor is declined as pH raises up, meaning that the interfacial tension is increasing with a higher pH. This could be due to the presence of basic groups, such as amides and amines, in the extracted asphaltene structures from the Athabasca crude oil. As a result of acid-basic neutralization, more asphaltenes are

adsorbed onto the acid water/oil interface, leading to an interfacial tension reduction in acid water environment. Similar trends of interfacial tension in acidic environments without electric field application have been observed for other Athabasca bitumen [28], [135], [138], [139]. Whereas in an alkaline water phase ($\text{pH} \geq 7$), the shape factor is increased as water pH goes up, meaning that the interfacial tension is decreasing with a higher pH. This reduction could be attributed to the presence of carboxylate functional group in asphaltene molecular structure [140]. They are released from the precursor in a basic environment and serve as new surfactants, leading to a reduction in interfacial tension. In general, it is observed that the amphoteric asphaltenes [141] show a stronger affinity towards the water/oil interface in both low and high pH environments, with the application of electric field. The functioning groups in asphaltenes become charged or partly charged in a low or high pH environment, thus presenting a more hydrophilic behavior and increasing surface activity [142]. In this way, the asphaltenes accumulates on the interface even easier with the application of electric field, since they are charged and influenced by electrostatic force.

Crumpling ratio results suggest that the crumpling ratio raise up with increased water pH and are plotted in the following figure.

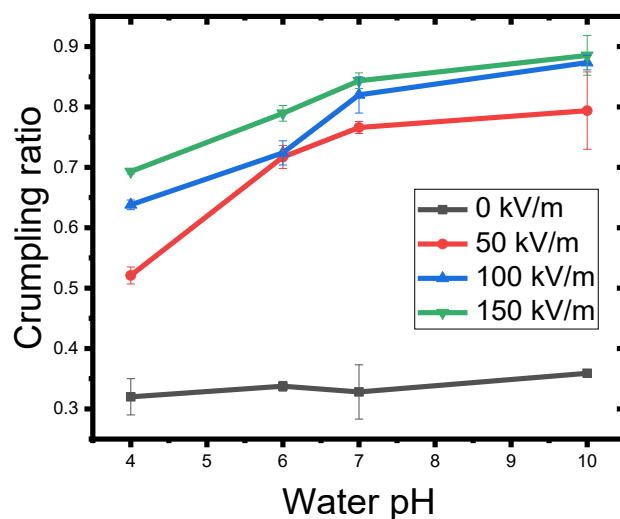
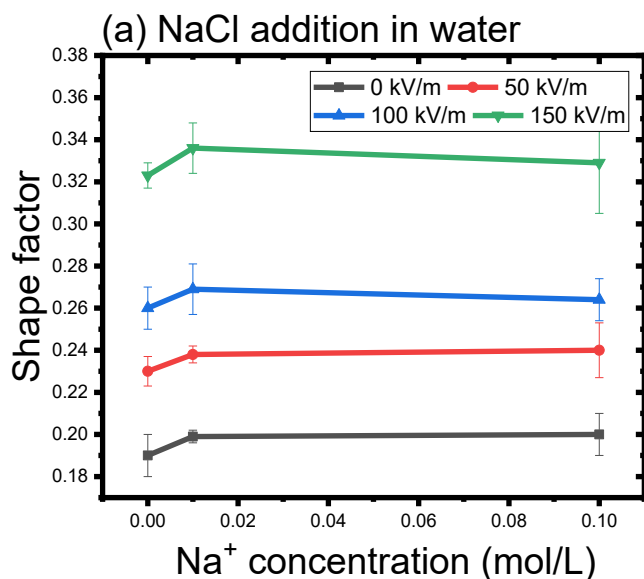


Figure 5 - 21: The crumpling ratio results of water phase at various pH suspending in 0.05 g/L model oil under different electric field strength.

In the alkaline water phase region ($\text{pH} \geq 7$), the crumpling ratio increases with higher water pH, which is consistent with the corresponding lower interfacial tension observed. However, in the acid water phase region ($\text{pH} \leq 6$), the crumpling ratio also increases with higher water pH, contradicted to shape factor results. This may be owing to a desorbable asphaltene layer formed in acidic environment that the asphaltene molecules detach from the interface during compression. Or the structure of the adsorbed asphaltene molecules in acidic environment under electric field is generally smaller, leading to a more compressible interfacial film and lower crumpling ratio.

5.6 Effect of salinity on shape factor and crumpling ratio under various electric fields

In oil production and transportation, the water coexisting with oil always contains salt. It is meaningful to investigate the effect of salt content and salt type on the shape factor under the influence of electric field, ranging from 0 kV/m to 150 kV/m. NaCl and CaCl₂ brine solutions at 0.01 mol/L and 0.1 mol/L are used as the aqueous phase in the emulsion system, representing monovalent salts and divalent salts respectively. The influence of chloride ions on the interfacial tension are not considered, as the stabilities of emulsions is not affected by different valance of chloride salts at the same concentration in water phase [143]. The shape factor results of NaCl and CaCl₂ additions are plotted as a function of salt content under various electric field strength as below.



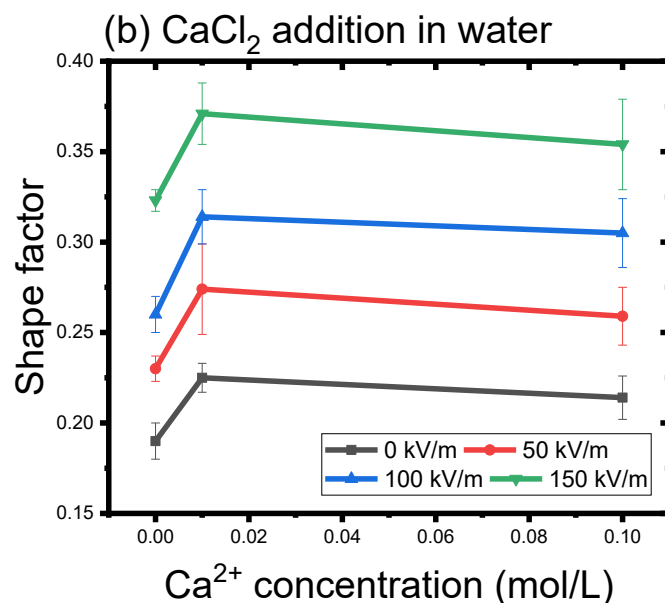


Figure 5 - 22: Shape factor results as a function of salt content with addition of: (a) NaCl, and (b) CaCl_2 at 0, 0.01 and 0.1 mol/L in the aqueous phase for pendant drop immersed in model oil under various electric field.

It is demonstrated in the figures at the same salt content, no matter mono- or divalent salts, a higher shape factor is observed at higher electric field strength. This trend is in accord with the results of other variables. Additionally, at the same electric field strength, the addition of either mono- or divalent salt at the same content lead to a higher shape factor, i.e. lower interfacial tension, than that of the deionized water. It is supported by many findings that the emulsion stability is enhanced with salt addition in normal conditions [30], under electric field application [144], and under microwave application [145]. The reason could be that as the aqueous phase is polarized under electric field, more cations move and accumulate at the interface, reducing the repulsive force between charged asphaltene molecules and thus enhancing asphaltene adsorption.

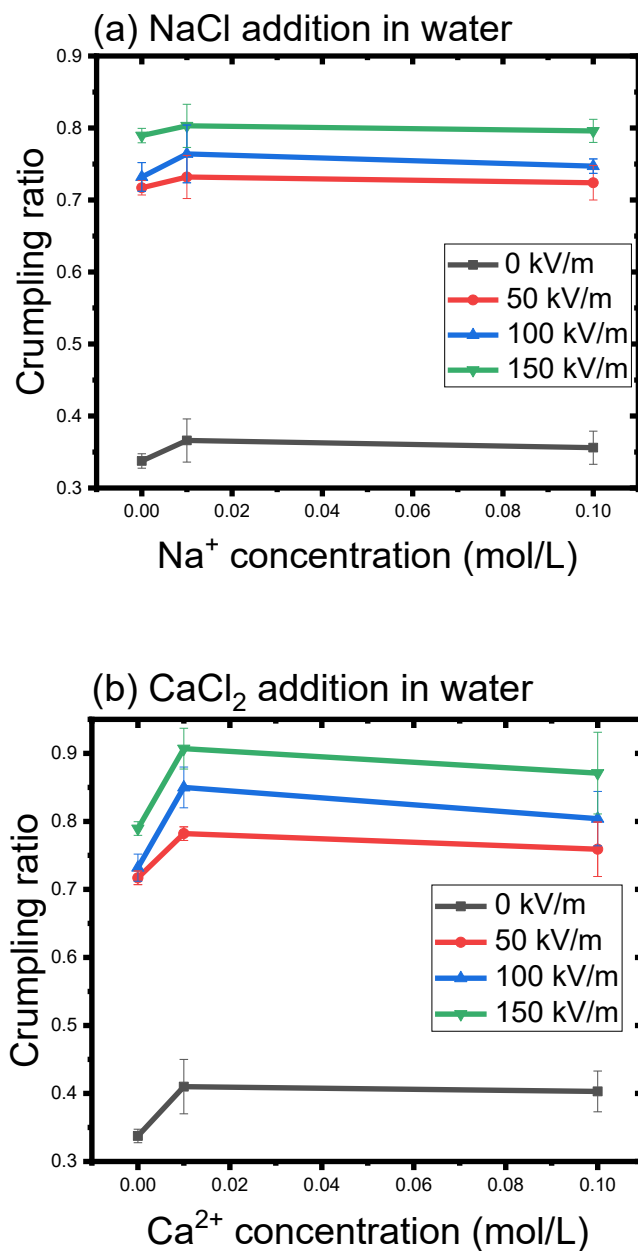


Figure 5 - 23: Crumpling ratio results as a function of salt content with addition of: (a) NaCl, and (b) CaCl₂ at 0, 0.01 and 0.1 mol/L in the aqueous phase for pendant drop immersed in model oil under various electric field.

As demonstrated in the above figures, at the same salt content of either monovalent or divalent salt, the stronger the applied electric field, the higher the crumpling ratio. Moreover, the addition of salts, either NaCl or CaCl₂, into the aqueous phase lead to a higher crumpling ratio of the emulsion system than that of the deionized water under applied external electric field, which is in accord with the lower interfacial tension results inferred by the higher shape factor mentioned before.

It is also implied in both shape factor and crumpling ratio results that a critical value of salt content exists where the asphaltene adsorption reaches the maximum for both NaCl and CaCl₂ salted water, as both the crumpling ratio and shape factor at 0.01 mol/L is higher than the ones at 0.1 mol/L. If the salt content is higher than this critical value, the crumpling ratio and shape factor of the interface start to decrease.

It is also shown in the figures that the shape factor and crumpling ratio at 0.01 mol/L of CaCl₂ are obviously higher than that of the deionized water, whereas the ones at 0.1 mol/L of NaCl addition displays only a slight increase from that of the deionized water. This is supported by findings from C. Perles et al. [144]. He suggested that the emulsion stability with an ionic strength higher than 0.1 to 0.3 mol/L, the exact value depending on the emulsion system, will tend to decrease and attain a close value with that of the deionized water. This could attribute to the salts contained in the aqueous phase attracting different components on the asphaltene molecular structure at high salt content when electric field is applied [146]. It is conjectured that smaller asphaltene molecules could be adsorbed more on the interface at high salt content, leading to a lower crumpling ratio and shape factor.

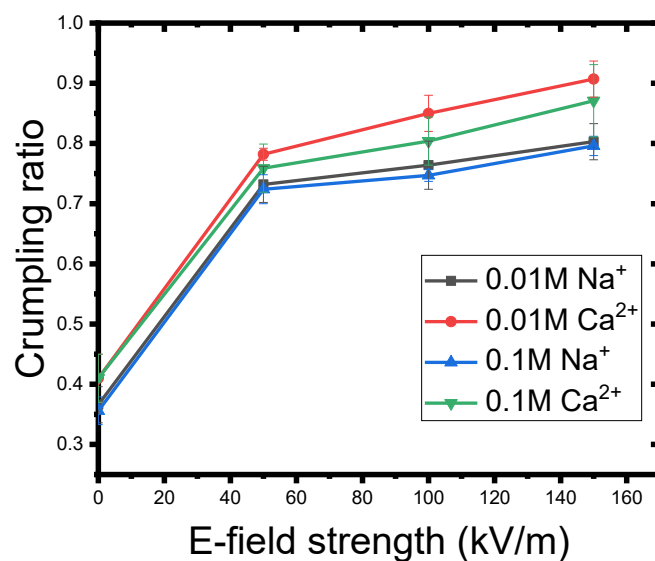


Figure 5 - 24: Crumpling ratio results as a function of electric field strength with addition of NaCl, and CaCl₂ at 0.01 and 0.1 mol/L in the aqueous phase for pendant drop immersed in model oil under various electric field.

The crumpling ratio results are also plotted as a function of electric field strength. It is suggested in the figure that the divalent salts Ca²⁺ are more effective than monovalent salts Na⁺ on enhancing asphaltene adsorption under electric field. This is in accord with findings from C. Perles et al. that divalent salts Ba²⁺ induce higher emulsion stability than monovalent salts Na⁺ and K⁺ [144]. This could be owing to the formation of a stronger complexes between divalent ions with asphaltene molecules adsorbed on the interface.

Chapter 6 Conclusions and Future Work

6.1 Conclusions

To understand the shape deformation under electric field and gain optimum drop shape for curve-fitting, a few variables, including the effect of electric field strength, electric field direction, and drop positions are investigated. Two types of drop deformation, either a flattening or an elongated drop shape exists in the studied system. For a pendant water drop in leaky dielectric fluid, the water drop can deform into a prolate, oblate shape in the direction of the electric field, or even presence no deformation in some special cases. The water drop deformation increases with stronger electric field applied and tends to detach from the glass capillary when it exceeds the limit. In pure solvent system, the shape change is reversible, indicated by the same IFT value at the same electric field strength. Whereas in surfactant system, the shape change is irreversible, since the IFT regains a value much lower than the original one after minutes of electric field application. The widest range of electric field can be applied when the electric field is applied in the same direction as gravity and the water drop is suspending at the middle position. In this way, the electric-induced force and gravity are in a balance, maintaining a moderate drop deformation.

The application of electric field creates extra shape deformation by the Maxwell stress on the water drop suspending in an oil phase, which deviates from the normal Laplacian one and induce calculation error in shape fitting. In this case, the interfacial tension calculation based on the shape factor is no longer accurate. New methods need to be brought up for interfacial tension calculation under external electric field and remove the effect of the induced Maxwell stress on shape

deformation. A potential experimental method by removing the electric field at the end of aging and allow extra time for drop relaxation is proposed and adopted in this study. This method assumes that the asphaltene films formed on water/oil interface is irreversibly adsorbed and more asphaltene adsorption onto the interface during relaxation is not considered. The real IFT results have shown that the interfacial tension decreases with higher electric field strength. And the reduction is much sharper with weak electric field application (≤ 50 kV/m) than strong electric field application (≥ 50 kV/m).

The trend above are further validated by more interfacial properties examined. The shape factor, crumpling ratio, and dilatational rheology results are consistent with the interfacial tension ones, suggesting that the asphaltene adsorption on the interface is enhanced under external electric field. This could be owing to the increased interfacial area with stronger electric field, and also the electrohydrodynamic (EHD) flow inducing fluid circulation in the dielectric media, which increases with higher electric field strength. Due to the EHD flow, the asphaltene molecules adsorbed on the interface keep rearranging and consolidating, making new sites for more adsorption.

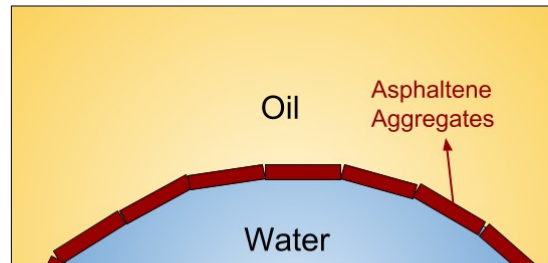
Different variables are also tested in this study, including the effect of asphaltene concentration, aging time, water pH, and salinity. It is shown that the higher the asphaltene concentration under electric field, the more asphaltene adsorbed, which is caused by a bigger asphaltene reservoir in the continuous phase. The asphaltene adsorption also increases with longer aging time under external electric field, with the turning point appears later under higher applied voltage, due to stronger electrohydrodynamic flow and faster asphaltene redistribution. As for the effect of water pH, stronger affinity of asphaltene molecules towards the water/oil interface in both low and pH environments is observed, evident with a lower interfacial tension. This phenomenon is amplified

under electric field since the asphaltene molecules accumulate and get charged on the interface, thus influenced by electrostatic force. However, crumpling ratio results imply that a partly reversible asphaltene adsorbed layer is formed in acidic environment that the asphaltene molecules desorb from the interface during contraction. Or the structure of the adsorbed asphaltene molecules in acidic environment under electric field is generally smaller, leading to a more compressible interfacial film and lower crumpling ratio. The effect of salinity is measured with NaCl and CaCl₂ salted water at different concentrations. The addition of salts into the aqueous phase leads to more asphaltene adsorption on the interfacial film than that of the deionized water. The reason is that when electric field is applied, more cations move and accumulate at the interface, reducing the repulsive force between charged asphaltenes. Asphaltene adsorption increases at low salt content but starts to decrease towards that of the deionized water at high salt content. This could be attributed to the salts contained in the aqueous phase attracting smaller asphaltene molecules on the interface at high salt content when electric field is applied. Additionally, divalent salts are more effective than monovalent salts on enhancing asphaltene adsorption under electric field.

It is suggested from the results that the asphaltene molecules containing polar groups tend to move to the polarized water drop faster due to EHD flow and form a more compact or thick adsorbed layer owing to rapid rearrangement by the EHD flow. Mechanisms on how the electric field is assisting water-water coalescence in model oil need to be further investigated, but one possible explanation holding a clue for this phenomenon is the patchy and heterogeneous interfacial film.

When electric field is applied, the interfacial area enlarges and some cracks form on the interfacial film, creating weak spots for further drop-drop coalescence.

(a) Without electric field application



(b) With electric field application

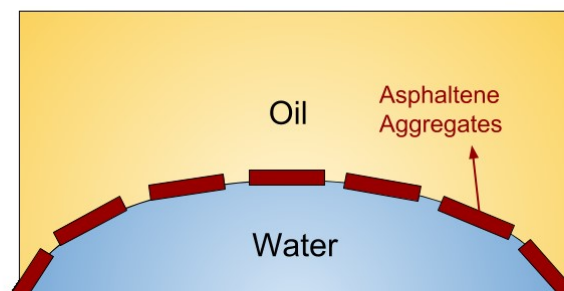


Figure 6 - 1: Schematics of the proposed mechanism on water drop-drop electrocoalescence in the oil phase. A homogeneous interfacial film of asphaltene is formed (a) without electric field application, but cracks are created (b) with electric field application, due to the enlarged interface.

6.2 Future work

Many aspects related to this work are not fully covered due to applicability limitations. Further investigations are required to establish a more comprehensive understanding of the effect of electric field on water/oil interfacial properties and the mechanisms of electrocoalescence.

1) A better way to seal the glass cell during experiment need to be developed, avoiding contaminating the system and bypassing the cables at the same time. This would prevent carbon dioxide from dissolving into the oil phase and reduce the chance of pH change in the system, also preventing toluene and heptane from evaporating. Otherwise the properties of the oil phase would change.

2) As safety is always the primary concern in lab, the experimental setup and operating procedures of this research is designed and conducted fully obeying the safety regulations. Therefore, the syringe and needle are designed by connecting a micrometer syringe and a glass capillary with a long rubber tube, to prevent any possibility of electric shock. A few drawbacks of this design exist, top of which is the inevitable heavy air loss at all the connection part. Even if Teflon tape and parafilm are applied and firmly winded around the connection, the water drop volume will still shrink during each 40 minutes aging time. In crumpling ratio measurement, this could result in a misjudgment in initial projected area of the droplet before retracting, and thus lead to crumpling ratio results error. A gas-tight manual syringe could help prevent air loss, and thus controlling droplet size more effectively. However, the needles connected with the gas-tight manual syringe are usually made of metal, which are dangerous in terms of high voltage application. Coating the metal needles with Teflon on the outside is a better solution. Another advantage of Teflon coating

is that it can prevent water drop from being attracted to the polarized glass capillary and presenting a flattening shape that is not as stable as a stretching one.

3) In the pursuit of the real interfacial tension, more methodologies need to be developed. The power off testing method brought up in this study is based on the assumption that asphaltene molecules are irreversibly adsorbed and more adsorption onto the interface during relaxation is not considered. Other methods that can solve the problem need to be developed. So far, the best solution is numerically fit the shape from the experiments to the advanced Laplacian one, where the Young-Laplace equation need to be modified to conclude an extra term for the Maxwell stress. The tricky part is the electric field simulation, since the existence of EHD flow exerts complexity in velocity and viscosity calculations.

4) An interfacial tension hysteresis exists when electric field is applied in a surfactant system, as shown in Figure 5-4, where surfactant adsorption is enhanced by the electric field. This interfacial tension hysteresis should be studied as a function of electric field application time under various electric field strength.

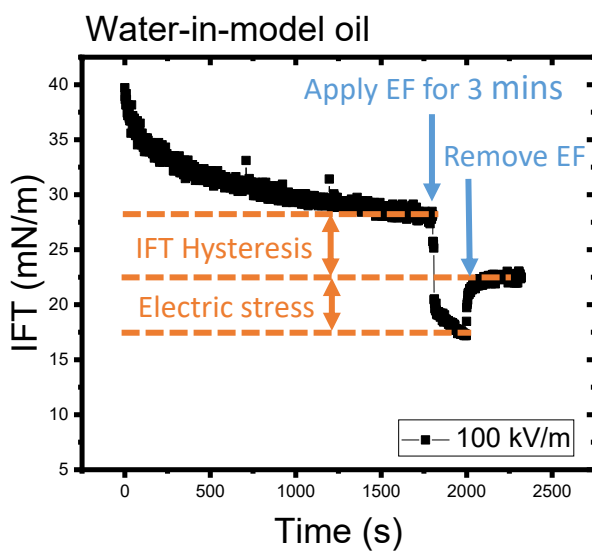


Figure 6 - 2: Interfacial tension of water/model oil interface as a function of time with interfacial tension hysteresis and electric stress marked. The water drop is aged at 0 kV/m for 30 minutes, followed by applying electric field at 100 kV/m for 3 minutes and then back to 0 kV/m.

5) To confirm whether the existence of another water drop in the neighborhood would affect the interfacial properties, more experiments with drop-drop configuration need to be conducted to measure the shape factor, crumpling ratio and elastic modulus using pendant drop tensiometry.

6) Electrocoalescence experiments with thin film draining apparatus also need to be tested. One method that can be utilized is to age the two water drops without the electric field and let them remain non-contacting. Then the electric field is applied while manually forcing the drops to approach, mimicking drops' attracting to each other by dielectrophoresis effect, until coalesce. Another method is to age the two water drops without the electric field and manually force drops overlap, mimicking water drops that are already in contact before electric-assisted demulsification application. Coalescence time can then be measured under various electric field strength.

7) To validate the proposed mechanism, the Brewster Angle Microscopy (BAM) can help with observing the asphaltene film structure under electric field application. And another way to better understand the crack on the interfacial film is to let the drop age without electric field first and then apply electric field for a certain application time, followed by conducting the crumpling process and calculating the crumpling ratio as a function of electric field application time. A drop is expected at short time application, when the asphaltenes have not occupied the cracks with further adsorption. Different electric field strength should also be tested, to investigate their effect

on the drop. It is expected that the stronger the electric field strength, the bigger the crack and the lower the crumpling ratio.

8) To understand the weak spots on the interface and how different parameters depend on the demulsifier, interfacial tension hysteresis, electric stress, shape factor and crumpling ratio should also be analysed with pendant drop tensiometry. Coalescence time should also be studied by comparing results with and without the electric field.

Bibliography

- [1] Ministry of Natural Gas Development and Minister Responsible for Housing, “Conventional versus Unconventional Oil and Gas,” 2007. [Online]. Available: https://www2.gov.bc.ca/assets/gov/farming-natural-resources-and-industry/natural-gas-oil/petroleum-geoscience/conventional_versus_unconventional_oil_and_gas.pdf. [Accessed: 11-Dec-2018].
- [2] Student Energy, “Definition of unconventional oil.” [Online]. Available: <https://www.studentenergy.org/topics/unconventional-oil>. [Accessed: 11-Dec-2018].
- [3] Energy Education, “Unconventional resource,” 2017. [Online]. Available: https://energyeducation.ca/encyclopedia/Unconventional_resource. [Accessed: 11-Dec-2018].
- [4] Wikipedia, “Unconventional Oil,” 2014. [Online]. Available: https://en.wikipedia.org/wiki/Unconventional_oil. [Accessed: 11-Dec-2018].
- [5] Government of Alberta, “What is oil sands?,” 2018. [Online]. Available: <http://www.energy.gov.ab.ca/OS/AOS/Pages/WOS.aspx>. [Accessed: 06-Dec-2018].
- [6] Alberta Energy Regulator, “Crude bitumen,” 2018. [Online]. Available: <https://www.aer.ca/providing-information/data-and-reports/statistical-reports/crude-bitumen>. [Accessed: 08-Dec-2018].
- [7] Government of Alberta, “Facts and Statistics,” 2017. [Online]. Available: <http://www.energy.gov.ab.ca/OS/AOS/Pages/FAS.aspx>. [Accessed: 07-Dec-2018].
- [8] Government of Alberta, “Upgraders and Refineries Facts and Stats,” 2018. [Online]. Available: <https://open.alberta.ca/dataset/98c15cad-c5d9-4d96-b39c-423210a3050c/resource/7367e817-4fea-4744-a80c-0a81ce5fc907/download/factsheet-upgraders-and-refineries.pdf>. [Accessed: 07-Dec-2018].
- [9] National Energy Board, “Canada’s Energy Futures 2017 Supplement: Oil sands,” 2017.
- [10] Alberta Energy Regulatory, “Crude Bitumen Production,” 2018. [Online]. Available:

- <https://www.aer.ca/providing-information/data-and-reports/statistical-reports/crude-bitumen-production>. [Accessed: 08-Dec-2018].
- [11] Government of Alberta, “Steam Assisted Gravity Drainage Facts and Stats,” 2017. [Online]. Available: <https://open.alberta.ca/dataset/f7c779ea-9776-4d59-a1b3-178d533f0ebc/resource/aac73d46-3ae0-478e-9b19-e64afa41b1f2/download/FSSAGD.pdf>.
 - [12] Alberta Energy Regulator, “Executive Summary,” 2018. [Online]. Available: <https://aer.ca/providing-information/data-and-reports/statistical-reports/executive-summary>. [Accessed: 11-Dec-2018].
 - [13] H. G. Saunders and F. A. Kamke, “Quantifying emulsified wax distribution on wood flakes,” *Forest Products Journal*, vol. 46, no. 3, pp. 56–62, 1996.
 - [14] T. Nakashima, M. Shimizu, and M. Kukizaki, “Particle control of emulsion by membrane emulsification and its applications,” *Adv. Drug Deliv. Rev.*, vol. 45, no. 1, pp. 47–56, 2000.
 - [15] A. Y. . Khan, S. Talegaonkar, Z. Iqbal, F. J. . Ahmed, and R. K. Khar, “Multiple emulsions: An overview,” vol. 3, no. 4, p. 429, 2006.
 - [16] S. P. Agarwal, R. Khanna, R. Karmarkar, K. Anwer, and R. K. Khar, “Shilajit : A Review,” vol. 405, no. February, pp. 401–405, 2007.
 - [17] H. Schubert and H. Armbruster, “Principles of formation and stability of emulsions,” *Int. Chem. Eng.*, vol. 32, pp. 14–28, 1992.
 - [18] Griffin and C. William, “Classification of surface-active agents by HLB,” *J. Soc. Cosmet. Chem.*, vol. 1, no. 5, p. 311, 1949.
 - [19] Wikipedia, “emulsion.” [Online]. Available: <https://en.wikipedia.org/wiki/Emulsion>. [Accessed: 19-Dec-2018].
 - [20] B. A. Khan, N. Akhtar, H. Muhammad, S. Khan, and K. Waseem, “Basics of pharmaceutical emulsions : A review,” vol. 5, no. 25, pp. 2715–2725, 2011.
 - [21] P. M. Claesson, E. Blomberg, and E. Poptoshev, “Surfaces forces and emulsion stability (Chapter 7),” pp. 285–287, 2004.

- [22] H. W. Yarranton, D. M. Sztukowski, and P. Urrutia, "Effect of interfacial rheology on model emulsion coalescence. II. Emulsion coalescence," *J. Colloid Interface Sci.*, vol. 310, no. 1, pp. 246–252, 2007.
- [23] F. Y. Ushikubo and R. L. Cunha, "Stability mechanisms of liquid water-in-oil emulsions," *Food Hydrocoll.*, vol. 34, pp. 145–153, 2014.
- [24] S. D. Taylor, J. Czarnecki, and J. Masliyah, "Disjoining pressure isotherms of water-in-bitumen emulsion films," *J. Colloid Interface Sci.*, vol. 252, no. 1, pp. 149–160, 2002.
- [25] H. W. Yarranton, D. M. Sztukowski, and P. Urrutia, "Effect of interfacial rheology on model emulsion coalescence. I. Interfacial rheology," *J. Colloid Interface Sci.*, vol. 310, no. 1, pp. 246–252, 2007.
- [26] D. Georgieva, V. Schmitt, F. Leal-Calderon, and D. Langevin, "On the possible role of surface elasticity in emulsion stability," *Langmuir*, vol. 25, no. 10, pp. 5565–5573, 2009.
- [27] P. Atten, "Electrocoalescence of water droplets in an insulating liquid," *Conf. Rec. - IAS Annu. Meet. (IEEE Ind. Appl. Soc.)*, vol. 1992–Janua, pp. 1407–1411, 1992.
- [28] K. Moran, "Roles of interfacial properties on the stability of emulsified bitumen droplets," *Langmuir*, vol. 23, no. 8, pp. 4167–4177, 2007.
- [29] M. F. Fingas, "Water-in-oil emulsions: formation and prediction," *J. Pet. Sci. Res.*, vol. 3, pp. 38–49, 2014.
- [30] X. Wang and V. Alvarado, "Effects of Aqueous-Phase Salinity on Water-in-Crude Oil Emulsion Stability," *J. Dispers. Sci. Technol.*, vol. 33, no. 2, pp. 165–170, 2012.
- [31] J. S. Eow, M. Ghadiri, and A. O. Sharif, "Electrostatic and hydrodynamic separation of aqueous drops in a flowing viscous oil," *Chem. Eng. Process.*, vol. 41, pp. 649–657, 2002.
- [32] D. Sun, S. C. Jong, X. Duan, and D. Zhou, "Demulsification of water-in-oil emulsion by wetting coalescence materials in stirred- and packed- columns," *Colloids Surf., A Physicochem. Eng. Asp.*, vol. 150, pp. 69–75, 1999.
- [33] J. Wu, Y. Xu, T. Dabros, and H. Hamza, "Effect of demulsifier properties on destabilization of water-in-oil emulsion," *Energy Fuel*, vol. 17, pp. 1554–1559, 2003.

- [34] D. Langevin and J. F. Argillier, “Interfacial behavior of asphaltenes,” *Adv. Colloid Interface Sci.*, vol. 233, pp. 83–93, 2016.
- [35] D. P. Ortiz, E. N. Baydak, and H. W. Yarranton, “Effect of surfactants on interfacial films and stability of water-in-oil emulsions stabilized by asphaltenes,” *J. Colloid Interface Sci.*, vol. 351, no. 2, pp. 542–555, 2010.
- [36] J. D. McLean and P. K. Kilpatrick, “Effects of asphaltene solvency on stability of water-in-crude-oil emulsions,” *J. Colloid Interface Sci.*, vol. 189, no. 2, pp. 242–253, 1997.
- [37] H. W. Yarranton, H. Hussein, and J. H. Masliyah, “Water-in-hydrocarbon emulsions stabilized by asphaltenes at low concentrations,” *Colloid Interface Sci.*, vol. 228, no. 1, pp. 52–63, 2000.
- [38] J. Sjöblom, E. Mingyuan, A. A. Christy, and T. Gu, “Water-in-crude-oil emulsions from the Norwegian continental shelf 7 . Interfacial pressure and emulsion stability,” vol. 66, pp. 55–61, 1992.
- [39] V. Pauchard, J. Sjö, S. Kokal, P. Bouriat, C. Dicharry, and H. Mu, “Role of Naphthenic Acids in Emulsion Tightness for a Low-Total-Acid-Number (TAN)/ High-Asphaltenes Oil †,” no. March 2007, pp. 1269–1279, 2009.
- [40] P. Chaverot, A. Cagna, S. Glita, and F. Rondelez, “Interfacial Tension of Bitumen - Water Interfaces . Part 1 : Influence of Endogenous Surfactants at Acidic pH †,” no. 9, pp. 790–798, 2008.
- [41] F. Alvarez-Ramírez and Y. Ruiz-Morales, “Island versus archipelago architecture for asphaltenes: Polycyclic aromatic hydrocarbon dimer theoretical studies,” vol. 27, pp. 1791–1808, 2013.
- [42] G. V. Chilingarian and T. F. Yen, “Bitumens, Asphalts, and Tar Sands,” *Elsevier*, pp. 57–187, 1978.
- [43] G. V. C. T.F. Yen, “Asphaltenes and Asphalts, 2,” *Elsevier*, pp. 65–80, 2000.
- [44] B. P. Tissot and D. H. Welte, “Petroleum Formation and Occurrence,” *Springer-Verlag*, pp. 10–699, 1984.

- [45] J. W. Bunger and N. C. Li, "Chemistry of Asphaltenes," *Am. Chem. Soc.*, pp. 1–140, 1984.
- [46] E. Y. Sheu and O. C. Mullins, "Asphaltenes, Fundamentals and Applications," *Plenum Press*, pp. 1–245, 1995.
- [47] S. S. Pollack, "Structural Studies of Asphaltics by X-Ray Small Angle Scattering," vol. 42, no. 6, pp. 623–629, 1970.
- [48] O. C. Mullins and E. Y. Sheu., *Structures and Dynamics of Asphaltenes*. 1998.
- [49] C. Y. Ralston, S. Mitra-kirtley, and O. C. Mullins, "Small Population of One to Three Fused-Aromatic Ring Moieties in Asphaltenes," vol. 13, no. 4, pp. 623–630, 1996.
- [50] L. Haraguchi, W. Loh, and R. S. Mohamed, "Interfacial and colloidal behavior of asphaltenes obtained from Brazilian crude oils," vol. 32, pp. 201–216, 2001.
- [51] H. Groenzin and O. C. Mullins, "Asphaltene Molecular Size and Structure," pp. 11237–11245, 1999.
- [52] O. C. Mullins, S. Mitra-Kirtley, and Z. Yifu, "The Electronic Absorption Edge of Petroleum," *Appl. Spectrosc.*, vol. 46, pp. 1405–1411, 1992.
- [53] G. W. Zajac, N. K. Sethi, and J. T. Joseph, "Molecular imaging of petroleum asphaltenes by scanning-tunneling-microscopy-verification of structure from C-13 and proton nuclear-magnetic-resonance data," *Scanning Microsc.*, vol. 8, no. 3, pp. 463–470, 1994.
- [54] D. . Borton *et al.*, "Molecular structures of asphaltenes based on the dissociation reactions of their ions in mass spectrometry," *Energy & Fuels*, vol. 24, pp. 5548–5559, 2010.
- [55] W. . Tang *et al.*, "Structural Comparison of Asphaltenes of Different Origins Using Multi-stage Tandem Mass Spectrometry," *Energy & Fuels*, vol. 29, pp. 1309–1314, 2015.
- [56] L. Barre, D. Espinat, E. Rosenberg, and M. Scarsella, "Colloidal structure of heavy crudes and asphaltene solutions," *Rev Inst Fr du Pet.*, vol. 52, no. 2, p. 161, 1997.
- [57] D. Fenistein and L. Barre, "Experimental measurement of the mass distribution of petroleum asphaltene aggregates using ultracentrifugation and small-angle X-ray scattering," *Fuel*, vol. 80, no. 2, p. 283, 2001.

- [58] D. Fenistein, L. Barre, D. Broseta, D. Espinat, A. Livet, and J. Roux, “Viscosimetric and neutron scattering study of asphaltene aggregates in mixed toluene/heptane solvents,” *Langmuir*, vol. 14, no. 5, p. 1013, 1998.
- [59] D. Fenistein, L. Barre, and D. Frot, “From aggregation to flocculation of asphaltenes, a structural description by radiation scattering techniques,” *Oil Gas Sci. Technol.*, vol. 55, no. 1, p. 123, 2000.
- [60] L. Barre, J. Jestin, A. Morisset, T. Palermo, and S. Simon, “Relation between nanoscale structure of asphaltene aggregates and their macroscopic solution properties,” *Oil Gas Sci. Technol.*, vol. 64, no. 5, p. 617, 2009.
- [61] L. Barre, S. Simon, and T. Palermo, “Barre L, Simon S, Palermo T. Solution properties of asphaltenes. *Langmuir* 2008;24: 3709 – 17,” p. 3709, 2008.
- [62] A. B. Andrews, W. Shih, and O. C. Mullins, “Molecular Size Determination of Coal-Derived Asphaltene by Fluorescence Correlation Spectroscopy,” *Soc. Appl. Spectrosc.*, vol. 65, no. 12, pp. 1348–1356, 2011.
- [63] M. H. Schneider, A. B. Andrews, S. Mitra-kirtley, and O. C. Mullins, “Asphaltene Molecular Size by Fluorescence Correlation Spectroscopy,” *Energy & Fuels*, vol. 21, pp. 2875–2882, 2007.
- [64] A. R. Hortal, B. Mart, and M. D. Lobato, “On the determination of molecular weight distributions of asphaltenes and their aggregates in laser desorption ionization experiments,” *J. mass spectrometry*, vol. 41, pp. 960–968, 2006.
- [65] A. E. Pomerantz, M. R. Hammond, A. L. Morrow, O. C. Mullins, R. N. Zare, and S. U. V, “Two-Step Laser Mass Spectrometry of Asphaltenes,” *J. AM. CHEM. SOC.*, vol. 130, no. 23, pp. 7216–7217, 2008.
- [66] H. Groenzin, O. Mullins, S. Eser, J. Mathews, M. Yang, and D. Jones, “molecular size of asphaltene solubility fractions,” *Energy & Fuels*, vol. 17, no. 2, pp. 498–503, 2003.
- [67] L. Buch, H. Groenzin, E. Buenrostro-Gonzalez, S. Andersen, C. Lira-Galeana, and M. OC., “Molecular size of asphaltene fractions obtained from residuum hydrotreatment,” *Fuel*, vol. 82, no. 9, pp. 1075–84, 2003.

- [68] H. Groenzin and O. Mullins, "Molecular size and structure of asphaltenes from various sources," *Energy & Fuels*, vol. 14, no. 3, pp. 677–84, 2000.
- [69] J. Sjöblom, S. Simon, and Z. Xu, "Model molecules mimicking asphaltenes," *Adv. Colloid Interface Sci.*, vol. 218, pp. 1–16, 2015.
- [70] S. Subramanian, S. Simon, and J. Sjöblom, "Asphaltene Precipitation Models: A Review," *J. Dispers. Sci. Technol.*, vol. 37, no. 7, pp. 1027–1049, 2016.
- [71] A. Cagna, G. Esposito, A.-S. Quinquis, and D. Langevin, "On the reversibility of asphaltene adsorption at oil-water interfaces," *Colloids Surfaces A Physicochem. Eng. Asp.*, vol. 548, no. February, pp. 46–53, 2018.
- [72] P. Tchoukov, F. Yang, Z. Xu, T. Dabros, J. Czarnecki, and J. Sjöblom, "Role of asphaltenes in stabilizing thin liquid emulsion films," *Langmuir*, vol. 30, no. 11, pp. 3024–3033, 2014.
- [73] D. Pradilla, S. Simon, and J. Sjöblom, "Mixed Interfaces of Asphaltenes and Model Demulsifiers, Part II: Study of Desorption Mechanisms at Liquid/Liquid Interfaces," *Energy and Fuels*, vol. 29, no. 9, pp. 5507–5518, 2015.
- [74] P. Qiao, D. Harbottle, P. Tchoukov, X. Wang, and Z. Xu, "Asphaltene Subfractions Responsible for Stabilizing Water-in-Crude Oil Emulsions. Part 3. Effect of Solvent Aromaticity," *Energy and Fuels*, vol. 31, no. 9, pp. 9179–9187, 2017.
- [75] D. PK and H. RJ., "Acid-base characteristics of petroleum asphaltenes as studied by non-aqueous potentiometric titrations," *Fuel*, vol. 63, no. 2, pp. 197–201, 1984.
- [76] A. Hutin, J. Argillier, and D. Langevin, "Mass transfer of asphaltenes between oil and water. OGST; 2015 (submitted for publication)," *OGST*, 2015.
- [77] L. Barre, J. Eyssautier, and O. C. Mullins, "L. Barre, J. Eyssautier, O.C. Mullins, The asphaltenes, Annu. Rev. Anal. Chem. 4 (2011) 393 – 418.," *Annu. Rev. Anal. Chem.*, vol. 4, pp. 393–418, 2011.
- [78] O. C. Mullins, "The Asphaltenes," *Annu. Rev. Anal. Chem.*, vol. 4, pp. 393–418, 2011.
- [79] H. Zeng, Y. Song, D. Johnson, and O. Mullins, "Critical nanoaggregate concentration of

- asphaltenes by low frequency conductivity,” *Energy & Fuels*, vol. 23, p. 1201, 2009.
- [80] D. Freed, N. Lisitza, P. Sen, and Y. Song, “A study of asphaltene nanoaggregation by NMR,” *Energy & Fuels*, vol. 23, p. 1189, 2009.
- [81] F. Mostowfi, K. Indo, O. Mullins, and R. McFarlane, “Asphaltene nanoaggregates and the critical nanoaggregate concentration from centrifugation,” *Energy & Fuels*, vol. 23, p. 1194, 2009.
- [82] E. Y. Sheu, “Petroleum Asphaltenes Properties, Characterization, and Issues,” vol. 4, no. 5, pp. 74–82, 2002.
- [83] O. C. Mullins *et al.*, “Advances in Asphaltene Science and the Yen – Mullins Model,” 2012.
- [84] O. C. Mullins, “The Modified Yen Model,” *Energy & Fuels*, vol. 24, pp. 2179–2207, 2010.
- [85] Y. Ruiz-morales, “Aromaticity in pericondensed cyclopenta-fused polycyclic aromatic hydrocarbons determined by density functional theory nucleus-independent chemical shifts and the Y-rule — Implications in oil asphaltene stability,” *NRC Res. Press*, vol. 87, pp. 1280–1295, 2009.
- [86] H. Sabbah, A. L. Morrow, A. E. Pomerantz, and R. N. Zare, “Evidence for Island Structures as the Dominant Architecture of Asphaltenes,” pp. 1597–1604, 2011.
- [87] J. Eastoe and J. S. Dalton, “Dynamic surface tension and adsorption mechanisms of surfactants at the air-water interface,” *Adv. Colloid Interface Sci.*, vol. 85, no. 2, pp. 103–144, 2000.
- [88] J. P. Rane, D. Harbottle, V. Pauchard, A. Couzis, and S. Banerjee, “Adsorption kinetics of asphaltenes at the oil-water interface and nanoaggregation in the bulk,” *Langmuir*, vol. 28, no. 26, pp. 9986–9995, 2012.
- [89] L. Y. Zhang, Z. Xu, and J. H. Masliyah, “Langmuir and Langmuir–Blodgett films of mixed asphaltene and a demulsifier,” vol. 19, no. 23, pp. 9730–41, 2003.
- [90] M. Jeribi, B. Almir-Assad, D. Langevin, I. Hénaut, and J. F. Argillier, “Adsorption

- kinetics of asphaltenes at liquid interfaces,” *J. Colloid Interface Sci.*, vol. 256, no. 2, pp. 268–272, 2002.
- [91] J. Roux, D. Broseta, and B. Deme, “SANS study of asphaltene aggregation: concentration and solvent quality effects,” *Langmuir*, vol. 17, no. 16, p. 5085, 2001.
 - [92] J. McLean and P. Kilpatrick, “Effects of asphaltene aggregation in model heptane- toluene mixtures on stability of water-in-oil emulsions,” *J Colloid Interface Sci*, vol. 196, no. 1, pp. 23–24, 1997.
 - [93] S. Mhatre, S. Deshmukh, and R. M. Thaokar, “Electrocoalescence of a drop pair,” *Phys. Fluids*, vol. 27, no. 9, 2015.
 - [94] S. E. Taylor, “Investigations into the electrical and coalescence behaviour of water-in-crude oil emulsions in high voltage gradients,” *Colloids Surf.*, vol. 29, no. 1, pp. 29–51, 1988.
 - [95] H. A. Pohl, “Some effects of nonuniform fields on dielectrics,” *J. Appl. Phys.*, vol. 29, no. 8, pp. 682–689, 1958.
 - [96] S. Mhatre, “Dielectrophoretic motion and deformation of a liquid drop in an axisymmetric non-uniform AC electric field,” *Sensors Actuators, B Chem.*, vol. 239, pp. 1098–1108, 2017.
 - [97] J. Q. Feng, “Dielectrophoresis of a deformable fluid particle in a nonuniform electric field,” *Phys. Rev. E - Stat. Physics, Plasmas, Fluids, Relat. Interdiscip. Top.*, vol. 54, no. 4, pp. 4438–4441, 1996.
 - [98] J. C. Baygents, N. J. Rivette, and H. A. Stone, “Electrohydrodynamic deformation and interaction of drop pairs,” *J. Fluid Mech.*, vol. 368, pp. 359–375, 1998.
 - [99] S. Mhatre and R. Thaokar, “Pin-plate electrode system for emulsification of a higher conductivity leaky dielectric liquid into a low conductivity medium,” *Ind. Eng. Chem. Res.*, vol. 53, pp. 13488–13496, 2014.
 - [100] M. R. Abdelaal and M. A. Jog, “Heat/mass transfer from a drop translating in steady and time-periodic electric fields: External problem,” *Int. J. Heat Mass Transf.*, vol. 55, no. 9–

- 10, pp. 2315–2327, 2012.
- [101] S. K. Griffiths and F. A. Morrison, “The transport from a drop in an alternating electric field,” *Int. J. Heat Mass Transf.*, vol. 26, no. 5, pp. 717–726, 1983.
- [102] J. S. Eow and M. Ghadiri, “Motion, deformation and break-up of aqueous drops in oils under high electric field strengths,” *Chem. Eng. Process.*, vol. 42, no. 4, pp. 259–272, 2003.
- [103] J. R. Melcher and G. I. Taylor, “Electrohydrodynamics: a review of the role of interfacial shear stresses,” *Ann. Rev. Fluid Mech.*, vol. 1, pp. 111–146, 1969.
- [104] G. Taylor, “Studies in Electrohydrodynamics. I. The Circulation Produced in a Drop by Electrical Field,” *Proc. R. Soc. A Math. Phys. Eng. Sci.*, vol. 291, no. 1425, pp. 159–166, 1966.
- [105] J.-W. HA and S.-M. YANG, “Deformation and breakup of Newtonian and non-Newtonian conducting drops in an electric field,” *J. Fluid Mech.*, vol. 405, p. S0022112099007223, 2000.
- [106] E. C. Hsu and N. N. Li, “Membrane recovery in liquid membrane separation processes,” *Sep. Sci. Technol.*, vol. 20, no. 2 and 3, pp. 115–130, 1985.
- [107] R. E. Khayat, A. Luciani, L. A. Utracki, F. Godbille, and J. Picot, “Influence of shear and elongation on drop deformation in convergent/divergent flows,” *Int. J. Multiph. Flow*, vol. 26, pp. 17–44, 2000.
- [108] J. S. Eow, M. Ghadiri, and A. Sharif, “Experimental studies of deformation and break-up of aqueous drops in high electric fields,” *Colloids Surfaces A Physicochem. Eng. Asp.*, vol. 225, no. 1–3, pp. 193–210, 2003.
- [109] S. Mhatre *et al.*, “Electrostatic phase separation: A review,” *Chem. Eng. Res. Des.*, vol. 96, pp. 177–195, 2015.
- [110] S. Mhatre and R. Thaokar, “Electrocoalescence in non-uniform electric fields: An experimental study,” *Chem. Eng. Process. Process Intensif.*, vol. 96, pp. 28–38, 2015.
- [111] C. Bezemer and G. A. Croes, “Motion of water droplets of an emulsion in a non-uniform

- field,” *Br. J. Appl. Phys.*, vol. 224, no. 6, pp. 168–169, 1955.
- [112] S. Mhatre, S. Simon, J. Sjöblom, and Z. Xu, “Demulsifier assisted film thinning and coalescence in crude oil emulsions under DC electric fields,” *Chem. Eng. Res. Des.*, vol. 134, pp. 117–129, 2018.
- [113] P. Atten, “Electrohydrodynamics of dispersed drops of conducting liquid: From drops deformation and interaction to emulsion evolution,” *IJPEST*, vol. 7, no. 1, pp. 2–12, 2013.
- [114] F. Ravera, G. Loglio, and V. I. Kovalchuk, “Interfacial dilational rheology by oscillating bubble/drop methods,” *Curr. Opin. Colloid Interface Sci.*, vol. 15, no. 4, pp. 217–228, 2010.
- [115] O. I. Del Río and A. W. Neumann, “Axisymmetric drop shape analysis: Computational methods for the measurement of interfacial properties from the shape and dimensions of pendant and sessile drops,” *J. Colloid Interface Sci.*, vol. 196, no. 2, pp. 136–147, 1997.
- [116] M. Hoorfar and A. W. Neumann, “Recent progress in Axisymmetric Drop Shape Analysis (ADSA),” *Adv. Colloid Interface Sci.*, vol. 121, no. 1–3, pp. 25–49, 2006.
- [117] J. D. Berry, M. J. Neeson, R. R. Dagastine, D. Y. C. Chan, and R. F. Tabor, “Measurement of surface and interfacial tension using pendant drop tensiometry,” *J. Colloid Interface Sci.*, vol. 454, pp. 226–237, 2015.
- [118] S. M. I. Saad, Z. Policova, and A. W. Neumann, “Design and accuracy of pendant drop methods for surface tension measurement,” *Colloids Surfaces A Physicochem. Eng. Asp.*, vol. 384, no. 1–3, pp. 442–452, 2011.
- [119] M. Nagel, T. A. Tervoort, and J. Vermant, “From drop-shape analysis to stress-fitting elastometry,” *Adv. Colloid Interface Sci.*, vol. 247, no. July, pp. 33–51, 2017.
- [120] F. K. Hansen and G. Rødsrud, “Surface tension by pendant drop. I. A fast standard instrument using computer image analysis,” *J. Colloid Interface Sci.*, vol. 141, no. 1, pp. 1–9, 1991.
- [121] M. A. Farah, R. C. Oliveira, J. N. Caldas, and K. Rajagopal, “Viscosity of water-in-oil

- emulsions: Variation with temperature and water volume fraction,” *J. Pet. Sci. Eng.*, vol. 48, no. 3–4, pp. 169–184, 2005.
- [122] D. C. Maia, J. B. V. S. Ramalho, G. M. S. Lucas, and E. F. Lucas, “Aging of water-in-crude oil emulsions : Effect on rheological parameters,” *Colloids Surfaces A Physicochem. Eng. Asp.*, vol. 405, pp. 73–78, 2012.
- [123] H. Fruhner and K. D. Wantke, “A new oscillating bubble technique for measuring surface dilational properties,” *Colloids Surfaces A Physicochem. Eng. Asp.*, vol. 114, pp. 53–59, 1996.
- [124] Y. H. Kim, K. Koczko, and D. T. Wasan, “Dynamic film and interfacial tensions in emulsion and foam systems,” *J. Colloid Interface Sci.*, vol. 187, no. 1, pp. 29–44, 1997.
- [125] C. H. Chang, K. A. Coltharp, S. Y. Park, and E. I. Franses, “Surface tension measurements with the pulsating bubble method,” *Colloids Surfaces A Physicochem. Eng. Asp.*, vol. 114, pp. 185–197, 1996.
- [126] G. Loglio, P. Pandolfini, R. Miller, A. Makievski, J. Krägel, and F. Ravera, “Oscillation of interfacial properties in liquid systems: Assessment of harmonic distortion,” *Phys. Chem. Chem. Phys.*, vol. 6, no. 7, pp. 1375–1379, 2004.
- [127] V. I. Kovalchuk *et al.*, “Frequency characteristics of amplitude and phase of oscillating bubble systems in a closed measuring cell,” *J. Colloid Interface Sci.*, vol. 252, no. 2, pp. 433–442, 2002.
- [128] Y. C. Liao, O. A. Basaran, and E. I. Franses, “Hydrodynamic effects on the oscillations of supported bubbles: Implications for accurate measurements of surface properties,” *Colloids Surfaces A Physicochem. Eng. Asp.*, vol. 250, no. 1–3 SPEC. ISS., pp. 367–384, 2004.
- [129] E. M. Freer, H. Wong, and C. J. Radke, “Oscillating drop/bubble tensiometry: Effect of viscous forces on the measurement of interfacial tension,” *J. Colloid Interface Sci.*, vol. 282, no. 1, pp. 128–132, 2005.
- [130] M. E. Leser, S. Acquistapace, A. Cagna, A. V. Makievski, and R. Miller, “Limits of oscillation frequencies in drop and bubble shape tensiometry,” *Colloids Surfaces A*

- Physicochem. Eng. Asp.*, vol. 261, no. 1–3, pp. 25–28, 2005.
- [131] L. Liggieri, V. Attolini, M. Ferrari, and F. Ravera, “Measurement of the surface dilational viscoelasticity of adsorbed layers with a capillary pressure tensiometer,” *J. Colloid Interface Sci.*, vol. 255, no. 2, pp. 225–235, 2002.
- [132] A. Bateni, S. S. Susnar, A. Amirfazli, and A. W. Neumann, “Development of a new methodology to study drop shape and surface tension in electric fields,” *Langmuir*, vol. 20, no. 18, pp. 7589–7597, 2004.
- [133] L. Y. Zhang, R. Lopetinsky, Z. Xu, and J. H. Masliyah, “Asphaltene monolayers at a toluene/water interface,” *Energy and Fuels*, vol. 19, no. 4, pp. 1330–1336, 2005.
- [134] L. Y. Zhang, P. Breen, Z. Xu, and J. H. Masliyah, “Asphaltene films at a toluene/water interface,” *Energy and Fuels*, vol. 21, no. 1, pp. 274–285, 2007.
- [135] B. M. Aguilera, J. G. Delgado, and A. L. Cárdenas, “Water-in-Oil Emulsions Stabilized by Asphaltenes Obtained from Venezuelan Crude Oils Water-in-Oil Emulsions Stabilized by Asphaltenes Obtained from Venezuelan Crude Oils,” vol. 2691, 2010.
- [136] N. Zaki, P. C. Schorling, and I. Rahimian, “Effect of asphaltene and resins on the stability of water-in-waxy oil emulsions,” *Pet. Sci. Technol.*, vol. 18, no. 7–8, pp. 945–963, 2000.
- [137] Y. Fan, S. Simon, and J. Sjöblom, “Interfacial shear rheology of asphaltenes at oil-water interface and its relation to emulsion stability: Influence of concentration, solvent aromaticity and nonionic surfactant,” *Colloids Surfaces A Physicochem. Eng. Asp.*, vol. 366, no. 1–3, pp. 120–128, 2010.
- [138] S. Basu, K. Nandakumar, and J. H. Masliyah, “A study of oil displacement on model surfaces,” *J. Colloid Interface Sci.*, vol. 182, no. 1, pp. 82–94, 1996.
- [139] K. . Takamura and E. E. Isaacs, *In AOSTRA Technical Handbook on Oil Sands, Bitumens and Heavy Oils*. 1989.
- [140] J. Drelich and J. D. Miller, “Surface and interfacial tension of the Whiterocks bitumen and its relationship to bitumen release from tar sands during hot water processing,” *Fuel*, vol. 73, no. 9, pp. 1504–1510, 1994.

- [141] A. L. Nenningsland, E. Herschbach, and J. Sj, “Extraction of Basic Components from Petroleum Crude Oil,” vol. 55, no. 11, pp. 1043–1050, 2010.
- [142] S. Poteau, J. F. Argillier, D. Langevin, F. Pincet, and E. Perez, “Influence of pH on stability and dynamic properties of asphaltenes and other amphiphilic molecules at the oil-water interface,” *Energy and Fuels*, vol. 19, no. 4, pp. 1337–1341, 2005.
- [143] A. L. Márquez, A. Medrano, L. A. Panizzolo, and J. R. Wagner, “Effect of calcium salts and surfactant concentration on the stability of water-in-oil (w / o) emulsions prepared with polyglycerol polyricinoleate,” *J. Colloid Interface Sci.*, vol. 341, no. 1, pp. 101–108, 2010.
- [144] C. E. Perles, P. L. O. Volpe, and A. J. F. Bombard, “Study of the cation and salinity effect on electrocoalescence of water/crude oil emulsions,” *Energy and Fuels*, vol. 26, no. 11, pp. 6914–6924, 2012.
- [145] M. Fortuny, C. B. Z. Oliveira, R. L. F. V. Melo, M. Nele, R. C. C. Coutinho, and A. F. Santos, “Effect of Salinity, Temperature, Water Content, and pH on the Microwave Demulsification of Crude Oil Emulsions [†],” *Energy & Fuels*, vol. 21, no. 3, pp. 1358–1364, 2007.
- [146] J. A. Rocha *et al.*, “Role of Aqueous Phase Chemistry, Interfacial Film Properties, and Surface Coverage in Stabilizing Water-in-Bitumen Emulsions,” *Energy and Fuels*, vol. 30, no. 7, pp. 5240–5252, 2016.